NASA CONTRACTOR REPORT

NASA CR-141426

THE ESTIMATION OF POINTING ANGLE AND σ° FROM GEOS-3 RADAR ALTIMETER MEASUREMENTS

G. S. Brown
W. J. Curry

FINAL REPORT

Prepared Under Contract No. NAS6-2520 by

Applied Science Associates, Inc.
105 East Chatham Street
Apex, North Carolina 27502

National Aeronautics and
Space Administration

Wallops Flight Center
Wallops Island, Virginia 23337
AC 804 824-3411

August 1977

1. Report No.	2. Government Accession No.	3. Recipient's Catalog No.
NASA CR-141426		

4. Title and Subtitle	5. Report Date
THE ESTIMATION OF POINTING ANGLE AND σ° FROM GEOS-3 RADAR ALTIMETER MEASUREMENTS	August 1977
	6. Performing Organization Code
7. Author(s)	8. Performing Organization Report No.
G. S. Brown and W. J. Curry	
9. Performing Organization Name and Address	10. Work Unit No.
Applied Science Associates, Inc. 105 East Chatham Street Apex, North Carolina 27502	11. Contract or Grant No. NAS6-2520
12. Sponsoring Agency Name and Address	13. Type of Report and Period Covered
National Aeronautics and Space Administration Wallops Flight Center Wallops Island, Virginia 23337	Final Report
	14. Sponsoring Agency Code

15. Supplementary Notes

16. Abstract

This report derives quantitative results for a technique for estimating the pointing angle of the GEOS-3 radar altimeter and σ° estimates using data provided by the altimeter. The pointing angle method employs the output of two gated integrators, one of which is located at a position on the average return waveform which is sensitive to attitude errors. The statistical error of the estimation technique is determined as a function of the effective receiver signal-to-noise ratio. The one-sigma error in the estimation technique at nadir is 0.33° for the Global Mode and 0.23° for the Intensive Mode; the difference is due to different placement of one of the gated integrators on the average return. The method results in a minimum statistical error in the vicinity of one-half a beamwidth pointing angle; for both modes the one-sigma error is less than 0.07°. Other sources of error are addressed and evaluated with inadequate calibration being of major concern. The impact of pointing error on the computation of σ° from radar data and the waveform attitude induced altitude bias is considered and quantitative results are presented. The Intensive Mode Clean vs. Clutter AGC calibration problem is analytically resolved. The logarithmic nature of the AGC loop is shown to give rise to a bias of 2.5 dB for the Intensive Mode and 0.14 dB for the Global Mode. The Clutter AGC data are shown to be the theoretically correct data set for transforming inflight AGC values into received power. Pointing angle and σ° processing algorithms are presented along with some initial data. These results confirm the use of Clutter AGC data in the Intensive Mode as the correct calibration set for σ° computations.

17. Key Words (Suggested by Author(s))	18. Distribution Statement
Radar Altimetry Attitude Determination Pointing Accuracy σ° Measurement	Unclassified - unlimited STAR Categories 18 and 32

19. Security Classif. (of this report)	20. Security Classif. (of this page)	21. No. of Pages	22. Price*
Unclassified	Unclassified	101	

*For sale by the National Technical Information Service, Springfield, Virginia 22151

TABLE OF CONTENTS

TABLE OF CONTENTS (Cont'd.)

1.0 INTRODUCTION

In both the so-called Intensive and Global modes, the GEOS-3 radar altimeter acquires altitude and backscattered power data; furthermore, in the Intensive mode, instantaneous and/or average return waveform data are also obtained. Upon further processing, these data will yield measurements of the geoid undulation, the normalized surface scattering cross section (σ°), and the rms height of the small scale surface perturbations*. The key to the transformation from raw radar data to these surface characteristics is an in depth understanding of the scattering of electromagnetic energy from rough surfaces. For most applications of the GEOS-3 data, the data transformation problem hinges, more specifically, on knowing what influences the time varying average return power waveform.

The impact of the radar upon the post detection average return power waveform is contained in the three following system parameters; the video point target response, the tracking loop jitter density, and the pointing angle of the radar antenna electrical boresight with respect to nadir [1]. The point target response of the radar is measured by the Sample and Hold (S&H) gates during the RF BIAS TEST in the BIT/CAL mode of operation. Furthermore, the tracking loop jitter density can be determined by histograming the tracking loop jitter which is obtained directly from the tracking loop output. Thus, the first two radar dependent factors are directly measurable and therefore can be properly accounted for. The pointing angle, on the other hand, is not measured and only its estimated range of variation is known. For certain early-mission orbits, estimates of the spacecraft z-axis pointing with respect to nadir were computed [2]. However, since the angle between the spacecraft z-axis and the radar antenna electrical boresight is not precisely known, such results do not help matters much.

Since an uncertainty in the actual pointing angle of the radar antenna can lead to larger error bounds on radar derived estimates of surface characteristics, it is clearly in order to investigate means for determining the pointing angle. This report presents the results of a study to estimate the radar pointing angle through the use of the average Plateau gate output and

---

*Small scale surface perturbations, as used here, refer to those surface features whose spatial wavelength is much smaller than the effective spot size of the radar.

the average Attitude/Specular gate output. In addition, error bounds on the estimate are obtained based upon the number of returns used to form the average. The pointing angle induced altitude bias is computed for the Global mode* and the variation of σ° with pointing angle is also presented.

1.1 Summary of Results

This report derives a relationship between the ratio of the outputs of the Attitude/Specular and Plateau integrating gates and the angle of the radar antenna boresight relative to nadir. The relationship is shown to be single valued and therefore amenable to use as a means of estimating the radar pointing angle. Estimation curves are obtained for both the Intensive and Global modes. Stationary approximations to the autocorrelation function for the predetection backscattered signal are obtained which are applicable over the delay extent of the Plateau and Attitude/Specular gates. With the inclusion of receiver noise and rather simple models of the IF and video filters, estimates of the ten second standard deviation of the pointing angle estimate are obtained as a function of the effective receiver signal-to-noise ratio. The one-sigma statistical error of the method is on the order of 0.33° at nadir for Global Mode and 0.23° at nadir for the Intensive Mode. This error decreases to less than 0.07° for both modes when the pointing angle exceeds 1°. Based upon the statistical error of the technique, the method is best suited for use when the pointing error is on the order of one half a beamwidth.

The effect of inadequate temperature dependent calibration of the Attitude/Specular and Plateau gates is shown to be a nonnegligible source of error in the estimation process. A five percent change in gate calibration is shown to give rise to an error which is a nonlinear function of the true pointing angle, i.e. the error is largest at nadir ($\approx 0.4^\circ$) and decreases to about 0.1° at one half a beamwidth pointing error. This error source is hypothesized to be the cause of disagreement between preliminary pointing angle estimates obtained during Global Mode and spacecraft-based sensor estimates.

---

*Attitude induced biases have previously been presented for the Intensive Mode in [1].

Curves are obtained for converting received power measurements into pointing angle corrected estimates of σ° for both Global and Intensive Modes. Waveform and attitude induced altitude bias is computed for the Global Mode and shown to be a major source of error relative to absolute altimetry. The effect of pointing angle upon waveheight estimation is discussed and dismissed assuming that the pointing error is less than one half a beamwidth.

The problem of a discrepancy between the AGC Clean and Clutter Intensive Mode calibration data is addressed and resolved using an analytical approach. The sample-by-sample AGC control voltage is modeled as an average of logarithms of the Plateau gate outputs. Because of this logarithmic dependence, the average of the AGC control voltage differs from the deterministic (Clean) result by a constant value, i.e. a bias. This bias is equivalent to a 2.5 dB separation between the Clean and Clutter calibration curves. The actual data indicates a separation of 3.5 to 4 dB; thus, there is a 1 to 1.5 dB residual error which cannot be accounted for. Considering the complexity of simulating a noise-like coded return, this residual error may well be due to experimental error. To within this residual error, the Clutter AGC curves are shown to be the proper calibration data for reducing inflight data. The bias for Global Mode is shown to be negligible, because the bias depends inversely upon the number of returns averaged prior to entering the AGC loop. For the Global Mode, the number of returns averaged was sixteen and the resulting bias is shown to be -0.14 dB. The analysis presented here not only resolves the GEOS-3 Clean vs. Clutter problem, but also sheds more light on the operation of logarithmic AGC systems for extended target scattering.

The final two sections of the report deal with the implementation and evaluation of the models developed in the previous sections. A simple closed-form algorithm for converting the angle estimation function into pointing angle estimates is presented for both operating modes. A limited comparison of radar derived angle estimates with attitude control system results indicates the apparent presence of a 0.6° to 0.8° bias in the Global Mode. This bias is attributed to inadequate integrating gate calibration. Intensive Model comparisons indicate reasonable agreement with no apparent bias. A typographical error in the Plateau gate calibration data has, unfortunately, been implemented in the basic data correction/calibration

program at WFC. Temperature dependent correction routines have been developed to overcome this problem in an ad hoc fashion.

Closed-form algorithms have also been developed for computing σ° from return power measurements. These algorithms also depend upon transmitted power and pointing angle. Global Mode σ° values compare very favorably with Skylab results for similar surface conditions. Intensive Mode values are some 3 dB lower than the Global Mode results. This was attributed to the use of Clean rather than Clutter AGC calibration data. An in-orbit test was conducted and it verified that the Clutter calibration data is the proper set. Correction routines have been developed to overcome the erroneous data calibration problem.

2.0 ESTIMATION OF THE RADAR POINTING ANGLE

2.1 Background

During study of the Skylab radar altimeter data, it was found that the pointing angle of the radar antenna boresight relative to nadir could be accurately determined from the shape of the post detection average return waveform [3]. This finding was a direct consequence of the fact that for near nadir pointing only the trailing edge portion of the AGC normalized average return was sensitive to a change in pointing angle. Figure 1 illustrates the behavior of the Skylab average return waveform for two different pointing angles. Of particular note in this figure is the fact that the leading edge of the average return is relatively insensitive to the change in pointing angle while the trailing edge exhibits a marked change. The pointing angle estimation procedures developed for Skylab involved comparison of the measured post detection average return waveform (in the trailing edge portion of the return) with computed waveforms [7]. Such a direct comparison was possible for Skylab because waveform samples of the return were obtained well into the trailing edge portion of the return. For a 1500 pulse average, the one-sigma error in the pointing angle estimate due to the statistical nature of the return was shown to be less than 0.05° [7] for, roughly, one half a beamwidth pointing error.

For the GEOS radar altimeter, no waveform point samplers, i.e., Sample and Hold gates, were located sufficiently far into the trailing edge portion of the return to directly apply the estimation procedures developed for Skylab.

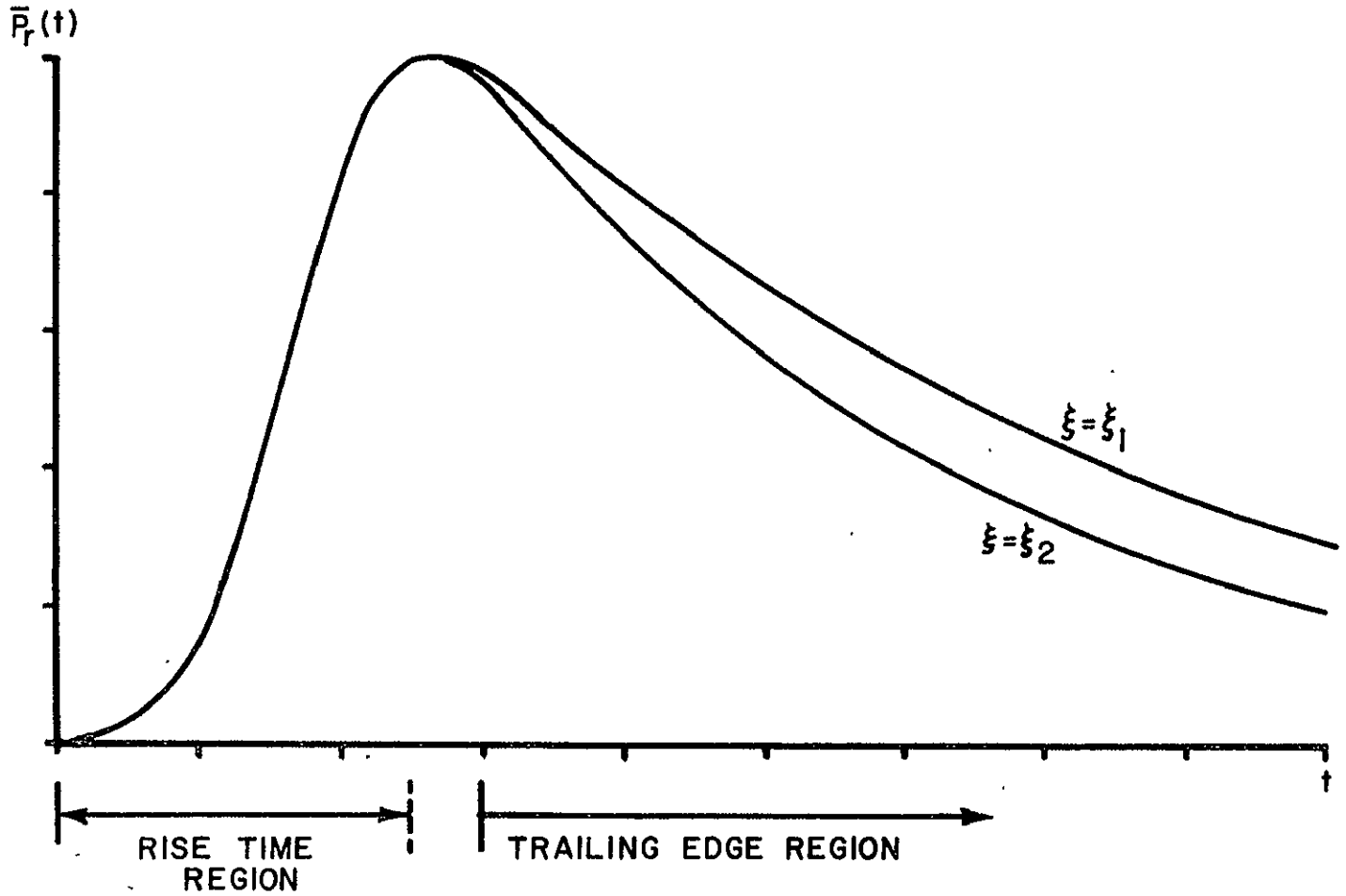

Figure 1. Typical shape of the average return power as a function of delay time for the Skylab radar altimeter.

However, the General Electric Company originally proposed an alternate implementation [4] whereby an integrating gate (called the Attitude/Specular gate) was located in the trailing edge portion of the return; the location of this integrating gate relative to the Ramp and Plateau (tracking) gates is shown in Figure 2 for both the Intensive and Global Modes. By comparing the output of the Attitude/Specular gate (which is sensitive to the pointing angle) to the output of the Plateau gate (which is much less sensitive to the pointing angle) the radar pointing angle could be indirectly measured. Preliminary analyses of this approach [4,1,5] indicated that the technique showed sufficient promise as to warrant further in depth analysis. The purpose of this section is to present the analysis for determining the estimated pointing angle and its statistical precision from the Plateau and Attitude/Specular integrating gate outputs.

2.2 The Estimation Function

Figure 3 is a block diagram [6] of those parts of the GEOS radar altimeter receiver which are essential to the angle estimation problem. It is important to note that the outputs of the integrating gates are passes through a one second averager before being telemetered to earth. The first step in the analysis comprises relating the filtered outputs of the integrating gates to the radar pointing angle.

2.2.1 The Average Integrating Gate Outputs

For the jth return voltage, the output of the IF filter/amplifier, which also contains the pulse compression network for the Intensive Mode (IM), may be represented as

$$x_j(t) = \left[v_{cj}(t) + n_{cj}(t)\right] \cos\omega_o t - \left[v_{sj}(t) + n_{sj}(t)\right] \sin\omega_o t \quad , \qquad (1)$$

where ω_o is the IF center frequency. The in-phase and quadrature return voltage components $v_{cj}(t)$ and $v_{sj}(t)$ are independent, zero mean, Gaussian random variables with a time varying variance equal to $K\overline{P}_r(t)$, i.e. the product of the average return power and a constant which depends upon the RF gain of the receiver and the AGC. Similarly, the in-phase and quadrature noise voltage components $n_{cj}(t)$ and $n_{sj}(t)$ are independent, zero mean,

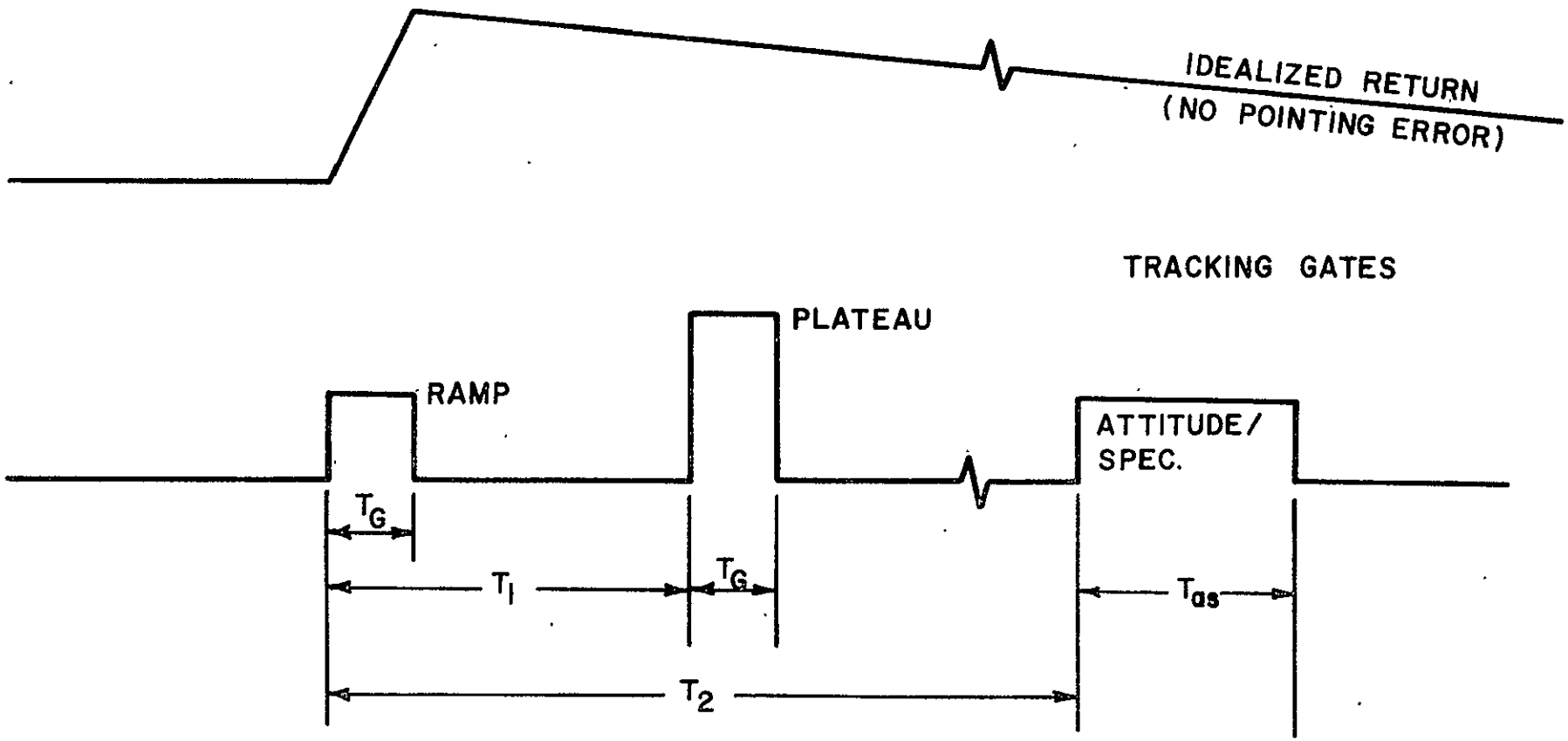

INTENSIVE MODE

T_G = 12.5 ns.

T_1 = 62.5 ns.

T_2 = 700 ns.

T_{as} = 200 ns.

GLOBAL MODE

T_G = 200 ns.

T_1 = 300 ns.

T_2 = 700 ns.

T_{as} = 200 ns.

Figure 2. Nominal GEOS tracking gates' lengths and locations for both Intensive and Global Modes.

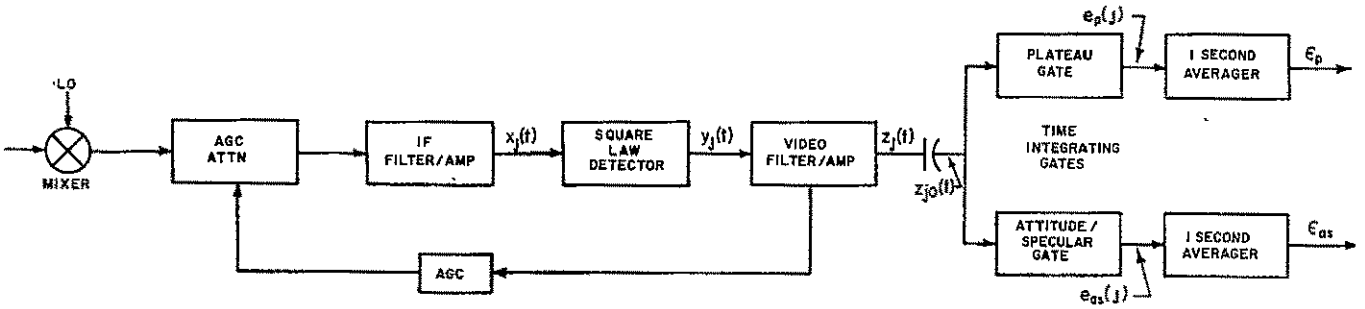

Figure 3. A simplified block diagram of the GEOS-3 radar altimeter receiver pertinent to the attitude estimation process.

Gaussian random variables with variance KN_o where $N_o = kT_e B_{IF}$ and k is Boltzman's constant, T_e is the effective receiver noise temperature, and B_{IF} is the IF filter/amplifier noise bandwidth. Squaring (1) and regrouping terms yields, for the output of the square law detector,

$$y_j(t) = \frac{1}{2}\left\{\left[v_{cj}(t)+n_{cj}(t)\right]^2 + \left[v_{sj}(t)+n_{sj}(t)\right]^2\right\}$$

$$+ \frac{1}{2}\left\{\left[v_{cj}(t)+n_{cj}(t)\right]^2 - \left[v_{sj}(t)+n_{sj}(t)\right]^2\right\}\cos 2\omega_o t$$

$$- \left[v_{cj}(t)+n_{cj}(t)\right]\left[v_{sj}(t)+n_{sj}(t)\right]\sin 2\omega_o t \qquad (2)$$

Since the video filter/amplifier has a low-pass characteristic with a bandwidth much less than $2f_o$, its output is given by

$$z_j(t) = \frac{1}{2}\left\{\left[v_{cj}(t)+n_{cj}(t)\right]^2 + \left[v_{sj}(t)+n_{sj}(t)\right]^2\right\} \circledast h_v(t) \ , \qquad (3)$$

where $h_v(t)$ is the impulse response of the video filter/amplifier and the symbol $\circledast$ denotes convolution. The series capacitor between the video amplifier and the two gates essentially blocks those components of $z_j(t)$ which, in the mean, are either constant or slowly varying with time. Thus, the input to the two gates is given by the following;

$$z_{jo}(t) = z_j(t) - \frac{1}{2}E\left\{\left[n_{cj}^2(t)+n_{sj}^2(t)\right] \circledast h_v(t)\right\} \qquad (4)$$

since $n^2(t) \circledast h_v(t)$ is the only term which yields a constant mean value.

The average output of either the Plateau or Attitude/Specular integrating gates is given by

$$\bar{e} = E\{e(j)\} = G\int_T^{T+\delta} E\left\{z_{jo}(t)\right\} h_G(T+\delta-t)\,dt \qquad (5)$$

where T is the time (in two-way time delay coordinates) at which the particular gate is switched on, δ is the gate length, G is the gain of the gate, and

$h_G(t)$ is the normalized impulse response of the integrating gate. Using (3) and (4), the average return voltage into the integrating gates is related to the IF average return power as follows;

$$E\left\{z_{jo}(t)\right\} = K\,\overline{P}_r(t) \circledast h_v(t) \tag{6}$$

The IF average return power may be expressed [1] as a convolution of the IF point target power response*, $P_{IF}(t)$, with the so-called flat surface impulse response, $P_{FS}(t)$. Interchanging the order of convolutions, (6) may be rewritten as

$$E\left\{z_{jo}(t)\right\} = K\,V_v(t) \circledast P_{FS}(t) \tag{7}$$

where $V_v(t)$ is the convolution of $P_{IF}(t)$ with the video filter/amplifier impulse response. $V_v(t)$ is the video voltage point target response and it is equivalent to the voltage waveform at the output of the video filter/amplifier during the so-called RF Bias Test of BIT/CAL for the GEOS altimeter. Substituting (7) into (5) yields the following expression for the average output of either the Plateau or Attitude/Specular gates;

$$\overline{e} = E\left\{e(j)\right\} = G\,K \int_{T}^{T+\delta} V_v(t) \circledast P_{FS}(t) h_G(T+\delta-t)\,dt \tag{8}$$

According to [6], the integrating gates are analog integrating circuits with a time constant equal to four times the gate width; thus, the normalized impulse response of the integrating gate is given by

$$h_G(T+\delta-t) = \frac{\exp\left[(T+\delta-t)/4\delta\right]}{\int_{T}^{T+\delta} \exp\left[(T+\delta-t)/4\delta\right] dt} \tag{9}$$

---

*For the Intensive Mode, the IF point target response is equivalent to the squared ambiguity function of the transmitted signal. For the Global Mode, the equivalence is with the cross-ambiguity function squared, because matched filtering is not used.

For near nadir operation, the appropriate flat surface impulse response has been shown [1] to be given by the following;

$$P_{FS}(t) = P_T \eta_{IF} \frac{G_o^2 \lambda^2 c \sigma^\circ(\psi_o)}{4(4\pi)^2 L_p L_r h^3} \exp\left(-\frac{4}{\gamma}\sin^2\xi - \frac{4c}{\gamma h} t \cos 2\xi\right)$$

$$\cdot I_o\left(\frac{4}{\gamma}\sqrt{\frac{ct}{h}}\sin 2\xi\right) \qquad (10)$$

for $t \geq 0$ and $P_{FS}(t) = 0$ for $t < 0$. In (10), P_T is the peak transmitted power, η_{IF} is the measured pulse compression ratio, G_o is the boresight gain of the radar antenna, λ is the radar wavelength, c is the speed of light (0.3m/ns.), σ° is the surface scattering cross section per unit scattering area, L_p is the two-way path attenuation, L_r comprises the appropriate radar losses, h is the altitude of the radar above the mean surface, and γ is a parameter related to the beamwidth of the antenna pattern (1.49×10^{-3} for GEOS-3). Also, in (10) and the remainder of the material in this report, time is measured relative to the total two-way delay time (2h/c) from the radar to the mean surface. The variable ξ in (10) is the pointing angle; it is defined as the angle between the electrical boresight of the radar antenna and the nadir axis. The angle ψ_o is defined by the following relationship;

$$\tan\psi_o = \left[ct/h\right]^{1/2} \qquad (11)$$

The video voltage point target was measured during preflight testing of the altimeter [6], and the results are shown in Figures 4 and 5 for the Intensive and Global Modes, respectively. A discretely sampled version of Figure 4 is also available from BIT/CAL data (RF Bias Test) obtained during actual operation of the altimeter. Examination of RF Bias Test data [8] obtained during inflight operation of the altimeter has indicated no significant changes in the Intensive Mode video point target response. No recording of the video point target response is accomplished in BIT/CAL for the Global Mode.

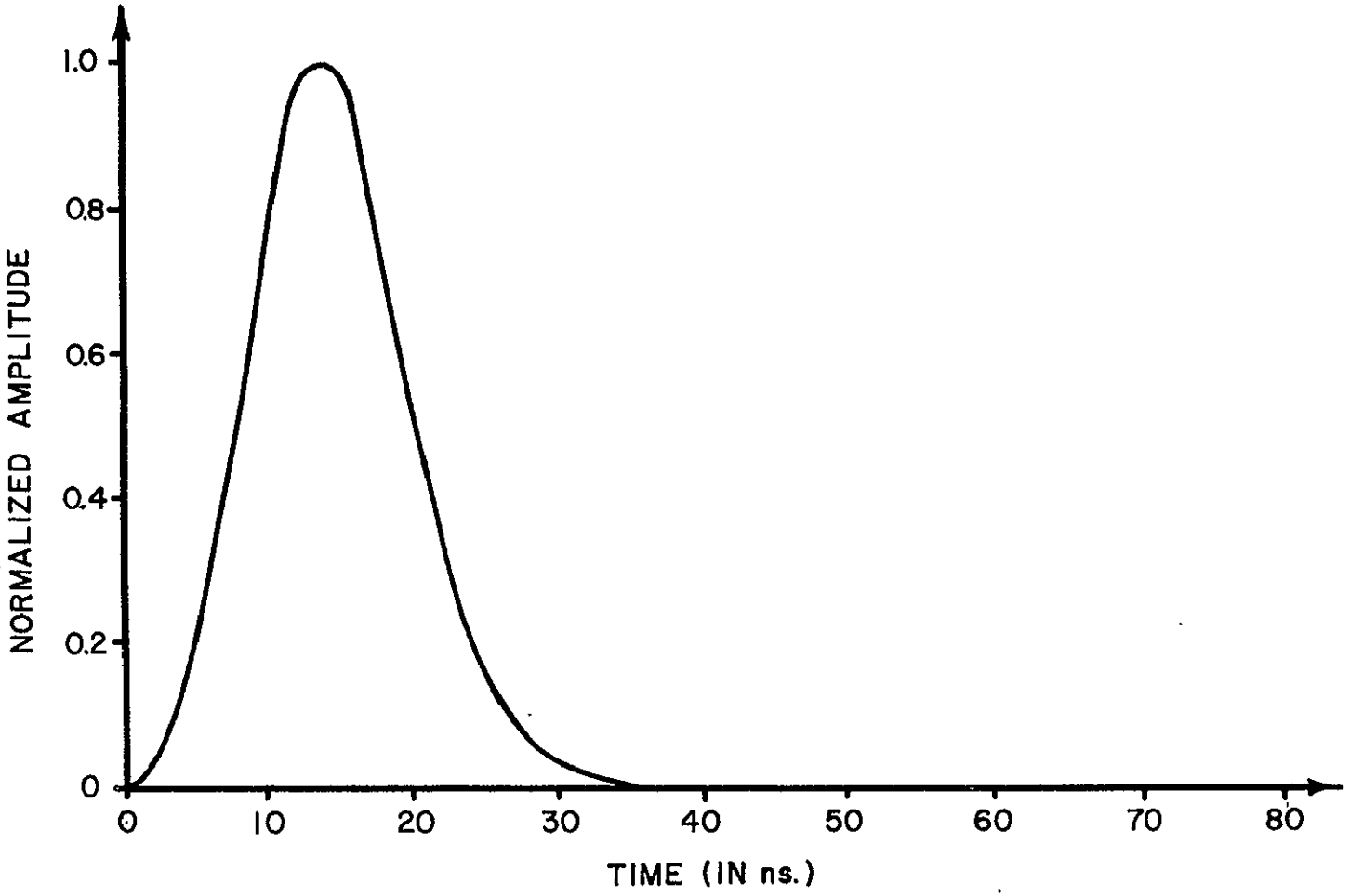

Figure 4. The Intensive Mode video voltage point target response, from [6].

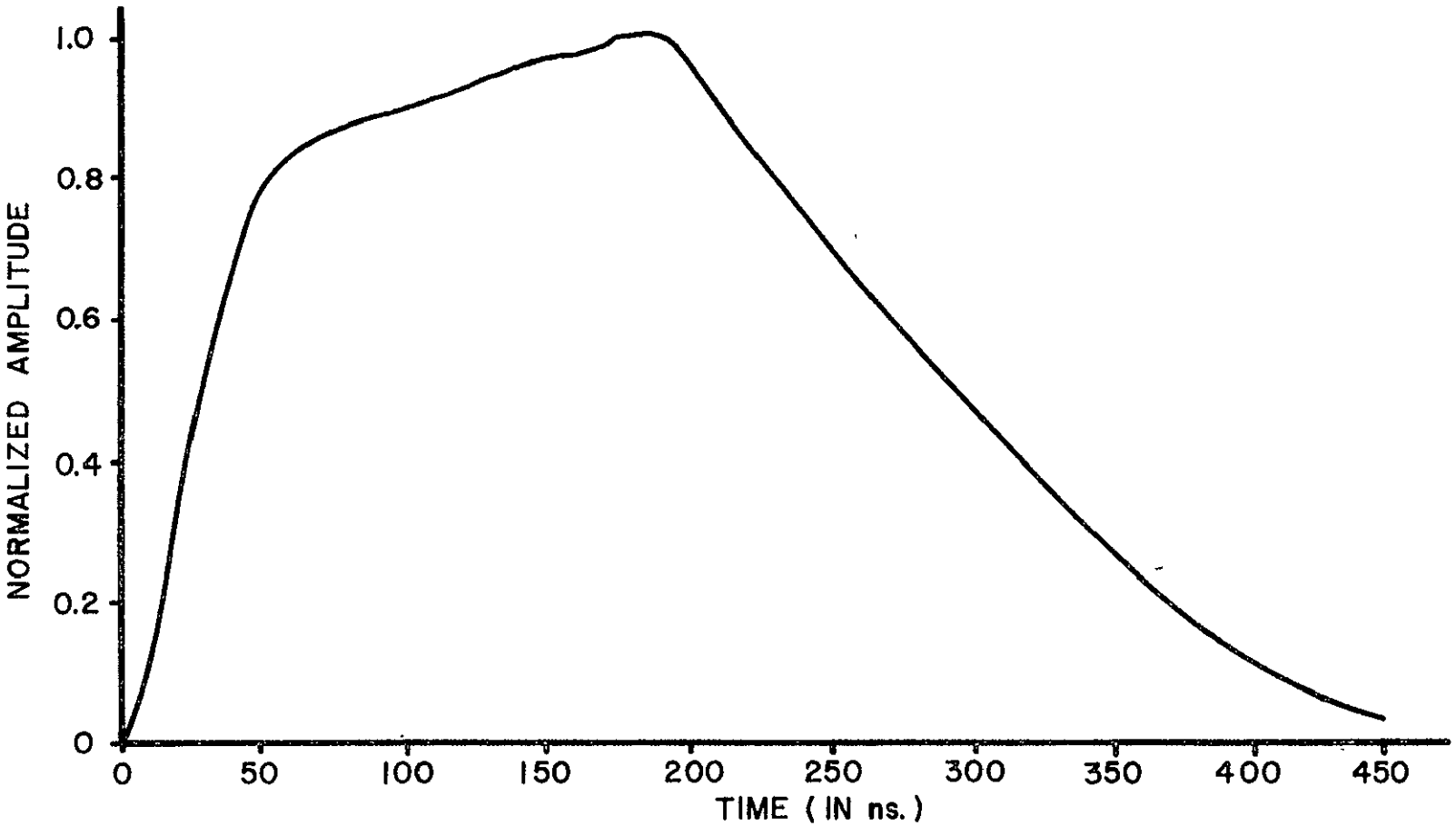

Figure 5. The Global Mode video voltage point target response, from [6].

2.2.2 The One Second Hardware Averager

The output of either the Plateau or Attitude/Specular integrating gate is, according to [6] and Figure 3, averaged for one second and then sampled by the telemetry system. The averaging process is accomplished by an analog filter, however, the transfer characteristics of this filter were not specifically detailed in [6]. For this reason, the analog averager or filter is modeled by a discrete process in which the output is formed by averaging the number of returns in a one second time interval. That is, the output of the one second averager in Figure 3 is approximated by the following;

$$\varepsilon \approx \frac{1}{M} \sum_{j=1}^{M} e(j) \tag{12}$$

where M is the number of returns integrated by either the Plateau of Attitude/Specular gates in a one second interval. For the Intensive Mode, M is equal to 100. In the Global Mode, M = 1600 for the Plateau gate and M = 100 for the Attitude/Specular gate; the difference is due to the fact that only the first return of the sixteen pulse burst (per prf) is integrated by the Attitude/Specular gate [6]. Table I summarizes the important

TABLE I

A Tabulation of Intensive and Global Mode Plateau and Attitude/Specular Gate Parameters

	GLOBAL MODE		INTENSIVE MODE	
	Plateau Gate	Attitude/ Specular Gate	Plateau Gate	Attitude/ Specular Gate
Relative Gate Gain, G*	$G_{p(g)}$	$G_{as(g)}$	$G_{p(i)}$	$G_{as(g)}$
Relative Gate Turn-On Time, T	300 ns	700 ns	62.5 ns	700 ns
Gate Width, δ	200 ns	200 ns	12.5 ns	200 ns
Number of Pulses Avgd. In 1 Sec, M	1600	100	100	100

*These gains are functions of the tracker temperature and input signal strength (near saturation); extensive calibration curves are given in [6]. The same Attitude/Specular integrating gate is used for both Global and Intensive Modes.

gate parameters for the Plateau and Attitude/Specular integrating gates for both the Global and Intensive Modes.

2.2.3 The Minimum Averaging Time and Its Effect Upon the Estimation Function

The ensemble average of the one second averaged integrating gate output is equal to the average gate output, i.e., $\overline{\bar{\varepsilon}} = \overline{e}(i)$. Using equations (8), (9), (10) and the waveforms in Figures 4 and 5 along with the gate parameters in Table I, the average output of the gates can be computed. It is now possible to construct a function of the Plateau and Attitude/Specular gate outputs which will result in a single-valued determination of the pointing angle; this function will be called the estimation function. It is obvious from (8) that this estimation function should be dependent upon the ratio of the Plateau and Attitude/Specular gate outputs in order to eliminate the unknown AGC dependent constant K. Furthermore, the estimation function should also be a function of the ratio of the gate outputs to the gate gains since this eliminates the need for detailed temperature corrections and is also consistent with Wallops Flight Center data processing products. A previous study has suggested the following form [1] for the estimation function;

$$\Delta = 1 - \frac{\varepsilon_{as}/G_{as}}{\varepsilon_p/G_p} \tag{13}$$

where ε_{as} and ε_p are the one second averaged outputs of the Attitude/Specular and Plateau gates, respectively, and G_{as} and G_p are the gate gains. However, defining the estimation function in terms of the one second averaged outputs, as above, suffers the drawback that the average estimation function, $\overline{\Delta}$, does not converge to the ratio of the average gate outputs. That is, since ε_p and ε_{as} are derived from at least a 100-pulse average, they will be essentially Gaussian with the following means and variances;

$$\overline{\varepsilon}_{as} = \overline{e}_{as} \qquad \overline{\varepsilon}_p = \overline{e}_p \tag{14}$$

$$\mathrm{Var}(\varepsilon_{as}) \approx \frac{\mathrm{Var}(e_{as})}{M_{as}} \qquad \mathrm{Var}(\varepsilon_p) \approx \frac{\mathrm{Var}(e_p)}{M_p} \tag{15}$$

where M_{as} and M_p are the number of pulses averaged to form the one second averaged Attitude/Specular and Plateau gate outputs (see Table I). In order to determine the average estimation function, the joint density function of $\varepsilon_{as} G_p / \varepsilon_p G_{as}$ must be computed. This density function can be obtained by the methods given in [9]; however, because the two processes ε_p and ε_{as} are nonzero mean Gaussian, the first moment is not easily calculated. An alternate approach [9, pg. 212] to computing the average of the estimation function is to expand $(1 - \varepsilon_{as} G_p / \varepsilon_p G_{as})$ in a Taylor series about $\varepsilon_{as} = \bar{\varepsilon}_{as}$ and $\varepsilon_p = \bar{\varepsilon}_p$ and only retain the significant terms (after averaging). This procedure is valid only when the probability masses of ε_{as} and ε_p are very concentrated near their "center of gravity", i.e., $\bar{\varepsilon}_{as}$ and $\bar{\varepsilon}_p$, and $(1 - \varepsilon_{as} G_p / \varepsilon_p G_{as})$ is smooth in the vicinity of this point. Reference 10 indicates the order of error this approximation can lead to when the above assumptions are violated; however, because of the degree of variance reduction brought about by the one second averaging, this approach can be safely used to compute the average estimation function. Therefore, using the Taylor series approach, the average estimation function can be shown to reduce to the following form:

$$\bar{\Delta} \approx 1 - \frac{\bar{\varepsilon}_{as} G_p}{\bar{\varepsilon}_p G_{as}} \left[1 + \frac{\mathrm{Var}(\varepsilon_p)}{(\bar{\varepsilon}_p)^2} \right] \tag{16}$$

Rewriting (16) in terms of the average gate outputs yields

$$\bar{\Delta} = 1 - \frac{\bar{e}_{as} G_p}{\bar{e}_p G_{as}} \left[1 + \frac{\mathrm{Var}(e_p)}{M_p (\bar{e}_p)^2} \right] \tag{17}$$

Equation (17) illustrates why it is not desirable to define the estimation as in (13); that is, the average estimation function depends upon the variance of the Plateau gate output. For the Global Mode, this dependence does not create a problem since M_p is 1600 and $\mathrm{Var}(e_p)$ is relatively insensitive to receiver noise. However, for the Intensive Mode, $M_p = 100$ and $\mathrm{Var}(e_p)$ is more strongly dependent upon the receiver noise because of the lower signal-to-noise margin. Thus, if the estimation function is defined as in (13), the average estimation function will depend upon the

receiver signal-to-noise ratio and this is not a desirable situation. The obvious way to overcome this problem is to increase M_p in (17) by at least an order of magnitude; then, the variance dependent term in (17) will be negligibly small and can be ignored. For this reason, the estimation function Δ should be defined in terms of at least a ten second average of the gate outputs, i.e.

$$\Delta = 1 - \frac{\tilde{\varepsilon}_{as}/G_{as}}{\tilde{\varepsilon}_p/G_p} \tag{18}$$

where

$$\tilde{\varepsilon}_{as} = \frac{1}{10M_{as}} \sum_{j=1}^{10M_{as}} e_{as}(j) \tag{19}$$

$$\tilde{\varepsilon}_p = \frac{1}{10M_p} \sum_{j=1}^{10M_p} e_p(j) \tag{20}$$

The remainder of this report will deal exclusively with the estimation function as defined in (18).

Ignoring the variance dependent term in (17), the average estimation function becomes

$$\overline{\Delta} = 1 - \frac{\overline{e}_{as}/G_{as}}{\overline{e}_p/G_p} \tag{21}$$

In (21), the gain normalized gate outputs are directly compatible with the gate output data products provided by Wallops Flight Center. Figure 6 illustrates how the average estimation function depends upon the radar antenna pointing antenna for both the Global and Intensive Modes. The greater slope of the curves as the pointing angle approaches a beamwidth (2.6°) reflects the fact that the average return waveform in the vicinity of the Attitude/-Specular gate changes more rapidly as the pointing angle approaches a beamwidth. The smaller slope of the Global Mode curve is a direct consequence

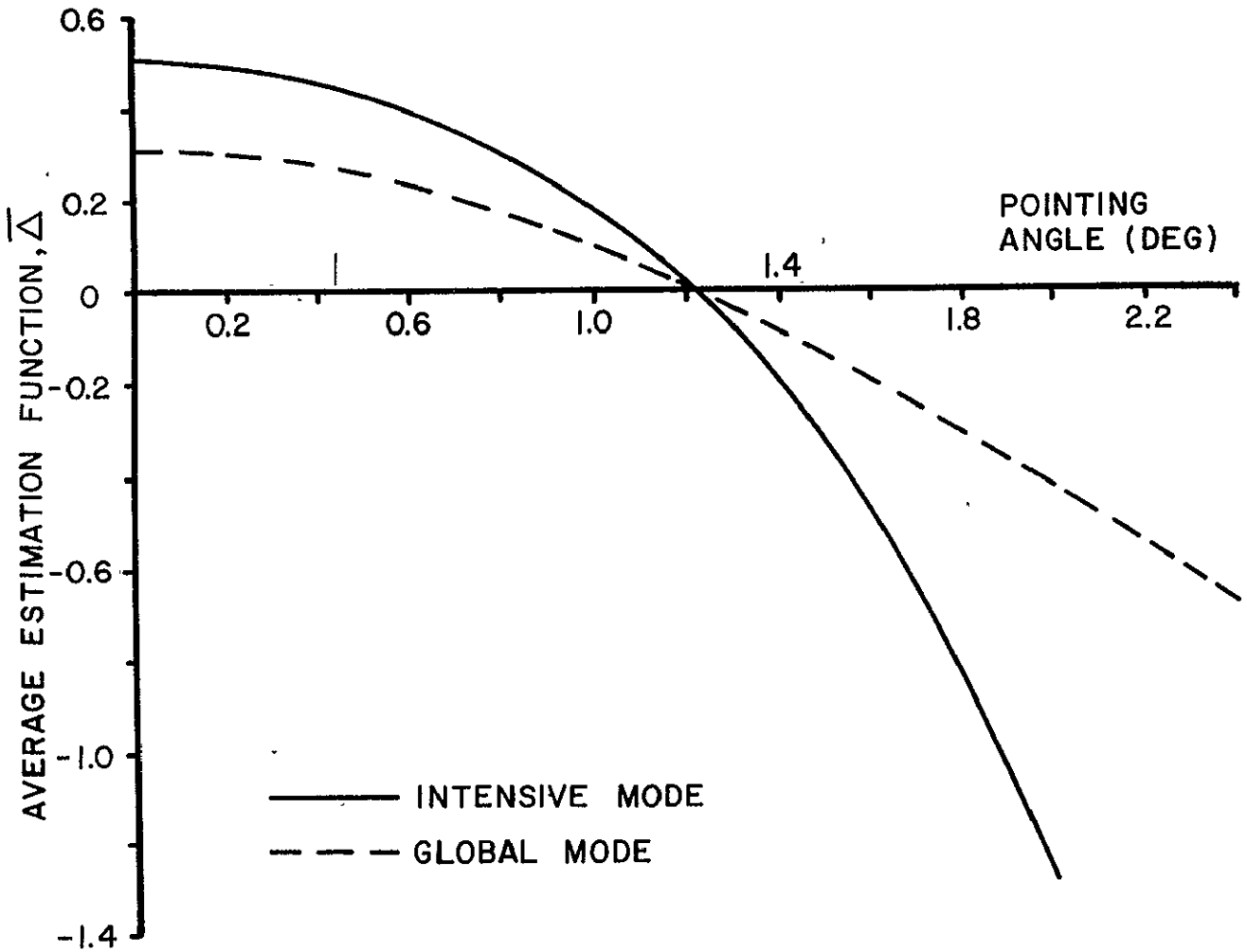

Figure 6. The average estimation function for Global and Intensive Modes.

of the placement of the Plateau gate on the average return by the tracking loop time discriminator. That is, for the Global Mode, the center of the Plateau Gate occurs approximately 400 ns after the start of the return (see Figure 2); at this relative delay time, the return shows a significant "droop" due to antenna pattern effects. Thus, both the Plateau and Attitude/-Specular gates encounter portions of the return which are dominated by antenna pattern induced droop. Similarly, as the pointing angle increases over the range shown in Figure 6, both gate outputs will also increase but at a different rates. For the Intensive Mode, the Plateau gate is located much nearer zero relative delay time and therefore is not effected by the antenna pattern; thus, the curve in Figure 6 for the Intensive Mode is primarily determined by the waveform in the vicinity of the Attitude/Specular gate.

2.3 The Precision of the Estimate

The previous section of this report was concerned with obtaining a relationship between the radar antenna pointing angle and the average Plateau and Attitude/Specular integrating gate outputs. This section will be devoted to computing the statistical uncertainty of the pointing angle estimate. This uncertainty is a direct consequence of the fading and fluctuating nature of the return and the nonnegligible influence of receiver noise. Since the analysis will be concerned with the variance of the integrating gate outputs, this phase of the investigation is closely related to the problem of determining the precision of the GEOS-3 split-gate tracker derived altitude estimates [11].

2.3.1 The Variance of the Gate Outputs

The average output of the integrating gates is given by (5); the variance of the output is as follows;

$$\mathrm{Var}(e) = G^2 \int_T^{T+\delta} \int_T^{T+\delta} E\left\{ z_{jo}(t_1) z_{jo}(t_2) \right\} h_G(T+\delta-t_1) h_G(T+\delta-t_2) dt_1 dt_2 - (\bar{e})^2 \qquad (22)$$

Substituting (3) and (4) in (22) and using the independent Gaussian property of v(t) and n(t) to simplify the resulting expectation operations [12], (22) reduces to the following form*

$$\mathrm{Var}(e) = G^2 \int_T^{T+\delta} \int_T^{T+\delta} \left\{ \left[R_v^2(t_1,t_2) + 2R_v(t_1,t_2)R_n(t_1,t_2) + R_n^2(t_1,t_2) \right] \right.$$

$$\left. \circledast h_v(t_1) \circledast h_v(t_2) \right\} h_G(T+\delta-t_1) h_G(T+\delta-t_2) dt_1 dt_2 \qquad (23)$$

where $R_v(t_1,t_2)$ and $R_n(t_1,t_2)$ are the autocorrelation functions for the IF in-phase or quadrature components of the return voltage and the noise, respectively. That is, the intrapulse autocorrelation function for the return is

$$R_v(t_1,t_2) = E\left\{ v_{cj}(t_1) v_{cj}(t_2) \right\} = E\left\{ v_{sj}(t_1) v_{sj}(t_2) \right\}$$

while the noise autocorrelation function is

$$R_n(t_1,t_2) = E\left\{ n_{cj}(t_1) n_{cj}(t_2) \right\} = E\left\{ n_{sj}(t_1) n_{sj}(t_2) \right\}$$

2.3.2 The Return Signal Autocorrelation Function

The autocorrelation of the noise is completely specified by the equivalent receiver noise temperature and the bandpass characteristics of the IF filter/amplifier. The return voltage intrapulse autocorrelation function is considerably more complex because, in general, it is nonstationary. Berger [13] has obtained an analytical expression for $R_v(t_1,t_2)$ under certain restrictive conditions. Generalizing his result and correcting some of his algebraic errors, it can be shown that the IF return voltage autocorrelation function is given by the following**,

---

*In the transformation from (22) to (23), it was assumed that the video filter/amp did not appreciably alter the shape of $\overline{P}_r(t)$; measurements presented in [6] indicate that this is a reasonable assumption.

**Equation (24) is valid if the scattering surface is noncoherent and the doppler spread in the return is small relative to the doppler extent of the radar ambiguity function; both of these conditions are satisfied for over-ocean operation of the GEOS-3 radar altimeter.

$$R_v(t_1,t_2) \approx K \int_0^\infty P_{IF}^{1/2}(t_1 - t)\, P_{IF}^{1/2}(t_2 - t)\, P_{FS}(t)\, dt \qquad (24)$$

where $P_{IF}^{1/2}(\cdot)$ is the square root of the IF point target power response and $P_{FS}(\cdot)$ is the flat surface impulse response, see equation (10). Equations (24) and (23) indicate a five-fold integration to accomplish the transformation from known quantities, i.e., $P_{IF}(t)$ and $P_{FS}(t)$, to the variance of the gate outputs. For this reason it is most necessary to accomplish as many of these integrations in closed form as possible.

2.3.2.1 Intensive Mode

Inspection of the IF point target power response measurements presented in [6] shows that a Gaussian form is a very good approximation for $P_{IF}^{1/2}(t_1)$ in the Intensive Mode, i.e.

$$P_{IF}^{1/2}(t_1) \approx \exp\left[-(t_1 - t_o)^2/4\sigma_i^2\right] \qquad (25)$$

where $\sigma_i \approx 5.3$ ns and $t_o \approx 2\sqrt{2}\,\sigma_i$ is time shift introduced to insure the proper timing between P_{IF} and P_{FS} in (24). In (24), since $P_{FS}(t)$ is nearly constant over the range of integration for which the product $P_{IF}^{1/2}(t_1-t)P_{IF}^{1/2}(t_2-t)$ is nonzero, the following approximation is valid;

$$R_v(t_1,t_2) \approx K\, P_{FS}\left(\frac{t_1+t_2}{2} - t_o\right) \int_0^\infty P_{IF}^{1/2}(t_1-t)P_{IF}^{1/2}(t_2-t)dt \qquad (26)$$

Substituting (25) in (26) yields

$$R_v(t_1,t_2) = K\sqrt{2\pi\sigma_i^2}\; P_{FS}\left(\frac{t_1+t_2}{2} - t_o\right) \exp\left[-(t_1-t_2)^2/8\sigma_i^2\right]$$
$$\cdot \left\{\frac{1}{2} + \frac{1}{2}\,\mathrm{erf}\left[\frac{t_1+t_2-2t_o}{2\sqrt{2}\,\sigma_i}\right]\right\} \qquad (27)$$

where erf$(\cdot)$ is the error function. Those parts of $R_v(t_1,t_2)$ which give rise to its nonstationary nature are functionally dependent upon the sum

of the two time coordinates t_1 and t_2. As noted previously, the flat surface impulse response varies rather slowly as t_1 and t_2 range over the appropiate time extent of the integrating gate, i.e. from T to $T+\delta$. Thus, the flat surface impulse response may be adequately approximated by its value at the mid-point of the gate, i.e.

$$P_{FS}\left(\frac{t_1+t_2}{2} - t_o\right) \approx P_{FS}\left(T+\delta/2 - t_o\right) \tag{28}$$

Using the values for T and δ shown in Table I, it may be verified that the argument of the error function is greater than two for both the Plateau and Attitude/Specular gates; thus, since $\text{erf}(t \geq 2) \approx 1$,

$$\text{erf}\left[\frac{t_1+t_2-2t_o}{2\sqrt{2}\,\sigma_i}\right] \approx 1 \quad ,$$

and (27) simplifies to the following;

$$R_v(t_1,t_2) \approx K\sqrt{2\pi\sigma_i^2}\; P_{FS}\left(T+\delta/2-t_o\right) \exp\left[-\left(t_1-t_2\right)^2/8\sigma_i^2\right] \tag{29}$$

Thus, for the Intensive Mode, the predetection intrapulse autocorrelation function is essentially stationary over the time extent of the Plateau and Attitude/Specular gates.

2.3.2.2 Global Mode

For the Global Mode, the situation is more complex because the shape of the IF point target power response is not easily represented by a simple function (see Figure 77 of [6]) such as a single Gaussian as in the case of the Intensive Mode. To take advantage of some of the approximations developed for the Intensive Mode, the square root of IF point target response was approximated by a four term series of Gaussian functions, i.e.

$$P_{IF}^{1/2}(t) \approx \sum_{m=1}^{4} a_m \exp\left[-\left(t-\beta_m\right)^2/2\sigma_m^2\right] \tag{30}$$

The amplitudes (a_m), time shifts (β_m), and spread factors (σ_m) were generated

by a computer program which minimizes the mean squared error between the measured function and the approximating series. A tabulation of these factors is shown in Table II.

Substituting (30) in (24), using the same rationale to remove the flat surface impulse response from inside the integral as in (26), and integrating term by term yields the following result;

$$R_v(t_1,t_2) \approx K\sqrt{2\pi}\sum_{k=1}^{4}\sum_{m=1}^{4} P_{FS}\left(\frac{\sigma_k^2(t_1-\beta_m)+\sigma_m^2(t_2-\beta_k)}{\sigma_k^2+\sigma_m^2}\right)\cdot\frac{a_m a_k \sigma_m \sigma_k}{\sqrt{\sigma_m^2+\sigma_k^2}}$$

TABLE II

Amplitudes, Time Shifts, And Spread Factors For The Four Term Gaussian Approximation To The Square Root Of The IF Power Point Target Response (Global Mode).

m	a_m	β_m	σ_m
1	0.615	55	25
2	0.705	125	50
3	0.412	190	50
4	0.66	300	85

Note: the units of β_m and σ_m are nanoseconds

$$\cdot \exp\left\{-\frac{\left[(t_1-t_2)-(\beta_k-\beta_m)\right]^2}{2\left(\sigma_k^2+\sigma_m^2\right)}\right\}\cdot\left\{\frac{1}{2}\right.$$

$$\left.+\frac{1}{2}\operatorname{erf}\left[\frac{\sigma_k^2(t_1-\beta_m)+\sigma_m^2(t_2-\beta_k)}{\sqrt{2}\,\sigma_k\sigma_m\sqrt{\sigma_m^2+\sigma_k^2}}\right]\right\} \tag{31}$$

Using the parameter values in Table II , it can be shown that the argument of the error function in (31) is always greater than two as t_1 and t_2 range over the Attitude/Specular gate. When t_1 and t_2 range over the Plateau gate, the argument is also greater than two except for pairs of indices

$$k=3 \quad , \quad m=4$$

$$k=4 \quad , \quad m=3$$

and

$$k=4 \quad , \quad m=4$$

Even for these terms, the error function argument is not appreciably smaller than two; also, since there are only three out of the sixteen terms in (31) for which the error function argument is less than two, their effect upon the sum will be further diminished. Consequently, the error function in (31) will be taken as one for both the Plateau and Attitude/Specular gates.

A remaining problem with (31) is that the argument of the flat surface impulse response depends upon both summation indices and it cannot be removed from inside the double sum. However, because of the exponential factor in (31) and the slowly varying nature of the flat surface impulse response, each term in the double series will be significant only in the neighborhood of $t_1 - t_2 = \beta_k - \beta_m$ or $t_1 = t_2 + \beta_k - \beta_m$. With this transformation, the argument of P_{FS} becomes $t_2 - \beta_k$ and (31) reduces to

$$R_v(t_1,t_2) \approx K\sqrt{2\pi}\sum_{k=1}^{4} P_{FS}(t_2-\beta_k)\sum_{m=1}^{4}\frac{a_m a_k \sigma_m \sigma_k}{\sqrt{\sigma_m^2+\sigma_k^2}}$$

$$\cdot \exp\left\{-\frac{\left[(t_1-t_2)-(\beta_k-\beta_m)\right]^2}{2\left(\sigma_k^2+\sigma_m^2\right)}\right\} \tag{32}$$

The β_k in the argument of P_{FS} is now replaced by an average value given by

$$\overline{\beta} = \frac{1}{4}\sum_{k=1}^{4}\beta_k = 167.5 \text{ ns}$$

and $P_{FS}(t_2 - \overline{\beta})$ is removed from inside the summation. This step is once again justified by noting that the flat surface impulse response is relatively slowly varying with time. As in the case of the Intensive Mode, t_2 in the argument of P_{FS} is replaced by $T + \frac{\delta}{2}$, i.e. the location of the mid point of either the Plateau or Attitude/Specular gate. Equation (32) therefore reduces to the following form;

$$R_y(t_1,t_2) \approx K\sqrt{2\pi}\, P_{FS}\left(T + \frac{\delta}{2} - \overline{\beta}\right)\sum_{k=1}^{4}\sum_{m=1}^{4}\frac{a_m a_k \sigma_m \sigma_k}{\sqrt{\sigma_m^2 + \sigma_k^2}}$$

$$\cdot \exp\left\{ - \frac{\left[(t_1-t_2) - (\beta_k-\beta_m)\right]^2}{2(\sigma_k^2 + \sigma_m^2)} \right\} \qquad (33)$$

It should be noted that (33) is a symmetric function of $t_1 - t_2$ because of the double summation.

The double sum in (33) was computed as a function of the time difference $(t_1 - t_2)$ and compared to a single Gaussian function. The following approximation was found to be very good;

$$\sum_{k=1}^{4}\sum_{m=1}^{4}\frac{a_m a_k \sigma_m \sigma_k}{\sqrt{\sigma_m^2 + \sigma_k^2}} \exp\left\{ - \frac{\left[(t_1-t_2) - (\beta_k-\beta_m)\right]^2}{2(\sigma_k^2 + \sigma_m^2)} \right\}$$

$$\approx \sigma_{go} \exp\left[-(t_1-t_2)^2/2\sigma_{g1}^2\right] \qquad (34)$$

where $\sigma_{go} = 102$ ns and $\sigma_{g1} = 161.37$ ns. Figure 7 shows the comparison between the normalized double sum and the single Gaussian approximation. The final form for the Global Mode autocorrelation function is

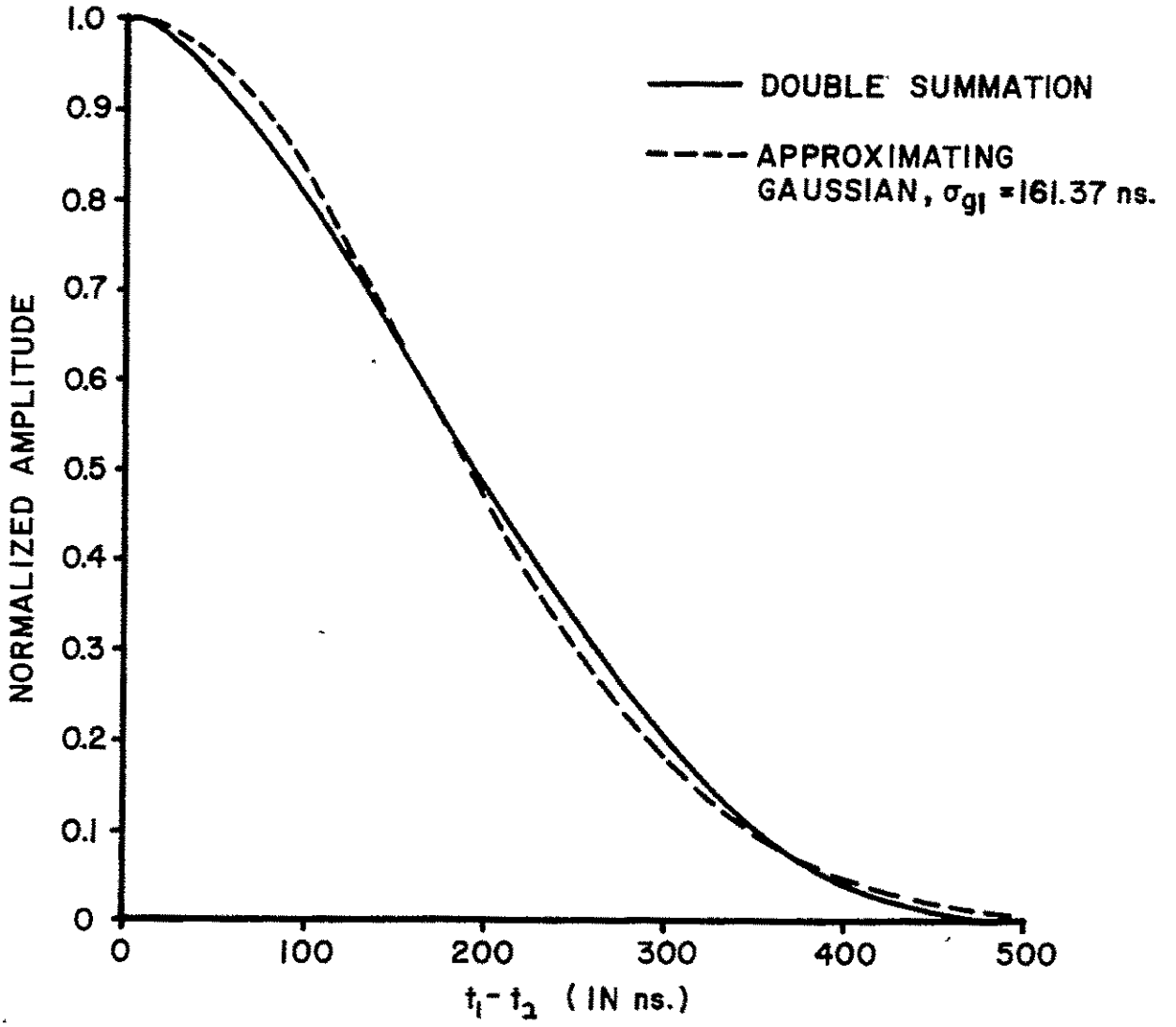

Figure 7. Comparison of signal autocorrelation coefficient and a Gaussian approximation for Global Mode.

$$R_v(t_1,t_2) \approx K\sqrt{2\pi\sigma_{go}^2}\; P_{FS}\left(T+\frac{\delta}{2}-\overline{\beta}\right)\exp\left[-(t_1-t_2)^2/2\sigma_{g1}^2\right] \qquad (35)$$

where

$$\sigma_{go} = 102 \text{ ns}$$
$$\overline{\beta} = 167.5 \text{ ns}$$
$$\sigma_{g1} = 161.37 \text{ ns}$$

It should be noted that the end purpose of the above sequence of approximations was to obtain an integrable form for the autocorrelation function. In performing these approximations, the slight nonstationary nature of the autocorrelation function in the Plateau gate region has been ignored and the resultant approximation is, no doubt, a smoothed version of the true function. However, equation (35) does contain the basic form of the Global Mode autocorrelation function and is probably more than adequate for a variance calculation.

2.3.3 The Noise Autocorrelation Function and Receiver Model

Now that the signal autocorrelation functions are known, the noise autocorrelation function must be obtained. As [11] indicates, even for a simple model of the IF and video filters, the problem is extremely tedious. To simplify the labor as much as possible and yet retain the basic character of the problem, the IF filter was modeled as a two-pole RC filter while the video filter was taken to be a single-pole RC filter. The 3 dB bandwidths were matched to the measurements presented in [6]; namely, for the IF filter

$$\text{Intensive Mode:}\quad BW_{IF} = 52.4 \text{ MHz}$$
$$\text{Global Mode}\quad :\quad BW_{IF} = 40.4 \text{ MHz}$$

and for the video filter

$$\text{Intensive Mode:}\quad BW_v = 50 \text{ MHz}$$
$$\text{Global Mode}\quad :\quad BW_v = 5 \text{ MHz}$$

For the two-pole IF filter, the autocorrelation function of the noise is given by the following;

$$R_n(t_1,t_2) = K(1.22kT_e)(BW_{IF})\left\{(4.88BW_{IF})|t_1-t_2|+1\right\} \cdot \exp\left[-4.88BW_{IF}|t_1-t_2|\right] \quad (36)$$

where k is Boltzman's constant and T_e is the equivalent noise temperature of the receiver front end.

Before proceeding further with the determination of the variance of the output of the integrating gates, equation (23) will be further simplified. First, in the double convolution of the video impulse response with the product of the noise and signal autocorrelations, the following approximation is made;

$$R_v(t_1,t_2)R_n(t_1,t_2)\circledast h_v(t_1)\circledast h_v(t_2) \approx R_v(t_1,t_2)\left[R_n(t_1,t_2)\circledast h_v(t_1)\circledast h_v(t_2)\right] \quad (37)$$

Equation (37) assumes that the noise decorrelates much more rapidly than the signal and, therefore, the video filter essentially only effects the noise. For the Global Mode, this is the case as will be shown later in this section. For the Intensive Mode, the video filter has little effect upon either the signal or the noise; thus (37) is more in the form of an identity, as will be shown. Also in equation (23), the exponential weighting of the integrating gates will be simplified to a uniform weighting, i.e. for t in $(T,T+\delta)$

$$h_G(T+\delta-t) \approx \frac{1}{\delta} \quad (38)$$

This simplification may be justified by noting that since the autocorrelation functions in (23) decorrelate rather rapidly over the range of integration, i.e. the extent of the gates, the integrations in (23) are insensitive to minor changes in the gate weighting. In other words, the integrals in (23) are much more sensitive to the autocorrelation functions than the form of the integrating gate impulse response. Thus, using the above approximations and the fact that the autocorrelation functions are essentially stationary, equation (23) may be simplified to the following form;

$$\mathrm{Var}(e) = \frac{G^2}{\delta^2}\left\{2\delta\int_0^{\delta}\left[\tilde{R}_v^2(\tau) + 2R_v(\tau)\tilde{R}_n(\tau) + \tilde{R}_n^2(\tau)\right]\left[1-\frac{\tau}{\delta}\right]d\tau\right\} \qquad (39)$$

where τ has replaced t_1-t_2 and

$$\tilde{R}_v^2(\tau) = R_v^2(\tau)\circledast h_v(\tau)\circledast h_v(\tau)$$

$$\tilde{R}_n^2(\tau) = R_n^2(\tau)\circledast h_v(\tau)\circledast h_v(\tau)$$

and

$$\tilde{R}_n(\tau) = \tilde{R}_n(\tau)\circledast h_v(\tau)\circledast h_v(\tau)$$

For the noise terms in (39), the double convolutions may be accomplished either directly or in the spectral domain. The calculations are straightforward but extremely tedious, as noted previously, so only the results will be presented. For the Global Mode,

$$\tilde{R}_n^2(\tau) = K^2\left[0.51\,k\,T_e\,B_{IF}\right]^2\left\{1.1845\,e^{-\alpha_2|\tau|} - 0.171\,e^{-2\alpha_1|\tau|} - 1.518(\alpha_2|\tau|)\,e^{-2\alpha_1|\tau|} + 1.455(\alpha_2|\tau|)^2\,e^{-2\alpha_1|\tau|}\right\} \qquad (40)$$

and

$$\tilde{R}_n(\tau) = 0.618\,K\left[0.51\,k\,T_e\,B_{IF}\right]\left\{1.319\,e^{-\alpha_2|\tau|} - 0.319\,e^{-2\alpha_1|\tau|} - 0.642(\alpha_2|\tau|)\,e^{-2\alpha_1|\tau|}\right\} \qquad (41)$$

where $\alpha_2 = 2\pi B_v$ and $\alpha_1 = 4.88\,B_{IF}$. For the Intensive Mode,

$$\tilde{R}_n^2(\tau) = K^2\left[1.01\,kT_e\,B_{IF}\right]^2 \left\{ 8.535\, e^{-\alpha_2|\tau|} - 7.535\, e^{-2\alpha_1|\tau|} - 2.532(\alpha_1|\tau|)\, e^{-2\alpha_1|\tau|} - 0.395(\alpha_1|\tau|)^2\, e^{-2\alpha_1|\tau|} \right\} \tag{42}$$

and

$$\tilde{R}_n(\tau) = 0.964\,K\left[1.01\,kT_e\,B_{IF}\right] \left\{ 11.296\, e^{-\alpha_2|\tau|} - 10.296\, e^{-2\alpha_1|\tau|} + 2.897(\alpha_1|\tau|)\, e^{-2\alpha_1|\tau|} \right\} \tag{43}$$

The effective receiver noise power at the receiver input, referred to the effective system bandwidth, is equal to $\left[\tilde{R}_n^2(0)\right]^{1/2}/K$.

2.3.4 Comparison of Autocorrelation Coefficients

From equations (29) and (35), the square of the return autocorrelation function may be written in the following form;

$$R_v^2(\tau) = R_v^2(0) \exp\left[-\tau^2/2\sigma^2\right] \tag{44}$$

where, for the Global Mode,

$$R_v^2(0) = K^2(2\pi\sigma_{go}^2)P_{FS}^2(\bar{T}+\frac{\delta}{2}-\bar{\beta})$$

$$\sigma^2 = \sigma_{gl}^2 \tag{45}$$

and for the Intensive Mode,

$$R_v^2(0) = K^2(2\pi\sigma_i^2)P_{FS}^2(\bar{T}+\frac{\delta}{2}-t_o)$$

$$\sigma^2 = 8\sigma_i^2 \tag{46}$$

The impulse response of the single pole RC video filter is

$$h_v(\tau) = \frac{\alpha_2}{2} e^{-\alpha_2|\tau|} \tag{47}$$

The double convolution of (47) with (44) may be accomplished in closed form with the following result;

$$R_v^2(\tau) \circledast h_v(\tau) \circledast h_v(\tau) = R_v^2(0) \frac{(\alpha_2\sigma)^2}{2} \left\{ \frac{1}{2} \sqrt{\frac{\pi}{2\sigma^2}} \left(1/\alpha_2 - \tau - \alpha_2\sigma^2\right) \right.$$

$$\cdot \exp\left(\alpha_2\tau + \alpha_2^2\sigma^2/2\right) \left[1 - \operatorname{erf}\left(\frac{\tau + \alpha_2\sigma^2}{\sqrt{2}\,\sigma}\right)\right]$$

$$+ \frac{1}{2} \sqrt{\frac{\pi}{2\sigma^2}} \left(1/\alpha_2 + \tau - \alpha_2\sigma^2\right) \exp\left(-\alpha_2\tau + \alpha_2^2\sigma^2/2\right)$$

$$\left. \cdot \left[1 + \operatorname{erf}\left(\frac{\tau - \alpha_2\sigma^2}{\sqrt{2}\,\sigma}\right)\right] + \exp\left(-\tau^2/2\sigma^2\right) \right\} \tag{48}$$

Equation (48) may be rewritten in a more simple form;

$$\tilde{R}_v^2(\tau) = \zeta_v R_v^2(0) \tilde{\rho}_v^2(\tau) \tag{49}$$

where for Global Mode $\zeta_v = 0.842$ and for Intensive Mode $\zeta_v = 0.783$ and $\tilde{\rho}_v^2(\tau)$ is normalized to a maximum value of one at $\tau = 0$.

Rewriting the noise and signal autocorrelation functions in (39) in a form similar to (49), the variance of the integrating gate output is given by

$$\text{Var}(e) = \frac{2G^2K^2}{\delta} \left[\frac{R_v^2(0)}{K^2}\right] \int_0^\delta \left\{ \zeta_v \tilde{\rho}_v^2(\tau) + 2\zeta_n \left[\frac{\tilde{R}_n^2(0)}{R_v^2(0)}\right]^{1/2} \rho_v(\tau)\tilde{\rho}_n(\tau) \right.$$

$$\left. + \left[\frac{\tilde{R}_n^2(0)}{R_v^2(0)}\right] \tilde{\rho}_n^2(\tau) \right\} \left[1 - \frac{\tau}{\delta}\right] d\tau \tag{50}$$

where, from equations (41) and (43), $\zeta_n = 0.618$ for the Global Mode and $\zeta_n = 0.964$ for the Intensive Mode. The noise autocorrelation coefficients in (50) are equal to the curly bracketed factors in equations (40) through (43). Figures 8 through 13 compare some of the autocorrelation coefficients in (50) for both before and after filtering. Figure 8 shows, for the Intensive Mode, that the video filter has little effect upon the noise alone and since the signal decorrelates more slowly than the noise, the assumption in (37) is justified. Figure 11 illustrates that for the Global Mode there is a significant difference in the noise and signal decorrelation times. Figure 8 also indicates the degree to which the radar in the Intensive Mode departs from an ideal matched filter, i.e. for matched filter conditions, $\rho_v(\tau) = \rho_n(\tau)$. Of particular note in Figures 8 through 13 is the fact that the video filter has a much more dramatic impact upon the noise than on the signal, especially, in Global Mode.

2.3.5 Definition of Signal-To-Noise Ratio (SNR)

In Equation (50), it is tempting to call the ratio $\tilde{R}_n^2(0)/R_v^2(0)$ the square of the signal-to-noise ratio; however, this point deserves some discussion. First, it must be remembered that $R_v^2(0)$ is not the same for the Plateau and Attitude/Specular gates; that is, the square of the average return power, i.e. $R_v^2(0)$, evaluated at the center of the Plateau gate is certainly different from the average power at the midpoint of the Attitude/Specular gate. This fact is illustrated in Figure 14 which shows how the ratio varies as a function of pointing angle and mode. This figure merely demonstrates the fact that as the pointing angle increases the peak in the average return power occurs later in time due to the increased delay time along the antenna boresight axis to the surface. In fact, as the pointing angle approaches or exceeds one beamwidth, the time at which the maximum occurs is given by

$$t \approx \left(\frac{h}{c}\right) \tan^2 \xi$$

This point raises the interesting question of how the altimeter signal-to-noise ratio should be defined! Usually, the term "signal" is taken to be the peak of the average return power; however, such a definition can be very misleading when considering large pointing angles. For example, when

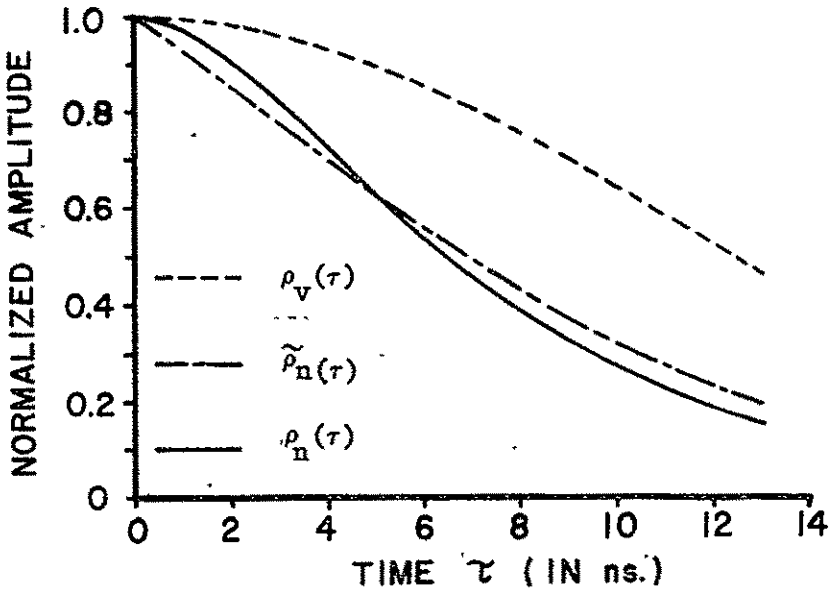

Figure 8. Comparison of the autocorrelation coefficients of the signal (no video filtering) and noise (before and after video filtering) for the Intensive Mode.

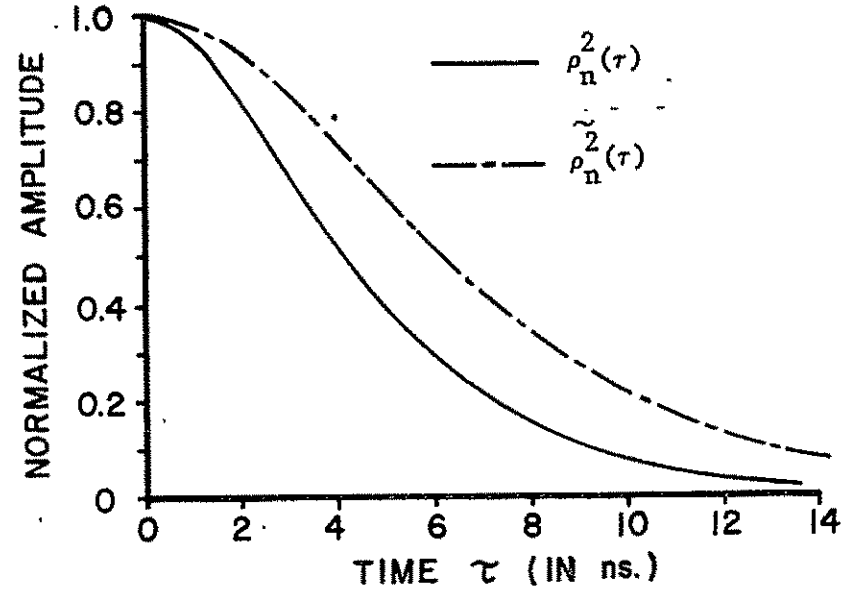

Figure 9. Comparison of the autocorrelation coefficients squared of noise before and after video filtering for the Intensive Mode.

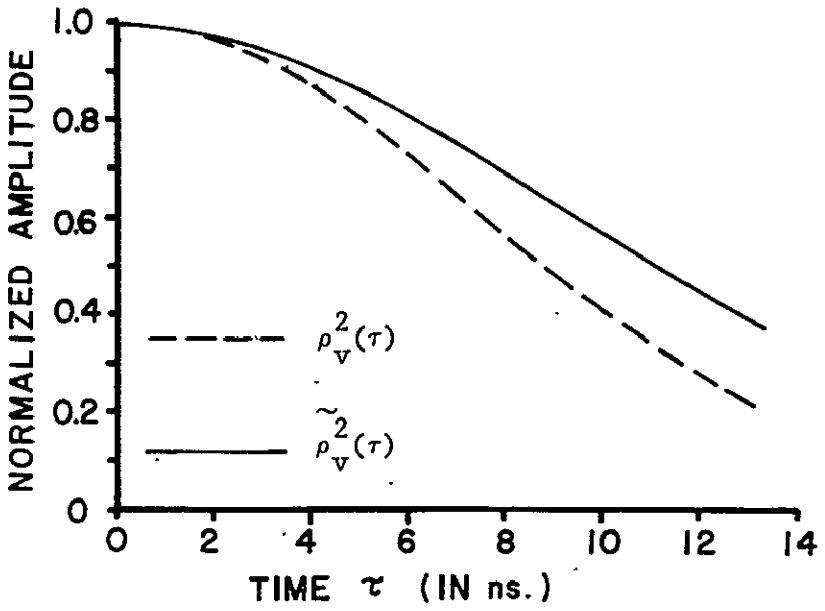

Figure 10. Comparison of the autocorrelation coefficients squared of the signal before and after video filtering for the Intensive Mode.

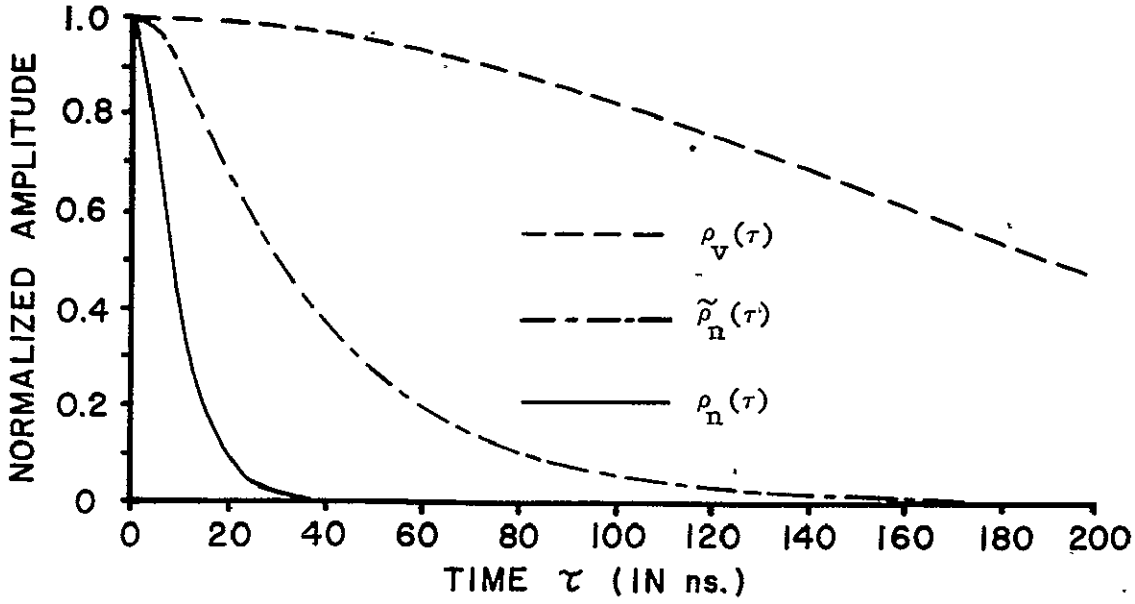

Figure 11. Comparison of the autocorrelation coefficients of the signal (no video filtering) and noise (before and after video filtering) for the Global Mode.

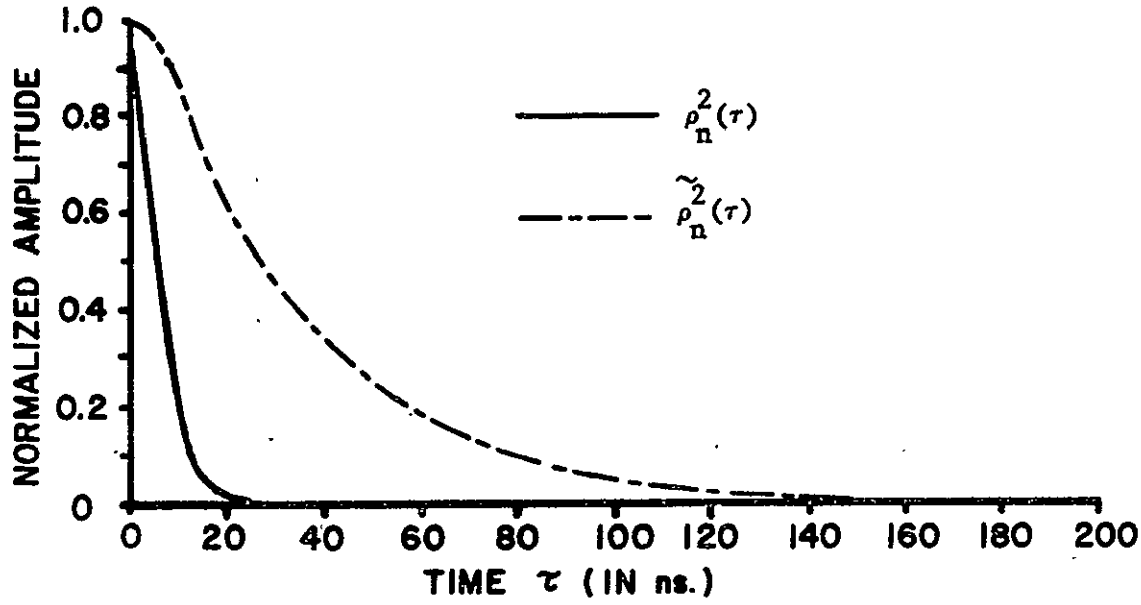

Figure 12. Comparison of the autocorrelation coefficients squared of the noise before and after video filtering for the Global Mode.

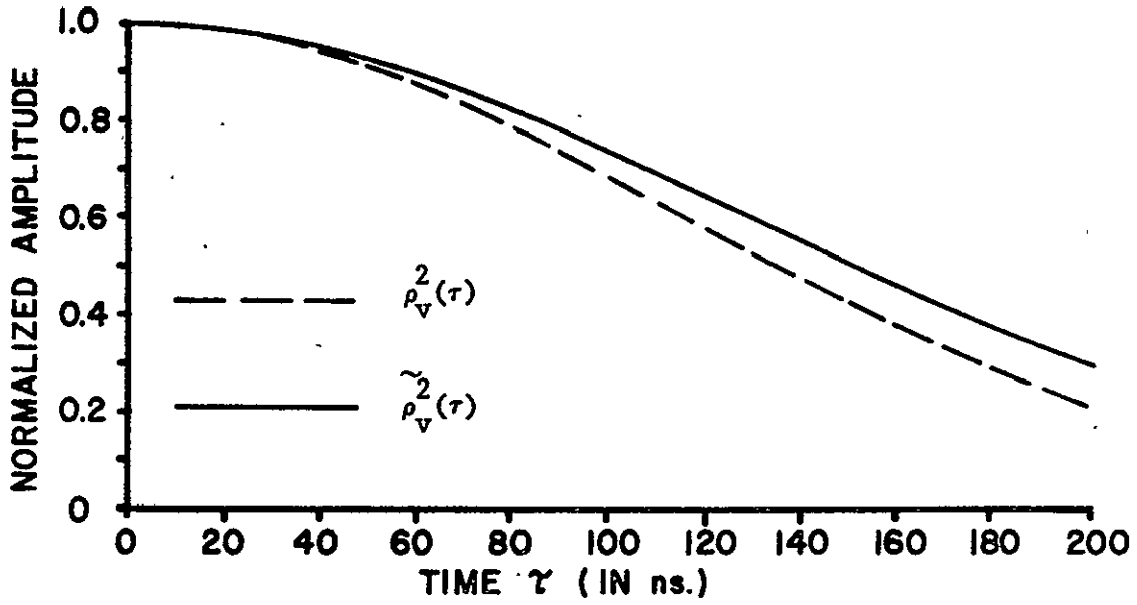

Figure 13. Comparison of the autocorrelation coefficients squared of the signal before and after video filtering for the Global Mode.

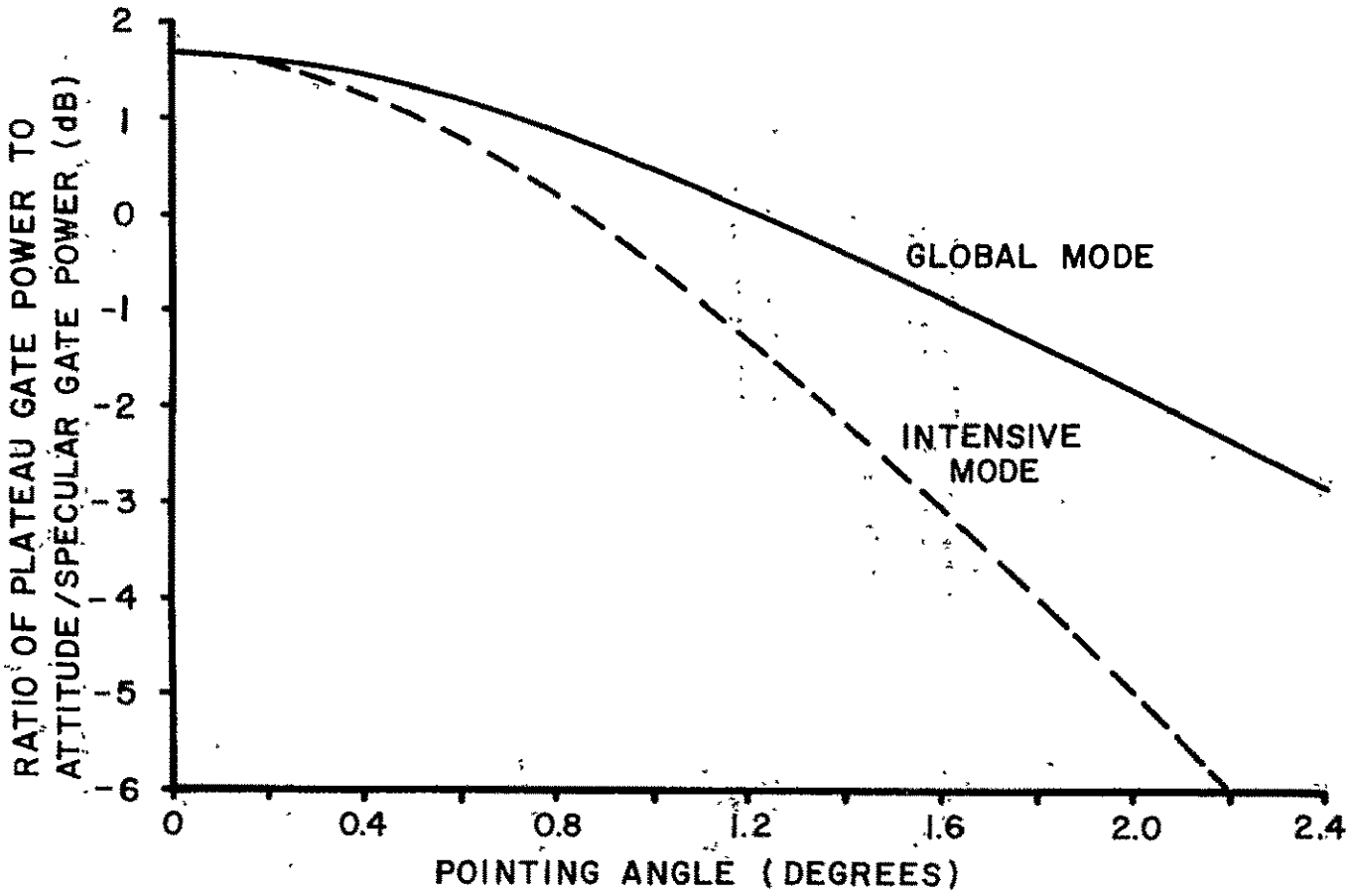

Figure 14. The ratio of the Plateau gate power to the Attitude/Specular

the pointing angle is small, the Plateau gate will measure the peak of the average return power. As the pointing angle increases, the Attitude/Specular gate will measure the peak and, finally, as the angle increases still further neither the Plateau gate nor Attitude/Specular gate will encompass the peak of the average return. In the latter case, the peak return power is not meaningful since it does not tell what the power level is in the vicinity of the tracking gates. Since maintaining track-lock is the most important function of the altimeter, it is the power in the Plateau (and Ramp) gate which is most relevent. For this reason, the term "signal" (as used in signal-to-noise ratio) will be defined as the average return power at the midpoint of the Plateau gate.

2.3.6 The Error for a Ten Second Average

With the above definition in hand, equation (50) should be rewritten as two equations; one for the Plateau gate and one for the Attitude/Specular gate. For the Plateau gate, define $R_{vp}^2(0) = R_v^2(0)$, and, similarly, for the Attitude/Specular gate, define $R_{va}^2(0) = R_v^2(0)$, then with $SNR = \left[R_{vp}^2(0)/R_n^2(0)\right]^{1/2}$, equation (50) can be rewritten for the Plateau and Attitude/Specular gates as follows;

$$\mathrm{Var}(e_p) = \frac{2G_p^2K^2}{\delta}\left[\frac{R_{vp}^2(0)}{K^2}\right]\int_0^{\delta}\left\{\zeta_v\,\tilde{\rho}_v^2(\tau) + \frac{2\zeta_n}{SNR}\,\rho_v(\tau)\,\tilde{\rho}_n(\tau) + \frac{1}{(SNR)^2}\,\tilde{\rho}_n^2(\tau)\right\}\left[1 - \frac{\tau}{\delta}\right]d\tau \tag{51}$$

and

$$\mathrm{Var}(e_{as}) = \frac{2G_{as}^2K^2}{\delta}\left[\frac{R_{va}^2(0)}{K^2}\right]\int_0^{\delta}\left\{\zeta_v\,\tilde{\rho}_v^2(\tau) + \frac{2\zeta_n}{SNR}\left[\frac{R_{vp}^2(0)}{R_{va}^2(0)}\right]^{1/2}\rho_v(\tau)\,\tilde{\rho}_n(\tau) + \frac{\left[\frac{R_{vp}^2(0)}{R_{va}^2(0)}\right]}{(SNR)^2}\,\tilde{\rho}_n^2(\tau)\right\}\left[1 - \frac{\tau}{\delta}\right]d\tau \tag{52}$$

For high SNR ($\gtrsim$ 20 dB), the different power levels in the two gates has no appreciable impact on the variances of the gate outputs. However, for low SNR and large pointing angles the difference in gate power levels tends to suppress the variance of the Attitude/Specular gate output as well it should since the Attitude/Specular gate "sees" the higher power level (see Figure 14).

Equations (51) and (52) determine the variance of the output of the integrating gates. The variance of the output of the one second averager along with the additional ground based averaging (to form a ten second average) is given by

$$\mathrm{Var}(\tilde{\bar{\varepsilon}}_{as}) \approx \frac{\mathrm{Var}(e_{as})}{10M_{as}} \tag{53}$$

and

$$\mathrm{Var}(\tilde{\bar{\varepsilon}}_{p}) \approx \frac{\mathrm{Var}(e_{p})}{10M_{p}} \tag{54}$$

Using the same technique as in Section 2.2 to determine the average estimation function, the variance of the estimation function is found to be as follows;

$$\mathrm{Var}(\Delta) \approx \left[\frac{\tilde{\bar{\varepsilon}}_{as}/G_{as}}{\tilde{\bar{\varepsilon}}_{p}/G_{p}}\right]^2 \left[\frac{\mathrm{Var}(\tilde{\bar{\varepsilon}}_{as})}{(\tilde{\bar{\varepsilon}}_{as})^2} + \frac{\mathrm{Var}(\tilde{\bar{\varepsilon}}_{p})}{(\tilde{\bar{\varepsilon}}_{p})^2}\right] \tag{55}$$

or, equivalently,

$$\mathrm{Var}(\Delta) = \left[\frac{\bar{e}_{as}/G_{as}}{\bar{e}_{p}/G_{p}}\right]^2 \left[\frac{\mathrm{Var}(e_{as})}{10M_{as}(\bar{e}_{as})^2} + \frac{\mathrm{Var}(e_{p})}{10M_{p}(\bar{e}_{p})^2}\right] \tag{56}$$

The average integrating gate output is given by equation (8), however to the same order of approximation used to find the variance of e, (8) can be approximated by the following;

$$\overline{e} \approx G R_v(0) \tag{57}$$

Substituting (51), (52) and (57) in (56) yields a result for the variance of the estimation function which involves three easily performed numerical integrations for each mode.

Using the curves in Figure 6, the variance estimates for Δ can be translated into variance estimates for the pointing angle ξ for a ten second average. Figure 15 shows the error as a function of pointing angle and SNR while Figure 16 shows similar results for the Intensive Mode. In comparing these two results, it is very interesting to note that although the Global Mode Plateau gate averages sixteen times as many returns per unit time as does the Intensive Mode, the resultant error for the two modes and high SNR are comparable. This is due to the fact that the estimation function curve for the Intensive Mode has a much greater slope than the Global Mode (see Figure 8). These curves clearly show that this technique for estimating the radar altimeter pointing angle is a most powerful approach.

2.4 Other Error Sources

The previous section has been concerned with the errors which are due to the random nature of the backscattered return and the influence of noise. In addition, there are two other sources which can significantly contribute to an erroneous estimate of the pointing angle.

2.4.1 σ° Variation With Angle of Incidence

The first of these other error sources involves the angular behavior of σ° for very near normal incidence. Throughout the previous analysis it has been implicitly assumed that σ° is constant over the range from zero degrees to the equivalent angle of the Plateau and Attitude/Specular gates. That is, in the equation for the flat surface impulse response, i.e. equation (10), $\sigma^\circ(\psi_o)$ has been assumed to be constant. Table III shows the relative time of occurrence of the midpoints of the gates and the corresponding angles of incidence on the mean flat surface. Since the greatest angle is about one degree, the above assumption on σ° is certainly not unreasonable. Previous radar altimeter measurements of a σ° [7, Chapter 8] indicate that

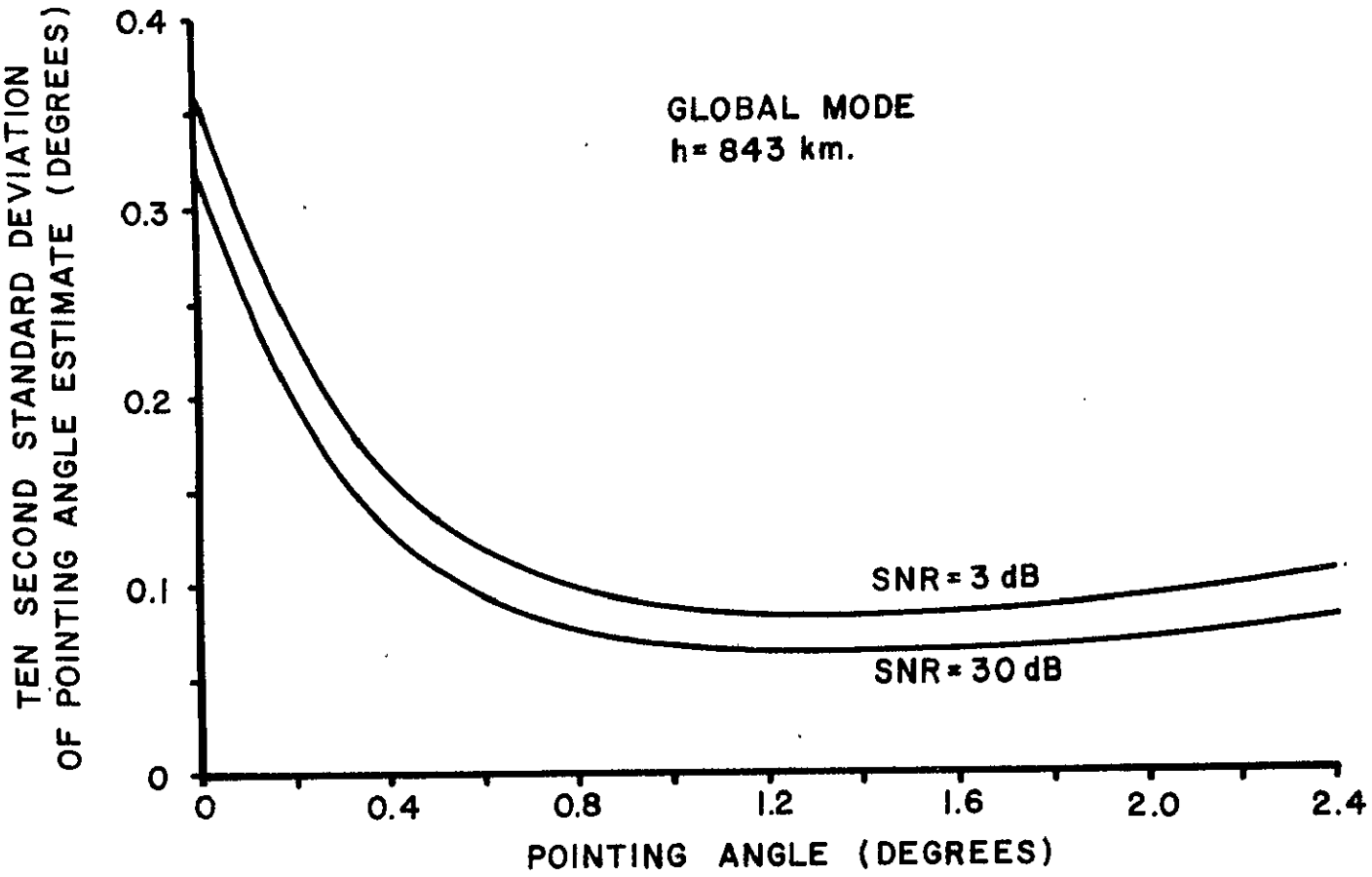

Figure 15. The precision of the pointing angle estimation technique for Global Mode.

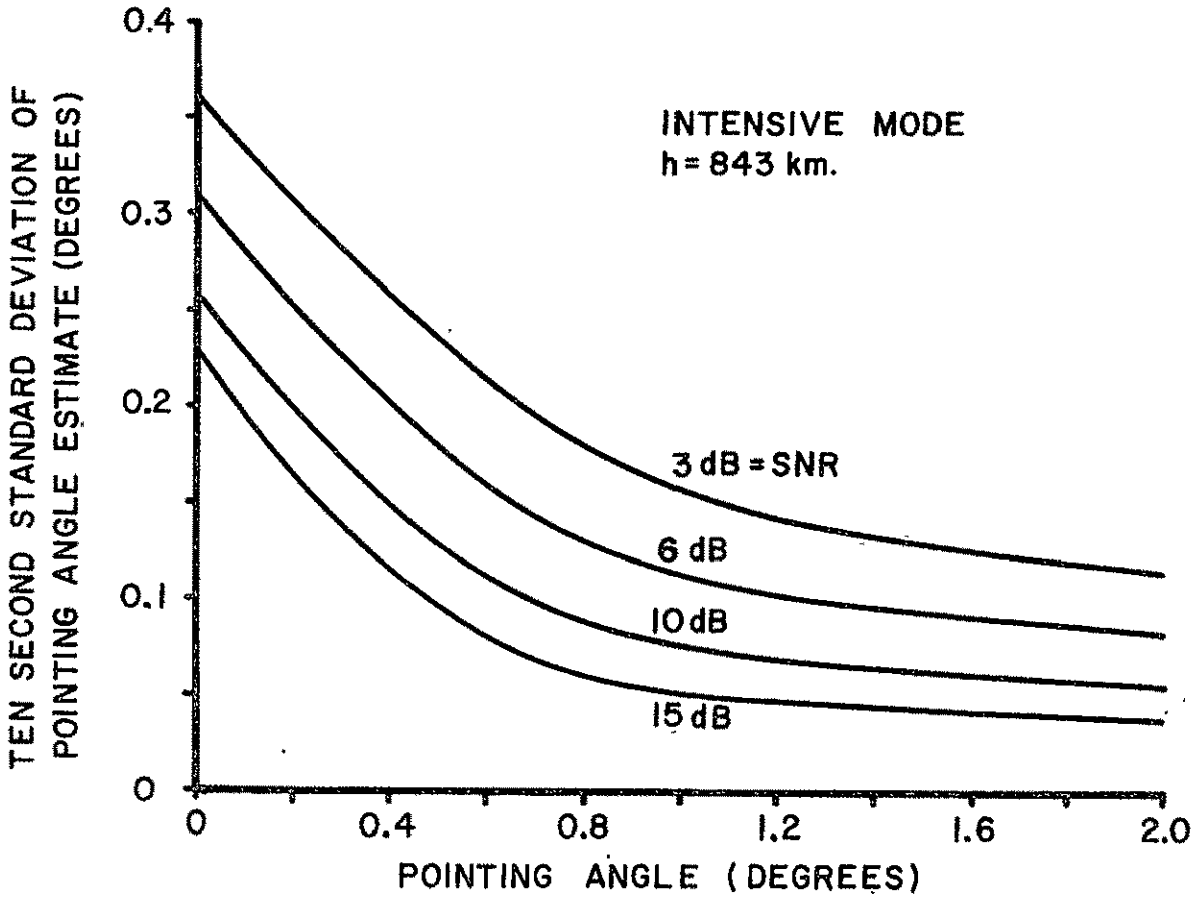

Figure 16. The precision of the pointing angle estimation technique for Intensive Mode.

TABLE III

The Angle of Incidence Corresponding to the Midpoints of the Plateau and Attitude/Specular Gates

	INTENSIVE MODE		GLOBAL MODE	
	Plateau Gate	Attitude/ Specular Gate	Plateau Gate	Attitude/ Specular Gate
Mid Point Relative Time (ns)	68.75	800	400	800
Corresponding Angle of Incidence (deg)	0.28	0.97	0.68	0.97

for the most ocean surface conditions, the assumption of a constant σ°, out to about one degree, is valid. Scattering data obtained by GEOS-3 have indicated that there are, however, cases where this assumption is violated. Such situations have been shown to occur when the surface has a very small mean square slope [7, Chapter 9]. Since a small mean square slope generally implies a lack of high frequency components in the surface height spectrum, ocean surfaces giving rise to this type scattering are possibly either void of any significant wind field or are covered by a more viscous material such as oil.

If σ° decreases over the equivalent angle of incidence range represented by the integrating gates, this can lead to an underestimate of the pointing angle. That is, if σ° decreases with angle of incidence, the trailing edge of the average return will decay faster than if σ° were constant. This increased decay, however, could very well be interpreted as a smaller pointing angle error. Of course, when the roll-off of σ° with angle of incidence is sufficiently rapid as to produce a return whose trailing edge is below the nadir return (for σ° assumed constant), the computed estimation function will exceed the maximum possible value given in Figure 6. This situation has been observed in the GEOS-3 data and is easily spotted

because the received power level increases significantly and the altitude data noise level decreases. The more troublesome case where σ° roll-off can result in an erroneous but nonzero estimate of the pointing angle can be spotted by observing the change in the trend of the pointing angle data. That is, for such cases, there will be a distinct change in the behavior of the pointing angle estimates which is not consistent with spacecraft dynamics. It should be noted that the estimation technique is generally not applicable over terrain due to the inhomogeneous nature of the scattering surface. In conclusion, a rapid roll-off of σ° with angle of incidence does not invalidate the technique but it does result in the possibility of erroneous estimates; however, suspicious data can be checked by methods discussed above.

2.4.2 Altimeter Calibration

All portions of the radar receiver modeled in this analysis are analog, see Figure 3, and are therefore subject to thermal and ageing effects. Since spacecraft power was not available to maintain a constant thermal environment, extensive thermal/vacuum testing and calibration of the altimeter were accomplished[6]. Because of launch constraints, this calibration was not quite as extensive as would have been desired under a less severe schedule. In regard to calibration of the Plateau and Attitude/Specular gate outputs, two problems have come to light since launch.

The first of these two problems comprised inadequate thermal/vacuum calibration of the Global Mode Plateau Gate. For this gate, input/output calibrations were accomplished only at room ambient temperature and pressure. As a consequence, the data correction processing performed by the Wallops Flight Center essentially accomplishes a single point thermal correction for the output of the Global Mode Plateau gate. A cursory examination of the temperature dependent calibration data in [6] for the Attitude/-Specular and Noise gates* clearly indicates that thermal effects are certainly not negligible. Unfortunately, there is no obvious means for overcoming this problem short of conducting special inflight tests in which the

*The 200 ns Attitude/Specular and Noise gates are common to both the Intensive and Global Modes and both were calibrated more extensively during Intensive Mode testing.

altimeter is switched back and forth between the Intensive and Global Modes. Assuming that the Intensive Mode is operating within its thermal calibration range, it should provide temperature independent estimates of the pointing angle. By comparing pointing angle estimates obtained from both modes, it may be possible to generate a pointing angle correction curve for the Global Mode. Such testing is recommended when operational considerations permit such a configuration of the altimeter.

As a sample of what effect inadequate calibration of the Global Mode Plateau gate can have, let the thermal environment be such that the effective gain (from detector output to one second averager output) changes by 5% from its preflight value. The average estimation function is given by (21), i.e.

$$\overline{\Delta} = 1 - \frac{\overline{e}_{as}/\hat{G}_{as}}{\overline{e}_{p}/\hat{G}_{p}} \tag{55}$$

where $\hat{G}_{as}$ and $\hat{G}_{p}$ are the gains obtained from preflight testing. However, according to (8) the average gate outputs may be written as

$$\overline{e}_{as} = G_{as} f_{as}$$

and

$$\overline{e}_{p} = G_{p} f_{p}$$

where G_{as} and G_{p} are the actual gains at the operating temperature of the tracking gates. Taking the differential of (55) with $G_{as} = \hat{G}_{as}$, i.e. no error for the Attitude/Specular gate, the change in the average estimation function corresponding to a change in G_{p} is given by

$$d\overline{\Delta} = (1 - \overline{\Delta}) \left(\frac{dG_{p}}{G_{p}} \right) \tag{56}$$

where if $G_{p} = \hat{G}_{p}$ the $dG_{p} = 0$. It should be noted from (56) that if G_{p} is larger than $\hat{G}_{p}$ then the change in $\overline{\Delta}$ is positive and the pointing angle estimate will be low, i.e. too small. Conversely, for a decrease in gain, the pointing angle estimate will be too large. Figure 17 illustrates the

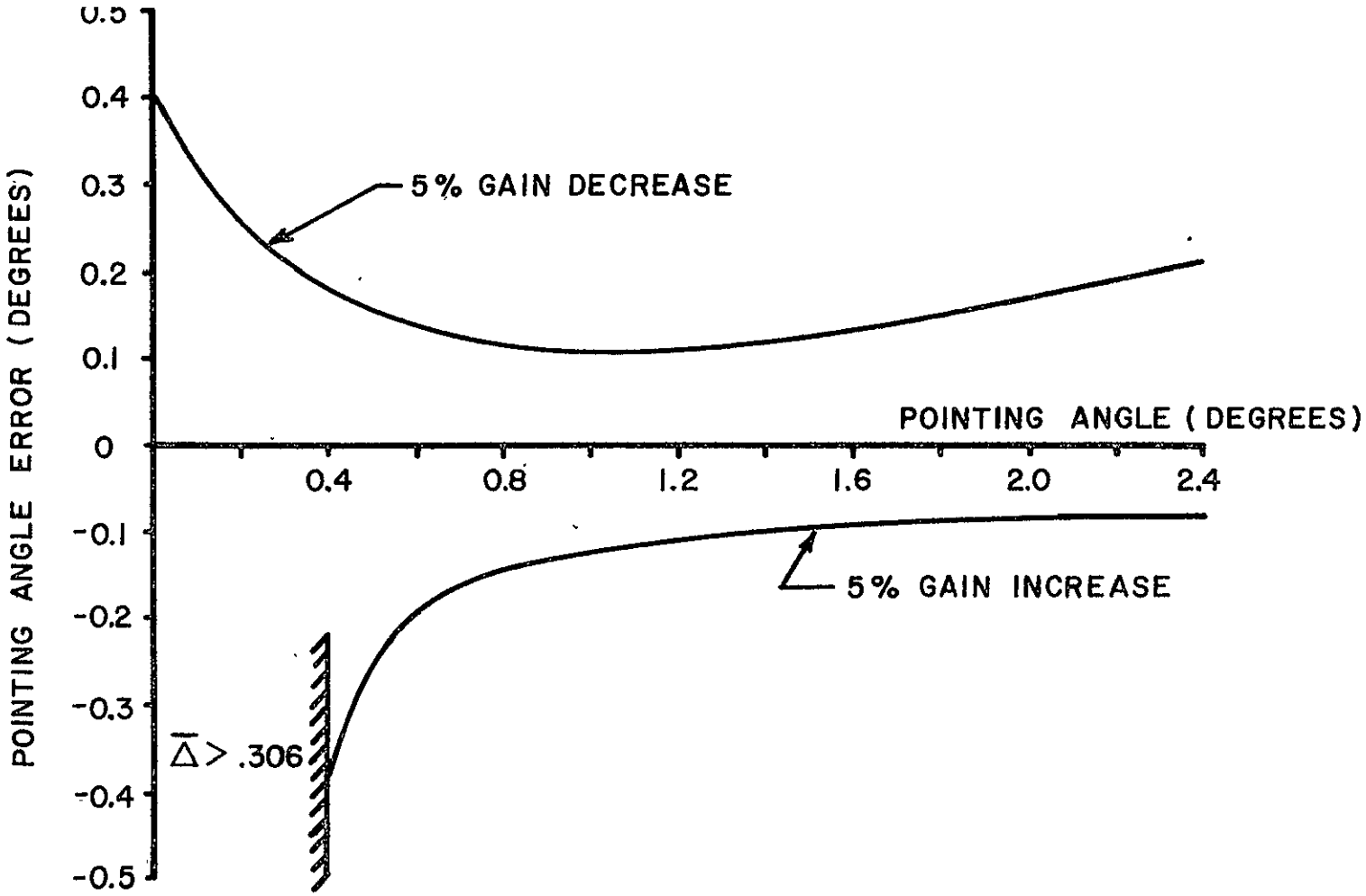

Figure 17. Pointing angle bias error for a 5% change in Plateau Gate gain for Global Mode.

pointing error resulting from a constant 5% change in the gain of the Global Mode Plateau gate.* If the gain increases by 5%, the computed estimation function will be greater than its maximum possible value of 0.306 for $\xi < 0.4°$, and no estimate of the pointing error is possible. For either an increase or a decrease in the gain, the error in the computed pointing angle is always greatest near $\xi = 0°$. Figure 18 is a plot of estimated versus true pointing angle for the 5% gain change.

A preliminary comparison of Global Mode pointing angle estimates with spacecraft derived attitude data from [2] indicates that thermal calibration may be a problem. That is, a plot of the radar estimated pointing angle versus the spacecraft sensor estimated angle is very similar in form to the upper curve in Figure 18. The mean error in the vicinity of zero pointing angle is higher, i.e. on the order of 0.7°. This would imply a gain increase of about 15%; however, the problem requires much further study. In particular, the data will be grouped by temperature to determine if, in fact, the temperature is a meaningful parameter in terms of data repeatability. In any case, there is a strong indication in the Global Mode pointing angle data reduced so far that inadequate gate calibration may be a major source of error.

The second calibration problem is similar to the first but it involves the Intensive Mode and is not as severe as the first in regard to its impact. During the very early operation of the Intensive Mode, the altimeter tended to run somewhat colder than was expected. Consequently, data were obtained at temperatures which were below the preflight calibration range and, thus, were only approximately corrected. Fortunately this problem will probably only result in the loss of some very early data since the operating temperature has increased back into the calibration range. Furthermore, since it is known when the data are outside of calibration range, i.e. by comparing the operating temperature with temperatures during calibration, one knows exactly when to suspect the data. Preliminary comparisons of Intensive Mode pointing angle estimates with spacecraft sensor derived attitude data indicates a much closer agreement than in the case of the Global Mode.

---

*The pointing angle error is defined as the difference between the true angle (computed from $\overline{\Delta}$) and the incorrect angle (computed from $\overline{\Delta} + d\overline{\Delta}$).

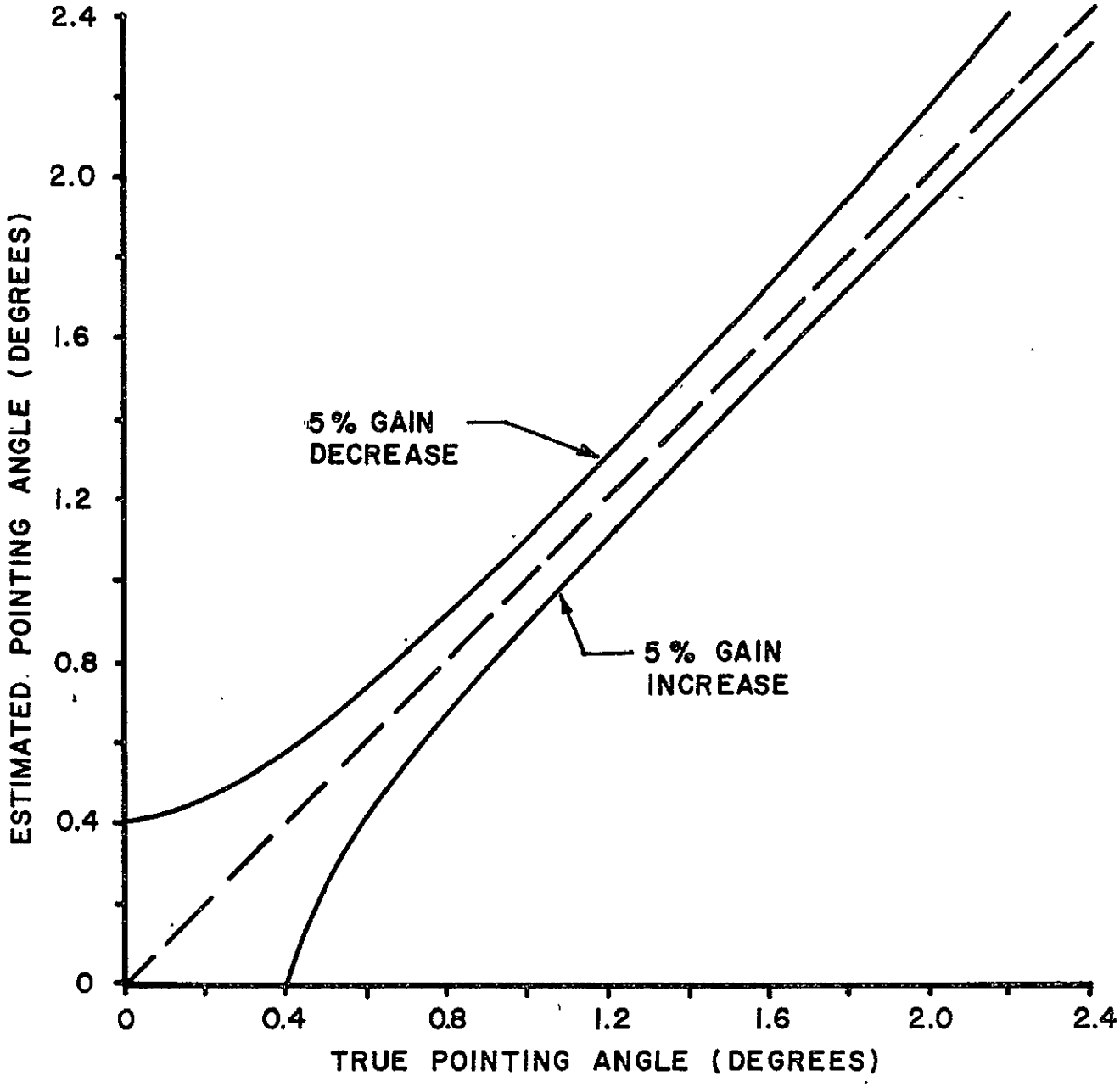

Figure 18. Estimated versus true pointing angle for a 5% change in Plateau gate gain in Global Mode.

3.0 THE IMPACT OF POINTING ERROR

The previous sections of this report have presented a technique for computing the radar antenna pointing angle and have estimated the accuracy and precision of the method. Given the fact that problems associated with inadequate calibration can be minimized, as per the discussion in the previous section, the method has the potential of providing very accurate pointing data. The need for such pointing estimates, for this mission, rests solely upon its potential to increase the accuracy of the primary altimeter data such as altitude, surface scattering cross section and waveheight estimates. Since the GEOS-3 altimeter antenna beamwidth is relatively large, the need for pointing angle correction is not as great as in the case of, say, Skylab [7]. However, this does not imply that it is a negligible effect; the corrections for pointing angle effects depend entirely upon the attitude excursions encountered during inflight operation of the altimeter. This section will consider the effects of pointing errors upon the following quantities; the normalized surface scattering cross section or σ°, the altitude data, and estimates of the ocean surface waveheight.

3.1 σ° Estimation

For the Global Mode, the average return power at the output of the radar antenna is given by

$$\bar{P}_r(t) = \frac{P_T G_o^2 \lambda^2 c}{4(4\pi)^2 L_r L_p h^3} \exp\left(-\frac{4}{\gamma}\sin^2\xi\right) \int_0^\infty P_\tau(t-t')\sigma^\circ(\psi') \cdot \exp\left[-\frac{4c}{\gamma h} t' \cos 2\xi\right] I_o\left(\frac{4}{\gamma}\sqrt{\frac{ct'}{h}}\sin 2\xi\right) dt' \qquad (57)$$

where $P_\tau(\cdot)$ is the transmitted waveform and

$$\tan\psi = \left[ct'/h\right]^{1/2} \qquad (58)$$

Since $\bar{P}_r(t)$ is a function of relative delay time, the question arises as to exactly where (in t) the measurement is made. Since the AGC control voltage, during tracking, is a filtered version of the Plateau gate output [6],

the received power measurement $\langle \overline{P}_r \rangle$ will be given by the following;

$$\langle \overline{P}_r(t) \rangle = \frac{\int_{300}^{500} \overline{P}_r(t) \exp\left[(500-t)/800\right] dt}{\int_{300}^{500} \exp\left[(500-t)/800\right] dt} \tag{59}$$

where time has the units of nanoseconds (see Figure 2).
That is, the actual power measurement is taken to be an exponentially weighted average of the received power over the Plateau gate. Assuming that $\sigma^\circ(\psi')$ is reasonably constant over the equivalent angular width of $P_\tau(t)$, it may be removed from inside the integral in (57), i.e.

$$\overline{P}_r(t) \approx \frac{P_T G_o^2 \lambda^2 c \sigma^\circ(\psi_o)}{4(4\pi)^2 L_r L_p h^3} \exp\left(-\frac{4}{\gamma}\sin^2\xi\right) \int_0^\infty P_\tau(t-t') \exp\left[-\frac{4c}{\gamma h} t' \cos 2\xi\right]$$

$$\cdot I_o\left(\frac{4}{\gamma}\sqrt{\frac{ct'}{h}}\sin 2\xi\right) dt' \tag{60}$$

where $\tan\psi_o = \left[ct/h\right]^{1/2}$. Rewriting (60) in the following form;

$$\overline{P}_r(t) \approx P_T\left[\frac{\sigma^\circ(\overline{\psi}_o)}{L_p}\right] F_G(t,\xi) \tag{61}$$

the average received power is given by

$$\langle \overline{P}_r(t) \rangle \approx P_T\left[\frac{\sigma^\circ(\overline{\psi}_o)}{L_p}\right] \frac{\int_{300}^{500} F_G(t,\xi) \exp\left[(500-t)/800\right] dt}{\int_{300}^{500} \exp\left[(500-t)/800\right] dt} \tag{62}$$

where $\overline{\psi}_o$ corresponds approximately to the midpoint of the Plateau gate, i.e.

$\bar{\psi}_o \approx 0.68°$. Since $\langle \bar{P}_r(t) \rangle$ and P_T are measured and $\sigma^\circ(\bar{\psi}_o)$ is to be computed, a plot of the ratio

$$\frac{\langle \bar{P}_r(t) \rangle}{P_T \left[\frac{\sigma^\circ(\bar{\psi}_o)}{L_p} \right]}$$

is convenient because it presents $\left[\sigma^\circ(\bar{\psi}_o)/L_p\right]$ as a function of received power, transmitted power and pointing angle. Figure 19 illustrates how the ratio depends upon pointing angle and may be used in conjunction with measurements of $\langle \bar{P}_r(t) \rangle$ and P_T to determine $\left[\sigma^\circ(\bar{\psi}_o)/L_p\right]$. The curves in Figure 19 were generated using the following parameters obtained from [6];

$$G_o = 36.5 \text{ dB}$$
$$\lambda = 0.02158 \text{ m}$$
$$c = 0.3 \text{ m/ns}$$
$$L_r = 0.8 \text{ dB}$$
$$h = 843 \text{ km}$$
$$\gamma = 1.49 \times 10^{-3} \text{ (2.4° antenna beamwidth)}$$

It should be noted that the results for the Global Mode in Figure 19 should not be used when there is an indication that $\sigma^\circ(\psi)$ may be changing rapidly with incidence angle.

For the Intensive Mode, the development follows that given for the Global Mode with exception that the waveform, $P_T(\cdot)$, requires more careful definition. The actual transmitted waveform comprises a 1.2 μs pulse whose carrier frequency is linearly swept at a fixed rate. The post-IF portion of the radar receiver operates on a compressed or deramped version of the expanded average return. Thus at first glance and as far as the measurement of σ° is concerned, it would appear that $P_T(\cdot)$ in (57) could be replaced by the ideal post compression waveform. With the exception of time sidelobes, this statement is true! That is, after compression in the receiver, the actual predetection point target response has, essentially, no time sidelobes, see Figure 4. Thus, for an extended target, the normal build-up of power due to integrated time sidelobes does not occur and the

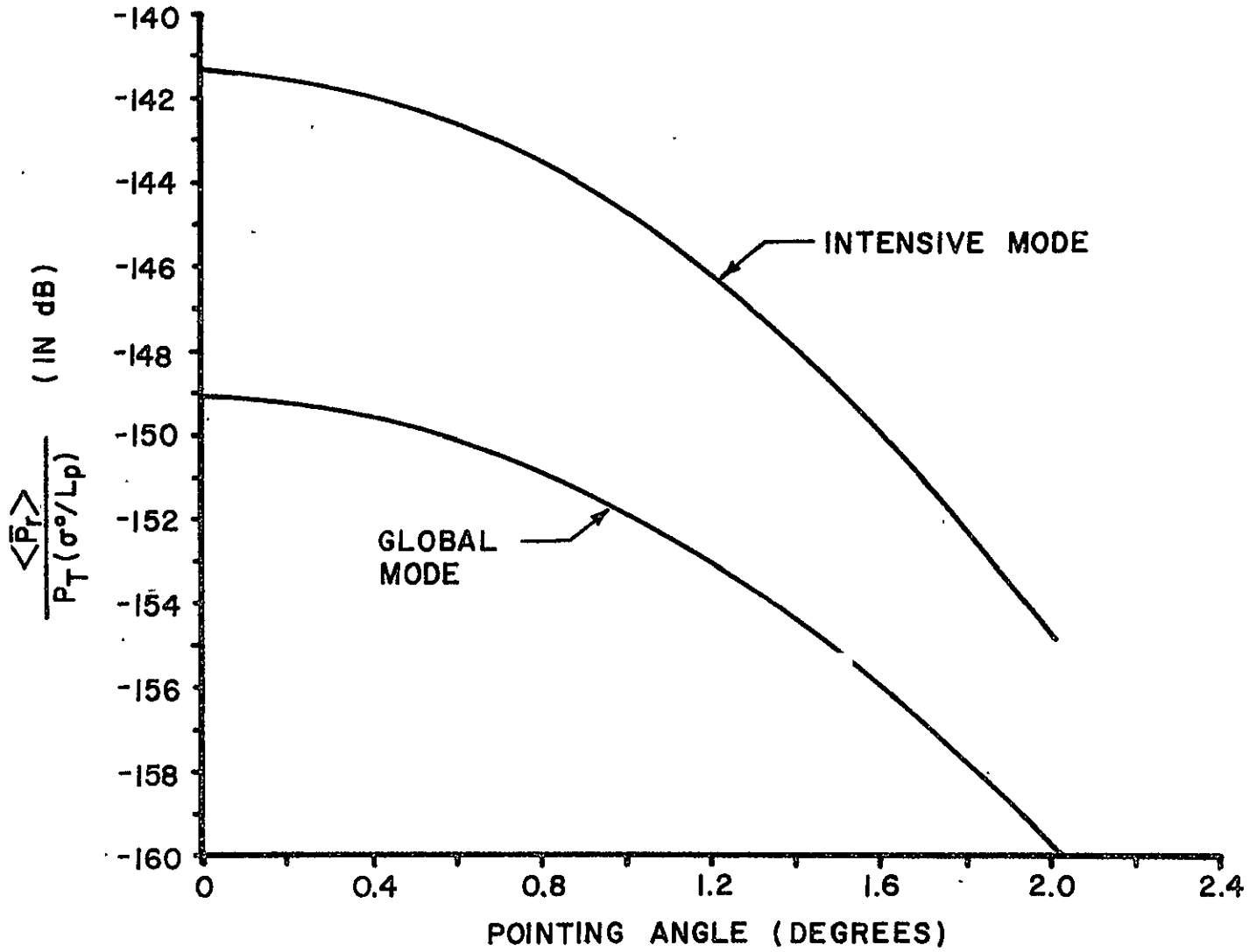

Figure 19. Variation of normalized received power with pointing angle for both the Global and Intensive Modes.

Plateau gate responds only to the integrated mainlobe of the point target response. Since the Plateau gate provides the AGC control voltage, from which the received power is inferred, the time sidelobes should be ignored. Therefore, for the Intensive Mode, $P_T(t-t')$ in (57) can, equivalently, be replaced by $100 \cdot P_{IF}(t-t')$ where 100 is the ideal compression gain* and $P_{IF}(t-t')$ is the IF point target response. This approach is different from the scheme used to calibrate the AGC but is entirely equivalent** to it, see [6].

With

$$F_I(t,\xi) = \frac{G_o^2 \lambda^2 c(100)}{4(4\pi)^2 L_r h^3} \exp\left(-\frac{4}{\gamma}\sin^2\xi\right) \int_0^\infty P_{IF}(t-t') \exp\left[-\frac{4c}{\gamma h} t' \cos 2\xi\right] \cdot I_o\left(\frac{4}{\gamma}\sqrt{\frac{ct'}{h}}\sin 2\xi\right) dt' \tag{63}$$

the mean return power, time-averaged over the Plateau gate, is given by the following;

$$\langle \bar{P}_r(t) \rangle \approx P_T\left[\frac{\sigma^\circ(\bar{\psi}_o)}{L_p}\right] \frac{\int_{62.5}^{75} F_I(t,\xi) \exp\left[(75-t)/50\right] dt}{\int_{62.5}^{75} \exp\left[(75-t)/50\right] dt} \tag{64}$$

where $\bar{\psi}_o$ is approximately equal to 0.28°. Figure 19 shows how the ratio

$$\frac{\langle \bar{P}_r(t) \rangle}{P_T\left[\frac{\sigma^\circ(\bar{\psi}_o)}{L_p}\right]}$$

varies with pointing angle for the Intensive Mode:

---

*The AGC calibration accounts for any differences between ideal and actual compression gain.

**The difference occurs because ideal pulse compression devices do not physically exist.

The curves in Figure 19 essentially illustrate the degree of correction that is necessary to account for the effect of pointing error in computing σ° from the received power data. If the pointing error is less than 0.8°, the maximum correction for the Global Mode is 1.75 dB while for the Intensive Mode it is 2.14 dB.

3.2 Global Mode Altitude Bias

The GEOS-3 altimeter employs a so-called split gate tracker to locate and follow the backscattered return. For such a tracker, the time of occurrence of the Ramp and Plateau integrating gates is constantly adjusted until, on the average, the following tracking law is satisfied;

$$2\bar{e}_r - \bar{e}_p = 0 \tag{65}$$

As shown in Figure 2, for an idealized return with a linear rise equal to δ and the gate widths also equal to δ and no pointing error, the leading edge of the Ramp gate will occur $2h/c$ seconds after detection of the transmitted pulse. As the pointing angle increases, the trailing edge of the return departs from its ideal behavior which causes $\bar{e}_p$ to change and the tracking point must also change. Thus, the leading edge of the ramp gate no longer occurs at $2h/c$, and the altitude estimate provided by the altimeter is biased. A bias will also result if the Ramp gate is not matched to the rise time portion of the average return waveform.

Figure 20 shows that the altitude bias for Intensive Mode is not a very sensitive function of pointing angle. This results from the fact that the Ramp gate width (12.5 ns) is very well matched to the average return rise time and the Plateau gate is reasonably insensitive to pointing errors. For the Global Mode, the situation is considerably different. Figure 21 illustrates the normalized video return presented to the tracking gates during the Global Mode for nadir pointing. Of particular note is the rather long rise time of the leading edge which is due, in great part, to the long trailing edge of the video point target response (see Figure 5). The nominal midpoint of the Plateau gate for an idealized return ($\sim$400 ns) occurs when there is a rather significant droop in the trailing edge of the return. Therefore, it is obvious that the Global Mode

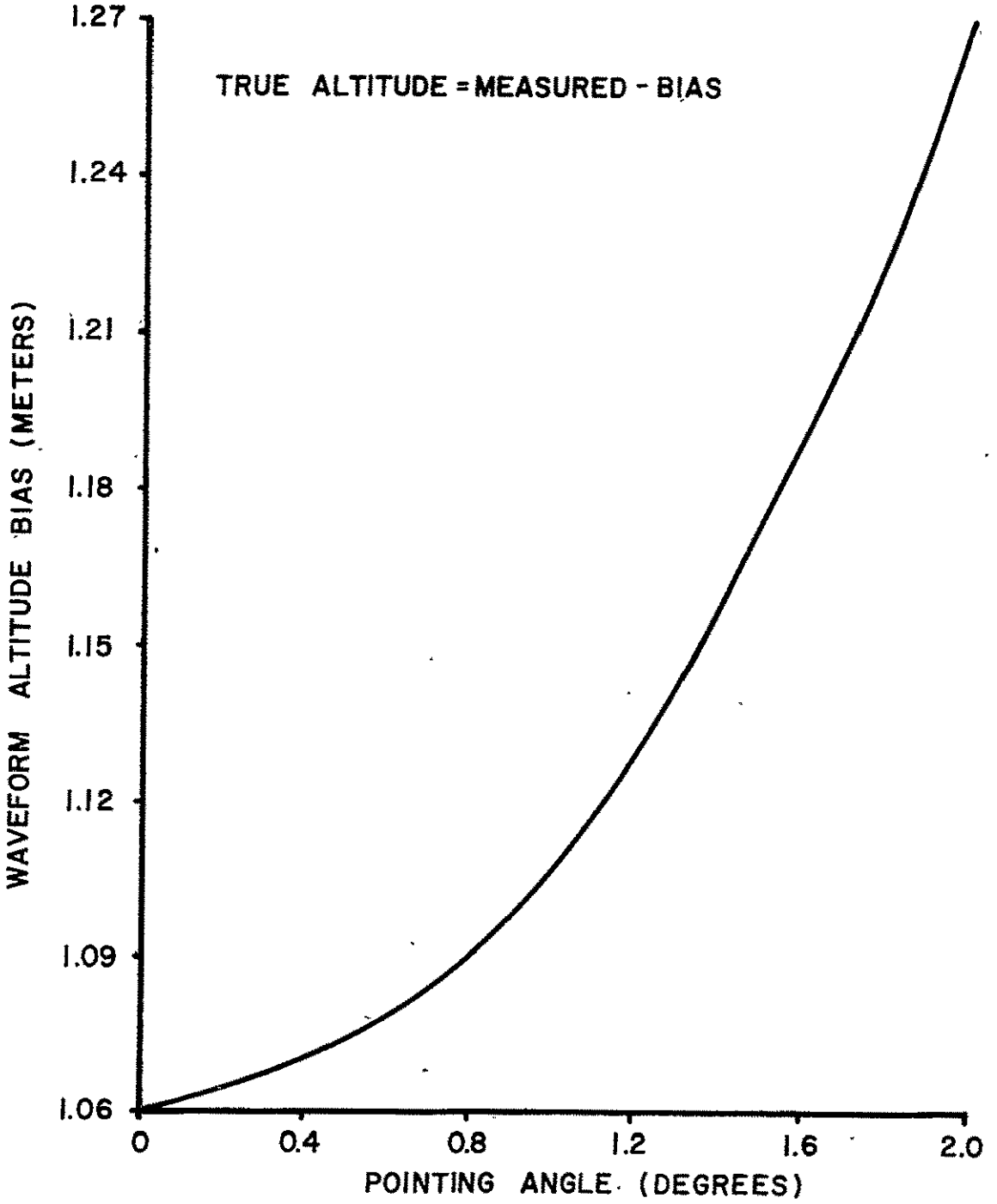

Figure 20. Intensive Mode waveform induced bias as a function of pointing angle (for $H_{1/3} \leq 0.5$ m).

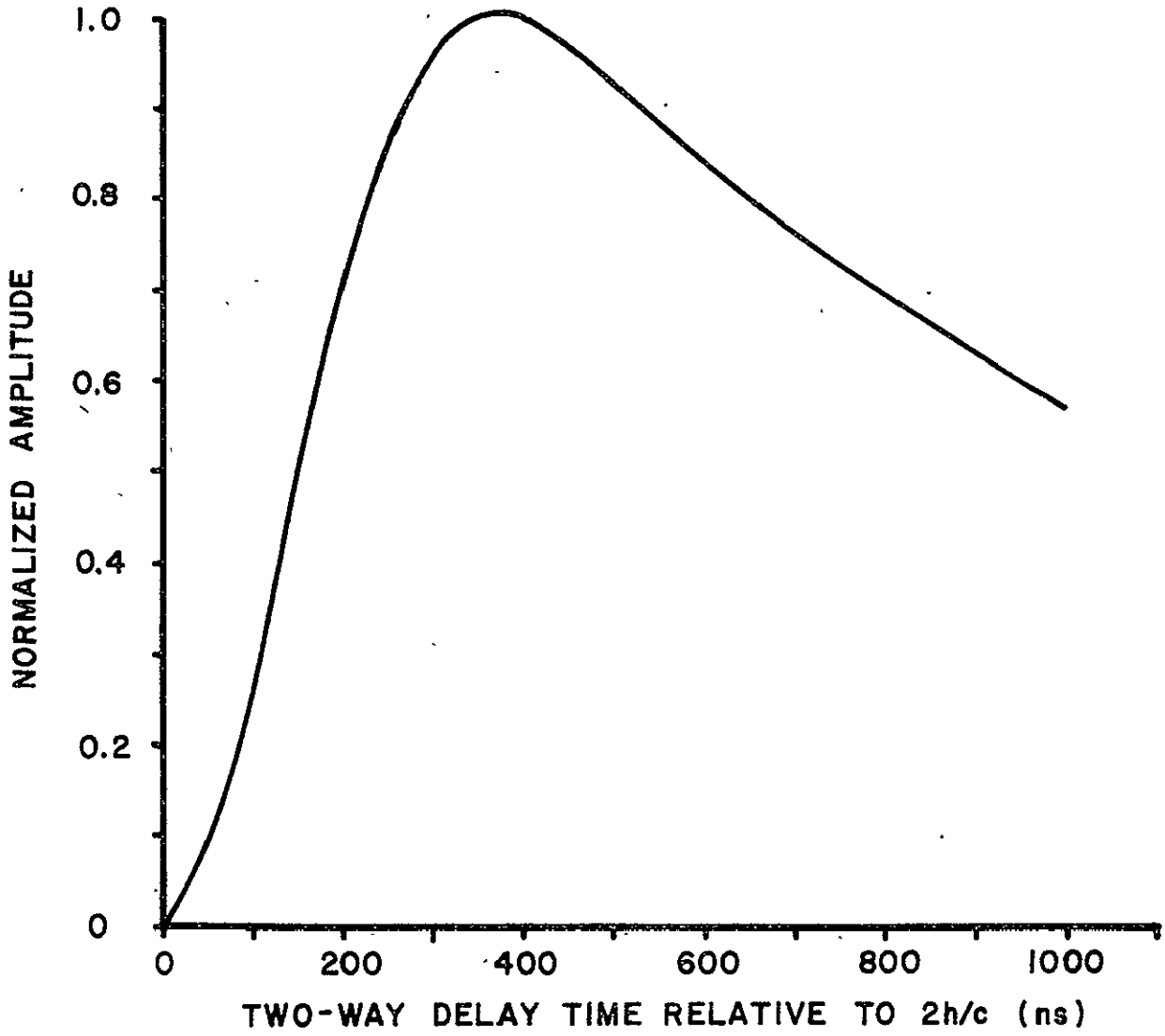

Figure 21. The normalized video average return voltage for the Global Mode and nadir pointing, i.e. $\xi = 0°$.

bias will be significantly different from the Intensive Mode.

Figure 22 shows the altitude bias as a function of pointing angle for the Global Mode. According to the definition of bias as given in the figure, the altimeter will always produce an altitude measurement which is too large, i.e. relative to 2h/c. Although not noted explicitly in the derivation of the estimation function and its variance, this shift in the location of the gates was properly accounted for in the actual computations. The results in Figure 22 clearly show that bias for the Global Mode is not negligible. It should be noted that the bias results presented in Figure 22 are only for the waveform and pointing induced effects; Reference [6, page 203] presents other bias factors which result from the GEOS-3 design. Reference 6 has also computed the waveform induced bias at nadir and obtains a value of 4.95 m as opposed to the 6.15 m shown in Figure 22. The difference is attributed to a slighly different result for the video average return waveform, i.e. compare Figure 20 with Figure 85 (page 205) of Reference 6.

3.3 Waveheight Estimation

According to the theory of linear random surface scattering, surface roughness tends to increase the rise time of the average return because of the range distributed nature of the specular points on the surface. To avoid the mathematical horrors associated with numerical deconvolution, one is usually content with measuring the increased rise time of the return and then translating this into an equivalent rms surface height via some straightforward model. The model normally requires an accurate computation of the so-called flat surface response, i.e the rms surface height is very small relative to the range extent of the video point target response. Fortunately, in the case of GEOS-3, the effect of pointing error upon the rise time extent of the flat surface response is negligible until the pointing angle approaches 1.2° (one half a beamwidth). For this reason, pointing errors can usually be ignored in waveheight estimation. However, if the pointing error does approach 1.2°, it should be properly accounted for or it will give rise to an overestimate of the surface waveheight. That is, pointing error tends to increase the rise time of flat surface return.

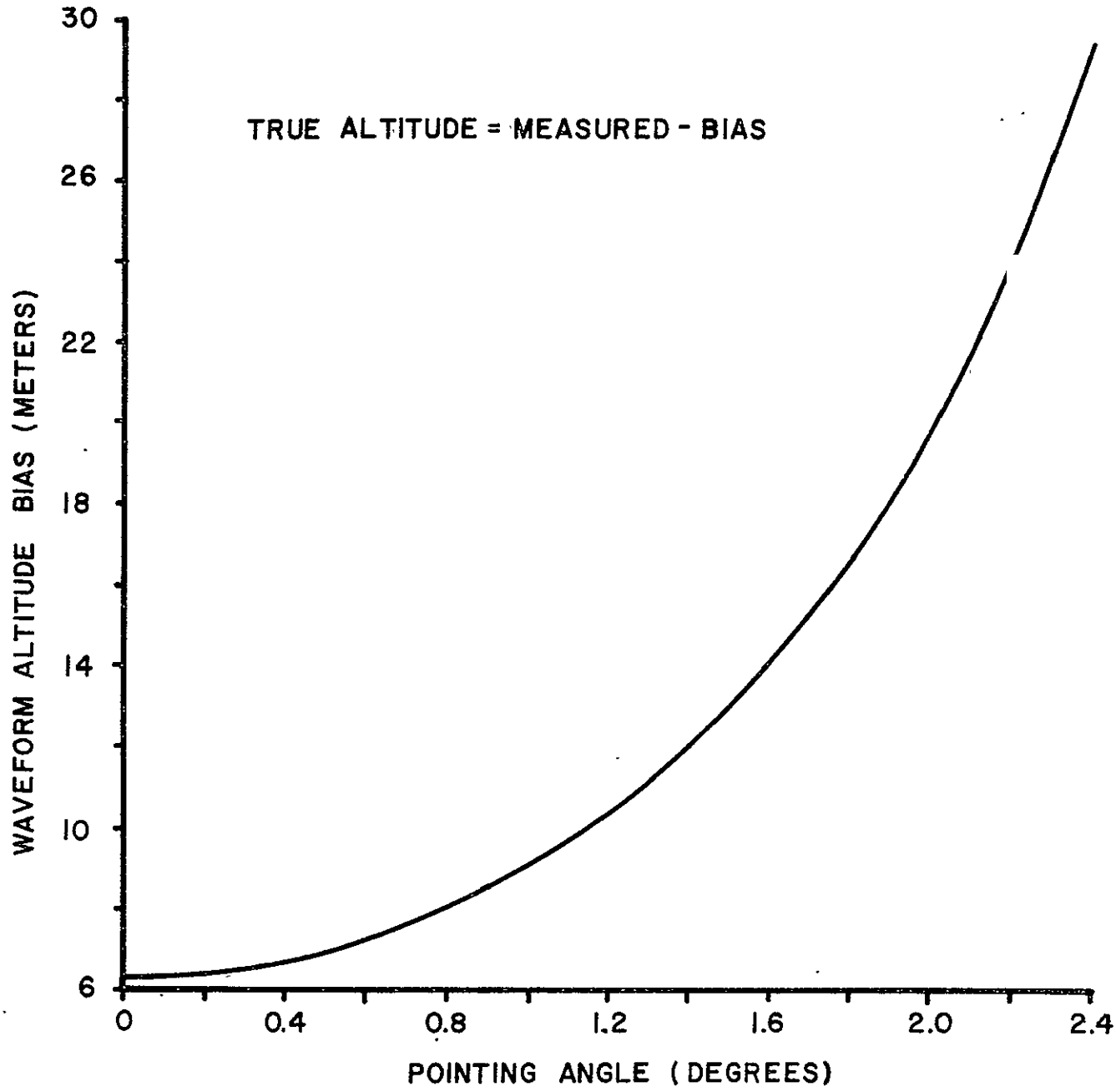

Figure 22. Global Mode waveform induced altitude bias as a function of pointing angle.

4.0 AGC CALIBRATION FOR FLUCTUATING TARGETS

As noted in section 3.1, the determination of σ° assumes an accurate measure of the average return power at the Plateau gate for both the Intensive and Global Modes. For the GEOS-3 altimeter, this measurement is accomplished by sampling a filtered replica of the AGC control voltage and, using preflight calibration curves, inferring the return power. The accuracy of this approach is, therefore, highly dependent upon the accuracy of the preflight calibration curves.

4.1 The Clean Versus Clutter Problem

Preflight calibration curves of AGC voltage versus average received power were obtained over a wide range of receiver temperatures and received power levels. In all cases, the average modulation waveform was tailored to simulate the expected inflight <u>average</u> return waveform. In addition, data were also obtained for the case where the basic waveform was, essentially, further modulated by a random noise source so as to simulate the fading and fluctuating nature of the backscattered return. When the simulated average return was not noise modulated, the data were referred to as the Clean AGC calibration curves; when the simulated return was noise modulated, the data were called Clutter AGC calibration curves. Although not representative of actual backscattered returns, the non-noise modulated or Clean AGC calibration data were obtained to cross check measurement techniques and basic AGC stability.

Since the AGC control voltage was determined by the power in the Plateau gate, it seemed reasonable to compare the Clean and Clutter AGC data. Because the Clutter data were obtained by averaging a large number of returns, the statistical error in the Clutter data was expected to be small; thus, the Clean and Clutter data were expected to be nearly identical. Figure 23 shows a comparison between Global Mode Clean and Clutter AGC data for nearly identical receiver temperatures. The agreement of the data is very good, the average difference is about 0.4 dB and this is certainly within measurement tolerances.* However, the comparison for the Intensive

*The majority of this 0.4 dB difference is due to the 0.6°C temperature difference between the two sets of data.

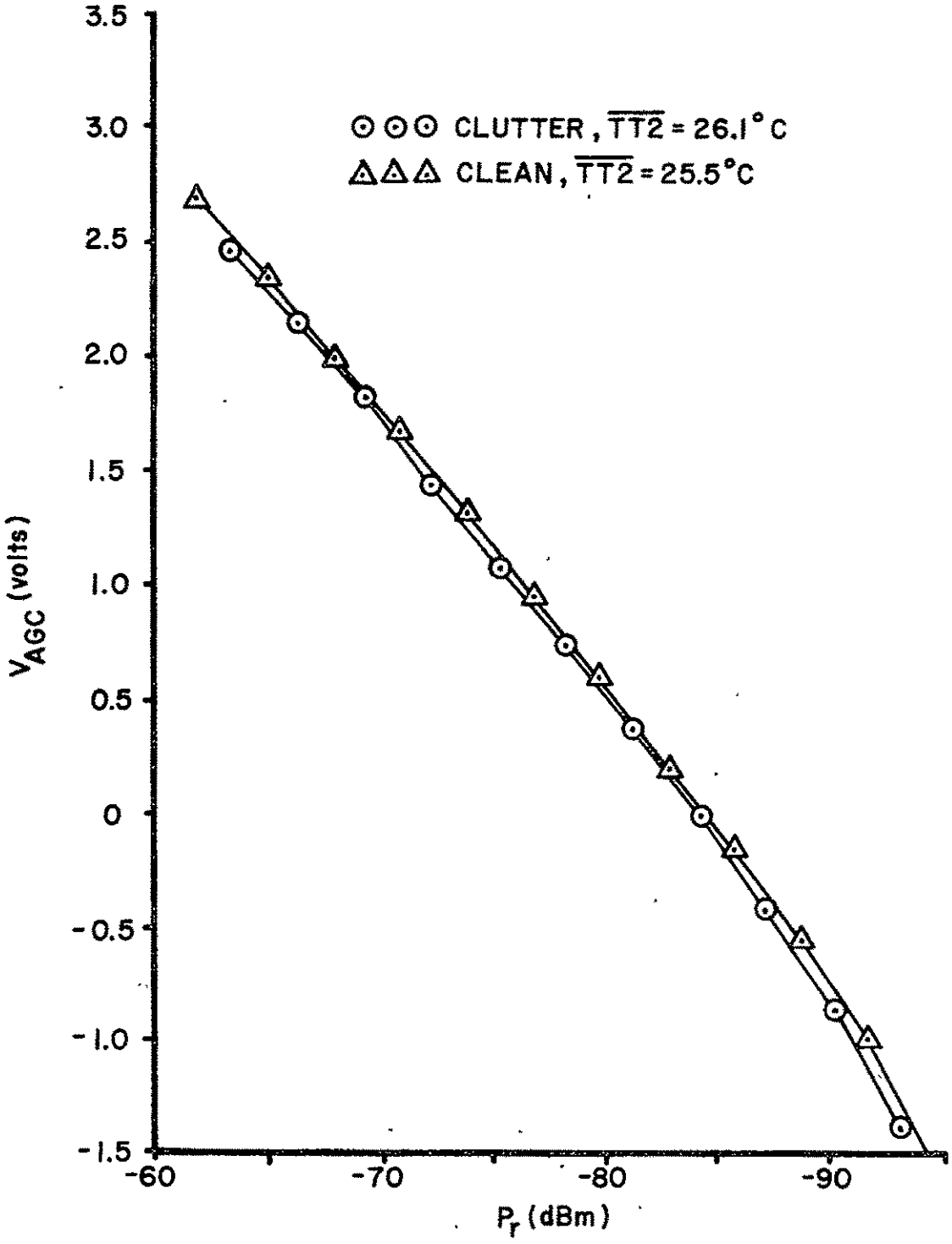

Figure 23. Global Mode Clean and Clutter AGC calibration data, from [6].

Mode was quite poor as shown in Figure 24. For these data, the differences ranged between 3.5 and 4 dB with the Clean data always indicating the higher voltage for equal Clean and Clutter power.

Extensive verification of the test procedures and techniques for the Intensive Mode Clutter data was accomplished by E. L. Hofmeister and B. N. Keeney of GE, but no obvious problems were found. The disparity was particularly troublesome because a decision had to be made as to which set of data for the Intensive Mode should be used to convert inflight AGC voltage measurements into received power. The Clean AGC curves were chosen to reduce the inflight date since the basic calibration process was considered to be more accurate. However, a preliminary analysis of σ° data resulting from both the Intensive and Global Modes showed that the Intensive Mode, using the Clean AGC curves, was yielding estimates of σ° which were consistently 3 to 4 dB below the estimates obtained from Global Mode. If, however, the Intensive Mode AGC voltage data were converted to received power using the Clutter curves, the 3 to 4 dB difference could be reduced to less than 1 dB. Thus, inflight data seemed to indicate that the Clutter calibration data should have been used to convert AGC voltage to received power.

Although the comparison of inflight σ° values resulting from both altimeter modes is a reasonable means for resolving the Clean vs. Clutter question, it still left much to be desired. In the first place, the error bounds in such a comparison mught be comparable to the 3.5 to 4 dB difference which was to be resolved. That is, because of varying surface conditions, spacecraft attitude and other factors, comparisons of this type are always subject to uncertainties. In addition, even if σ° comparisons did show which set of calibration data should be used, it would not answer the basic question of why the difference in the first place. Because future altimeters will also probably employ AGC systems of the GEOS type, it seemed imperative to find the source of the discrepancy. Since the calibration process was thoroughly checked and verified, it appeared that the discrepancy might be due to some fundamental difference between how the altimeter responded to a deterministic and a random signal. For this reason, the basic operation of the AGC loop was more thoroughly investigated.

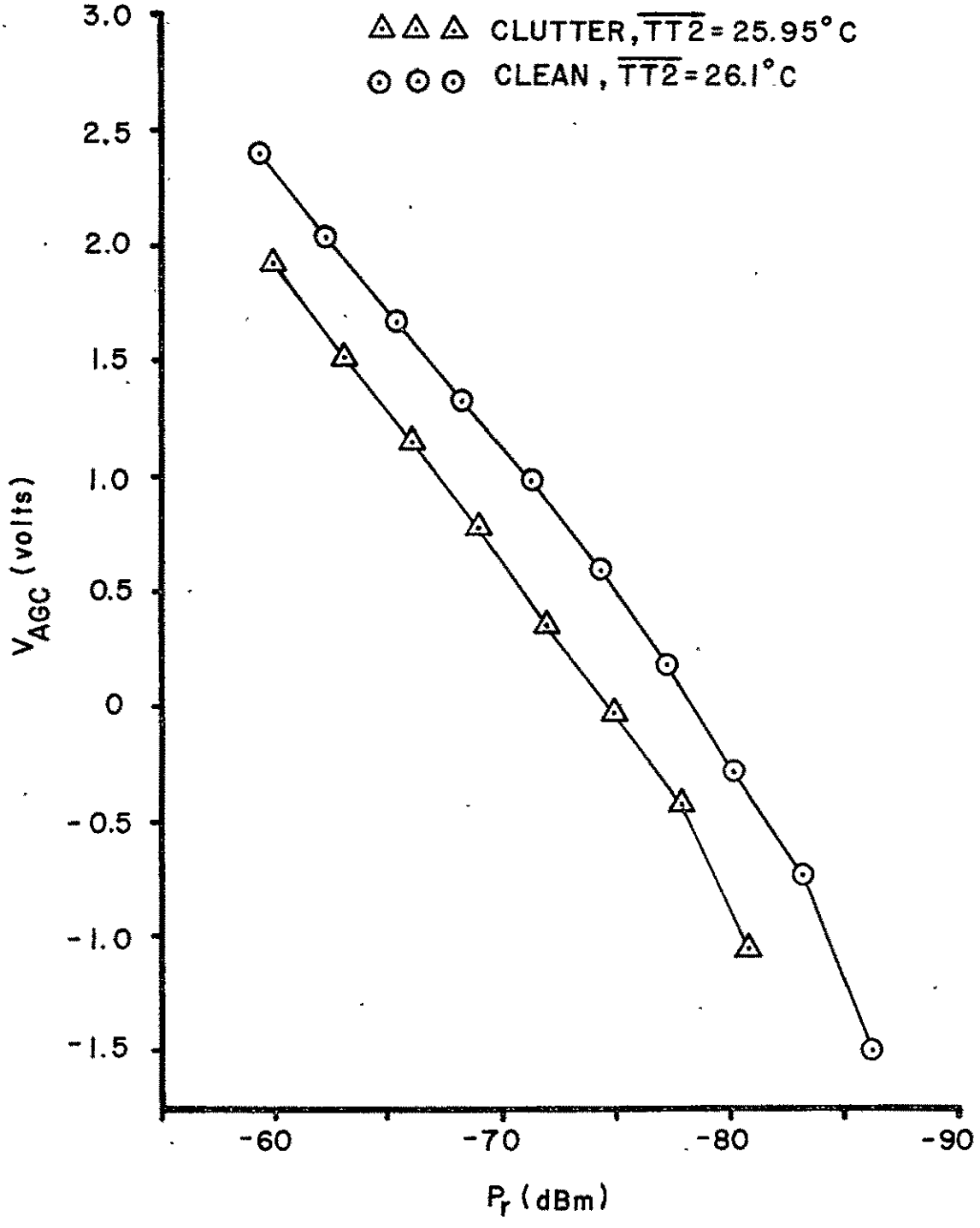

Figure 24. Intensive Mode Clean and Clutter AGC calibration data, from [6].

4.2 A Self-Consistent Solution To The Clean vs. Clutter Problem

A solution to the Clean vs. Clutter problem must satisfy the following conditions. First, the solution must comprise no unjustified assumptions in regard to the physics of the process. Second, as the experimental results in Figure 23 indicate, the Clean and Clutter AGC curves for the Global Mode must nearly overlap. Third, the solution must very nearly account for the discrepancy between the Clean and Clutter data for the Intensive Mode. It should be noted however that, in the final analysis, the proposed solution must be verified by tests and measurements on the actual hardware!

The results in Figures 23 and 24 indicate that for a non-fluctuating received power (Clean case), the AGC control voltage V may be expressed as a logarithmic function of the received power,* P_r, i.e.

$$V \approx a + b\left[10 \log(P_r)\right] \tag{66}$$

Equation (66) is strictly true only over a limited range of P_r values; however, for the present, it serves to illustrate some very important points. It is necessary, next, to know how V responds to a fluctuating received power on a sample-by-sample basis rather than on the average as presented in Figures 23 and 24. To a first order, at least, (66) should nearly represent the sample-by-sample case but with V dependent upon some finite pulse average of the received power (due to filtering in the AGC loop). Although it is more reasonable to represent this average as a weighted average of the pulse-by-pulse power, the problem will be simplified to an equivalent uniform average of discrete values. This assumption will not significantly alter the results to be presented. The next question is as follows; should (66) be replaced by a "finite pulse average of logs", i.e.

$$V_1 = a + b\left\{\frac{1}{m}\sum_{i=1}^{m} 10 \log\left[P_r(i)\right]\right\} \tag{67}$$

or a "log of the finite pulse average", i.e.

---

*The symbol log will be used for $\log_{10}$ while ℓn will be used for $\log_e$.

$$V_2 = a + b\left\{10\log\left[\frac{1}{m}\sum_{i=1}^{m} P_r(i)\right]\right\} \quad ? \tag{68}$$

Using the Clean AGC data there is no way to resolve this question and the AGC details in [6] are also insufficient in this regard. Both of the above equations merely state that any observation of the AGC control voltage is based upon a finite pulse average of received power.

Consider for the moment that either equation (or both) may be true. First of all, it must be realized that although P_r was explicitly written in both equations, this is incorrect for a sample-by-sample description of the control voltage. That is, the AGC loop is not excited by the received power, per se, but rather by a voltage which is proportional to the output of the Plateau integrating gate, see Figure 25. Since the Plateau gate is nearly "matched" to the video point target response, the statistics of the gate output are virtually identical to the statistics of input voltage.* Thus, the output of the Plateau gate is nearly equal to (GP_r/K) where K is the AGC attenuation, G is the system gain from antenna output to Plateau gate output (excluding the AGC attenuator), the probability density of P_r is exponential, i.e.

$$f(P_r) = \frac{G}{K\bar{P}_r}\exp\left(-\frac{P_r G}{K\bar{P}_r}\right)U(P_r) \quad , \tag{69}$$

and $\bar{P}_r$ is the average received power at roughly the mid point of the Plateau gate. For the Intensive Mode, GP_r/K is fed directly to the AGC loop for each pulse. For the Global Mode, sixteen returns resulting from a single pulse burst are first averaged and then fed to the AGC loop.** Thus, the AGC block diagram in Figure 25 may be replaced by its equivalent in Figure 26. Figure 26 clearly shows that the effective input to the AGC loop is $G\tilde{P}_r$ where for the Intensive Mode $\tilde{P}_r \approx P_r$, and for the Global Mode

---

*This statement is theoretically demonstrated, for the first two moments, in Section 2 for both altimeter modes, and experimental verification for the Intensive Mode is given in [6, page 145].

**This fact is ignored in Section 5.2 (AGC Analysis) of [6], however it is clearly stated on page 90 of [6] in text and is shown in the second sheet of Figure 7 of [6].

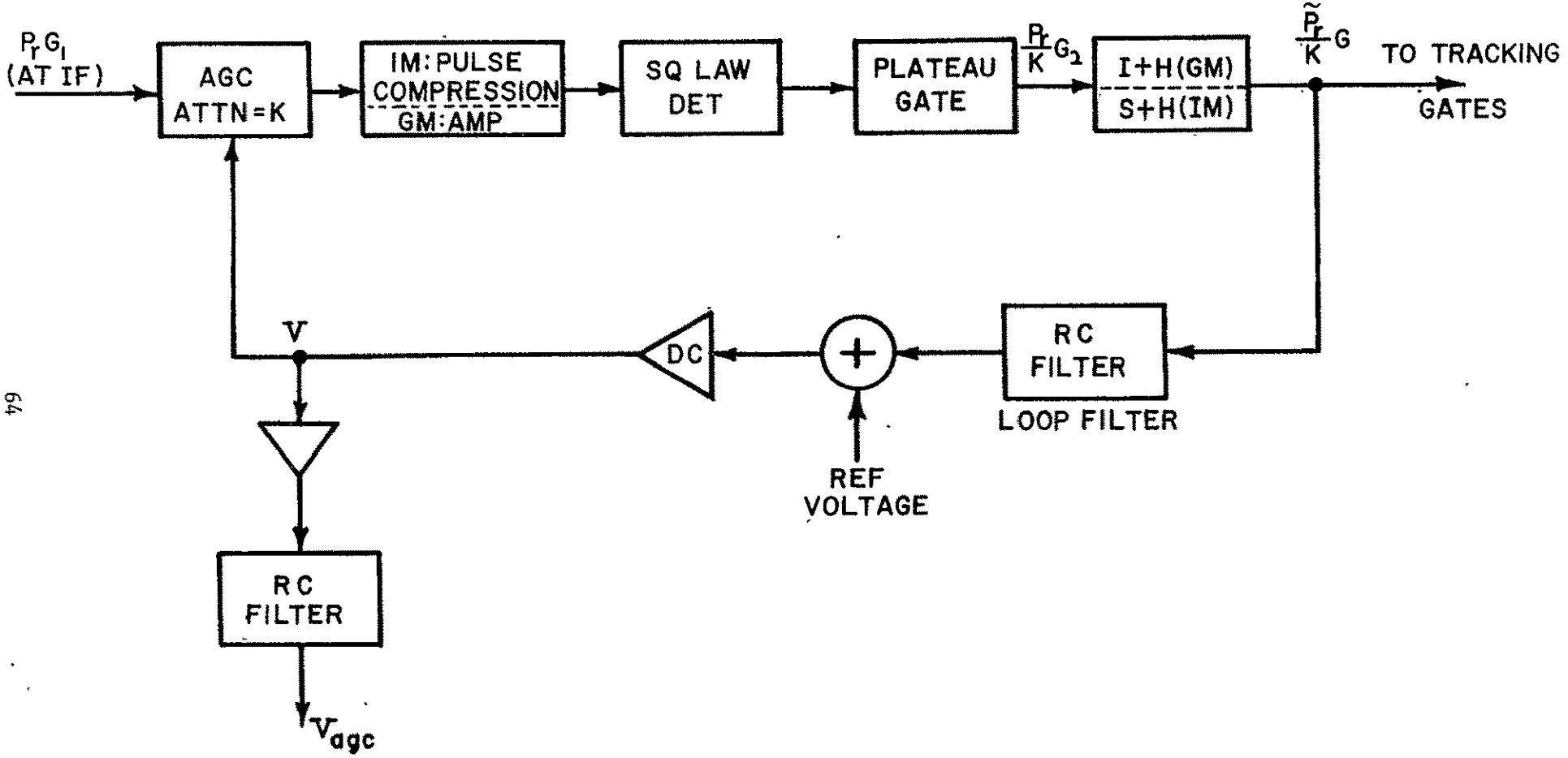

Figure 25. Block diagram of the AGC loop.

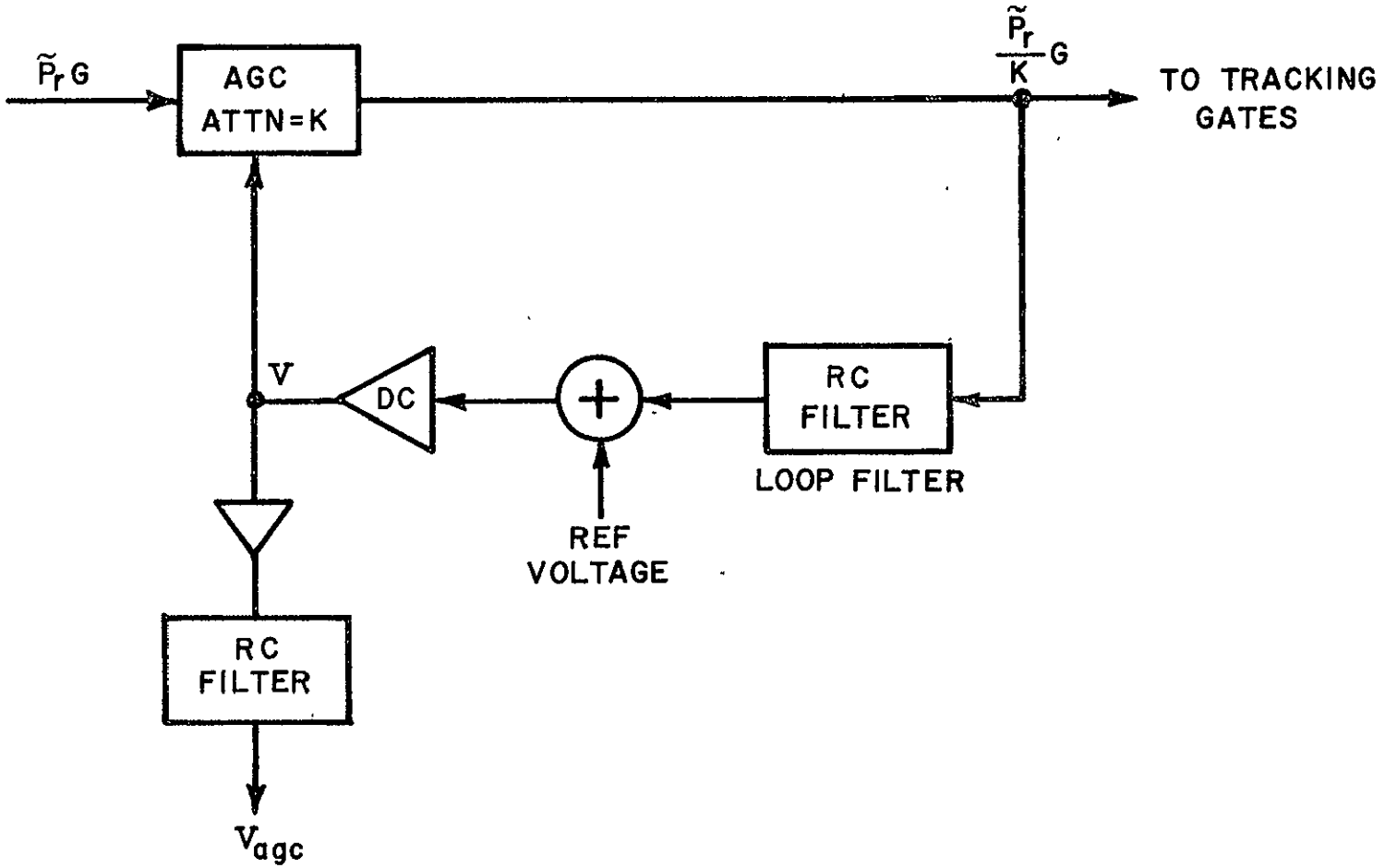

Figure 26. Equivalent AGC block diagram.

$$\tilde{P}_r(i) \approx \frac{1}{16} \sum_{j=1}^{16} P_r(j,i) \; * \tag{70}$$

Also, in equations (67) and (68), $P_r(i)$ should now be replaced by $\tilde{P}_r(i)$.

The reason for replacing the true AGC system by the equivalent system in Figure 26 is to emphasize the fact that in the case of the Global Mode the AGC input is actually a sixteen pulse average while the Intensive Mode input is not averaged. Thus, the probability density function for $\tilde{P}_r$ is exponential for the Intensive Mode and is given by the gamma density [14] for the Global Mode, i.e.

$$f(\tilde{P}_r) = \frac{N^N}{(\overline{P}_r)^N \Gamma(N)} (\tilde{P}_r)^{N-1} \exp(-N\tilde{P}_r/\overline{P}_r) \, U(\tilde{P}_r) \tag{71}$$

where $N = 16$. This sixteen pulse averaging is the reason why the statistical fluctuations in V_{agc} are much lower for Global Mode than for the Intensive Mode.

Using the gamma density for the Global Mode the average of the AGC control voltage can be computed for both possible forms of V, i.e. equations (67) and (68). Since the average of the control voltage for the Clutter case must equal the Clean results, both (67) and (68) must satisfy the following identity for the Global Mode;

$$\overline{V} = a + b\left\{10 \log \overline{P}_r\right\} \tag{72}$$

For (67), the average control voltage is given by

$$\overline{V}_1 = a + b \; E\left\{\frac{1}{m} \sum_{i=1}^{m} 10 \log\left[\tilde{P}_r(i)\right]\right\}$$

Since the $\tilde{P}_r(i)$, $i = 1,2,\ldots,m$, are independent

---

*The double indexing of P_r for the Global Mode is necessary because of the pulse burst operation. In (70), i denotes the burst number while j denotes the pulse number within a burst.

$$\overline{V}_1 = a + 10b\, E\left\{\log(\tilde{P}_r)\right\} = a + kb\, E\left\{\ell n(\tilde{P}_r)\right\}$$

where $k = 4.3429$. The probability density function of $y = \ell n(\tilde{P}_r)$ is easily shown to be

$$f(y) = \frac{N^N}{(\overline{P}_r)^N \Gamma(N)} \exp\left[Ny - \frac{N}{\overline{P}_r}\exp(y)\right] \qquad -\infty \le y \le \infty \tag{73}$$

Thus, the mean value of V_1 is given by

$$\overline{V}_1 = a + \frac{kbN^N}{(\overline{P}_r)^N \Gamma(N)} \int_{-\infty}^{\infty} y \exp\left[Ny - \frac{N}{\overline{P}_r}\exp(y)\right] dy \tag{74}$$

Integrals of this form are evaluated in the Appendix with the following result;

$$\overline{V}_1 = a + \frac{kb}{\Gamma(N)}\left[\Gamma(N)\ell n(\overline{P}_r) - \Gamma(N)\ell n(N) + \Gamma'(N)\right] \tag{75}$$

or

$$\overline{V}_1 = a + kb\left[\ell n(\overline{P}_r) - \ell n(N) + \frac{\Gamma'(N)}{\Gamma(N)}\right] \tag{76}$$

Equation (76) may be simplified to the following;

$$\overline{V}_1 = a + b\left\{10\log(\overline{P}_r) - k\ell n(N) + k\psi(N)\right\} \tag{77}$$

where $\psi(N)$ is the digamma function which is defined for integer values of N as follows;

$$\psi(N) = \begin{cases} -\gamma & N = 1 \\ -\gamma + \sum_{k=1}^{N-1} k^{-1} & N \ge 2 \end{cases}$$

and γ is Euler's constant, i.e. $\gamma = 0.5772$. With $P_{bias}(N) = -k\ell n(N) + k\psi(N)$, (77) may be written as

$$\overline{V}_1 = a + b\left\{10\log(\overline{P}_r) + P_{bias}(N)\right\} \tag{78}$$

Equation (78) indicates that the average AGC control loop voltage differs from the deterministic or Clean case by the term $bP_{bias}(N)$. Stated another way, (78) implies that if the Clean curves were used to estimate the average fluctuating power, one would obtain a biased estimate of the average received power. This statement merely reflects the well known fact that a logarithmic system (such as the AGC loop) produces a biased estimate of the average fluctuating power [15]. The fact that the bias is a function of the filtering prior to the AGC loop is shown in Table IV. For $N = 16$, the bias is -0.14 dB; this means that if equation (67) is the proper description of the AGC loop control voltage, then the Clean and Clutter data in Figure 23 should differ by no more than 0.14 dB. The data in Figure 23 clearly show this degree of agreement. Thus, equation (67) produces a result which agrees with both the Clean data and the average Clutter data for the Global Mode.

TABLE IV

AGC Loop Bias As A Function Of The Number Of Independent Returns Averaged Prior To The AGC Loop

N	P_{bias} (dB)
1	-2.51
2	-1.18
3	-0.76
4	-0.57
8	-0.28
12	-0.18
16	-0.14
20	-0.11

If the control voltage is as described in (68), the average is given by

$$\overline{V}_2 = a + bk\,E\left\{\ell n\left[\frac{1}{m}\sum_{i=1}^{m}\tilde{P}_r(i)\right]\right\}$$

or

$$\overline{V}_2 = a + bk\,E\left\{\ell n\left[\frac{1}{Nm}\sum_{i=1}^{m}\sum_{j=1}^{N}\tilde{P}_r(j,i)\right]\right\}$$

Since the $\tilde{P}_r(j,i)$ are independent for each i and j, the probability density of x, where

$$x = \frac{1}{Nm}\sum_{i=1}^{m}\sum_{j=1}^{N}\tilde{P}_r(j,i)$$

is given by

$$f(x) = \frac{(Nm)^{Nm}}{(\overline{P}_r)^{nM}\,\Gamma(nM)}\,(\tilde{P}_r)^{Nm-1}\exp\left[-(Nm\tilde{P}_r)/\overline{P}_r\right]U(\tilde{P}_r) \qquad (79)$$

Thus, the average control loop voltage is given by

$$\overline{V}_2 = a + b\left\{10\log_{10}(\overline{P}_r) + P_{bias}(Nm)\right\} \qquad (80)$$

where the analysis for $\overline{V}_1$ has been used to deduce this result. Since $m > 10$ for the Global Mode [6], the product $Nm > 160$ and $P_{bias}(Nm)$ is negligible. It is interesting to note that whereas the bias in $\overline{V}_1$ depended only upon pre-loop filtering, i.e. N, the bias in $\overline{V}_2$ depends on both pre-loop and loop filtering, i.e. Nm.

The results for $\overline{V}_1$ and $\overline{V}_2$ both agree, to within experimental error, with the data in Figure 23 for the Global Mode; that is, the Clean and Clutter curves are nearly identical. Thus, the problem of choosing which function is a proper representation for the AGC loop control voltage still persists. Referring to Figure 25, the AGC control voltage V is a scaled and offset replica of the output from the loop filter. Since the filter is linear, the output represents the average of a number of inputs. If the

inputs are $10\log[\tilde{P}_r(i)]$, $i = 1,2,\ldots,m$, then equation (67) clearly represents a linear process which is characteristic of an averaging filter. Conversely, there does not appear to be any obvious way for (68) to be the result of a linear averaging process. That is, let $q(\tilde{P}_r(i))$ be the ith input to the loop filter in Figure 25. The output of the loop is then equal to

$$\frac{1}{m}\sum_{i=1}^{m} q\left(\tilde{P}_r(i)\right)$$

hence, for (68) to be valid, the following equation must be satisfied;

$$10\log\left[\frac{1}{m}\sum_{i=1}^{m}\tilde{P}_r(i)\right] = \frac{1}{m}\sum_{i=1}^{m} q\left(\tilde{P}_r(i)\right) \qquad (81)$$

This equation has no solution for $q\left(\tilde{P}_r(i)\right)$ other than the trivial one which implies no averaging by the loop filter. Thus, based on the logarithmic behavior of the control voltage and the linear nature of the loop filter, it is concluded that V_1 is a realizable representation for the control voltage and V_2 is not! For this reason, V_2 will be dropped from further consideration.

For the Intensive Mode, the average AGC control voltage is given by the Global Mode result* with N = 1; that is, for the Intensive Mode, the Plateau gate output is fed directly to the AGC loop on a pulse-by-pulse basis. Thus,

$$\overline{V}_1 = a + b\left\{10\log(\overline{P}_r) - 2.51\right\} \qquad (82)$$

since the Plateau gate output is not filtered or averaged prior to its input to the AGC loop. Since the slope constant b is positive, (82) implies that the Clutter curves will be below the Clean curves as in Figure 24. The results in Figure 24 indicate that the difference between the Clean and Clutter curves varies from about 3.5 to 4 dB while (82) shows that the theoretical difference should be no more than 2.51 dB. Thus, there still is

*The constants a and b are the same as may be verified by comparing IM and GM Clean curves.

some discrepancy which cannot be accounted for. With the thought that the residual difference may be due to the linear approximation in (66), the control voltage was assumed to be more accurately represented by a quadratic expression of the form

$$V_d = a_1 + b_1\, 10\log(P_r) + c_1\left[10\log(P_r)\right]^2 \tag{83}$$

for the Clean or deterministic data and

$$V_r = a_2 + b_2\, 10\log(\overline{P}_r) + c_2\left[10\log(\overline{P}_r)\right]^2 \tag{84}$$

for the Clutter or random data. The coefficients (a_1,b_1,c_1) and (a_2,b_2,c_2) were determined by a least square fit of the data in Figure 24 to the expressions in (83) and (84). Substituting

$$\frac{1}{m}\sum_{i=1}^{m} 10\log\left[P_r(i)\right]$$

for $10\log(\overline{P}_r)$ in (84), the average $\overline{V}_r$ was analytically determined. Comparing the difference between (83) and (84) with the difference between (83) and $\overline{V}_r$, resulted in a voltage difference which translated into the same 1 to 1.5 dB discrepancy as before. This fact merely confirmed the suspicion that the probability density of $10\log\left[P_r(i)\right]$ was so concentrated about $10\log(\overline{P}_r)$ that a linear approximation was sufficient, at least on a piecewise basis.

In conclusion, 2.5 dB of the 3.5 to 4 dB difference between the Intensive Mode Clean and Clutter AGC calibration curves has been accounted for. This 2.5 dB difference results from the logarithmic relation between received power and the AGC control voltage and the lack of any filtering or averaging between the Plateau gate output and the AGC loop input. The difference does not exist in Global Mode because of the sixteen pulse averaging between the Plateau gate output and the AGC loop input. The analysis presented here clearly shows that the Clutter data should be used to convert inflight AGC voltages into received power, except for BIT/CAL where the Clean curves should be used. The residual discrepancy of 1 to 1.5 dB cannot be accounted for at this time. If it could be attributed to

measurement error, the Clutter curves could be moved closer to the Clean curves by 1 to 1.5 dB to account for the error. However, given the complexity of simulating a noise-like coded return such as in the case of the Intensive Mode Clutter data, it is not completely clear what the source of the error is. In the author's opinion, achieving an accuracy of 1 to 1.5 dB for such a system is a great credit to the engineers who designed, built and tested the GEOS-3 radar altimeter. It is anticipated that during the lifetime of the mission many opportunities will arise in which similar Intensive and Global Mode data sets can be compared and analyzed with the purpose of resolving the final 1 to 1.5 dB discrepancy in the Intensive Mode Clutter calibration data.

5.0 PROCESSING FOR AND INITIAL ESTIMATES OF POINTING ANGLE

The altimeter antenna boresight angle with respect to nadir is a matter of interest in the refinement of certain altimeter derived target features such as radar cross section and ocean waveheight as well as the altitude data. Though the degree of effect upon the accuracy of the various quantities of interest is variable, it is certainly not always negligible. The theoretical development of the estimation technique and its error bounds is given in section 2. This section will be concerned with the application of the formal results to actual GEOS-3 data.

5.1 Altimeter Pointing Angle Estimation Algorithm

Basically, there are only two measurements which the GEOS-3 altimeter produces that are used in pointing angle computation; the one-second averaged Plateau integrating gate output and the Attitude/Specular integrating gate output. From these, the "average estimation function" is computed from the following;

$$\overline{\Delta} = 1 - \frac{\overline{ASG}}{\overline{APG}} \tag{85}$$

where $\overline{APG}$ represents an average of the Plateau gate outputs (processed to remove the effect of the gate's transfer function gain) and $\overline{ASG}$ represents the same for the Attitude/Specular gate. For the GEOS-3 prf, $\overline{ASG}$ and $\overline{APG}$

must be based upon at least a ten second average for (85) to correspond to the estimation function given by (19). Using the theoretical curves of $\overline{\Delta}$ as a function of pointing angle shown in Figure 6, (85) can be used to estimate the altimeter pointing angle.

The GEOS-3 telemetry system operates in two different data rate modes in which the Plateau and Attitude/Specular gate outputs are sampled at slightly different rates [17]. However, in both cases, the telemetry data rate permits an oversampling of the outputs since the basic gate outputs represent one-second averaged values and the telemetry sampling is at least two times per second. Processing of GEOS-3 data is largely organized on a per frame basis so it is convenient to define intervals in terms of frames. A low data rate major frame period is 2.048102 seconds, so five of these frames adequately cover a ten second interval. High data rate frames are 3.276964 seconds long, so three of these comprise very nearly ten seconds of data.

Numerical approximation algorithms were developed to facilitate the transformation from $\overline{\Delta}$ to ξ (in degrees). For Global Mode, the expression is as follows;

$$\xi = \left[8.14848 - 10.2796 \ln(\overline{\Delta}+1.9033)\right]^{1/2} \tag{86}$$

where ξ is restricted to be less than 2.4°. For the Intensive Mode, the approximate expression is

$$\xi = \left[5.0935 \ln(1.9976 - \overline{\Delta}) - 2.04346\right]^{1/2} \tag{87}$$

and ξ should be limited to less than about 2°. Table V compares pointing angles computed from (86) and (87) with those obtained from Figure 6 as a function of the estimation function, $\overline{\Delta}$.

GEOS-3 altimeter data presently exists in various forms, but the easiest to manage and transport is magnetic tape. This necessitates a computer program to access the data, find values of interest, and make the necessary computations. Such a program (in Fortran) has been developed and is currently running on the Wallops Flight Center ECLIPSE computer. The program utilizes a subroutine written by Dr. G. S. Hayne of Applied Science

TABLE V

Comparison Of Pointing Angles As Obtained From Figure 6 With The Numerical Approximations Of Equations 86 and 87

GLOBAL MODE

$\overline{\Delta}$	ξ : Figure 6	ξ : Eqn. 86
0.306	0°	0.01°
0.2725	0.4°	0.396
0.1736	0.8°	0.798°
0.0148	1.2°	1.205°
-0.1943	1.6°	1.625°
-0.4362	2.0°	2.05°
-0.6795	2.4°	2.46°

INTENSIVE MODE

$\overline{\Delta}$	ξ : Figure 6	ξ : Eqn. 87
0.504	0°	0.0003°
0.458	0.4°	0.393°
0.308	0.8°	0.793°
0.020	1.2°	1.196°
-0.472	1.6°	1.6004°
-1.278	2.0°	2.0°

Associates, Inc., which reads into core one entire frame of either high or low rate data from external data files on tape or disk. These external data dumps must be in the GAP or ARC form.

This program is versatile in that either Global or Intensive mode data (at a high or low data rate) can be used. A test is made during program execution to branch to the appropriate program segments for each case. All the quantities of interest are tested for value bounds, and, if within bounds, are used in the computations. If not, a message designating an out-or-range condition is printed and the program skips to the next consecutive ten second interval. At present, there is no overlapping as in a sliding-window average and each value reported by the program represents a completely unique, ten second interval. The time shown in the printout is the start time for the middle frame in each ten second interval. Plateau, Attitude/Specular, AGC, altimeter status, transmitted power, estimated pointing angle (from $\overline{\Delta}$), and σ° averages are also printed. Since each status word represents an average, anything other than a whole number will imply a status change during the respective ten second averaging interval. If this occurs during automatic tracking, a loss of track is thereby indicated. Sometimes, very strong returns may be encountered. In such cases, the resultant values of $\overline{\Delta}$ will exceed an upper bound and no estimate of pointing angle can be made. When this occurs, an easily distinguishable value of -9999.99 is assigned to the pointing angle and σ° estimates. In such cases, however, all the other reported averages are given, and often a very high AGC or a loss of track may be noted. Figure 27 presents an abbreviated listing of an output for Global Mode Pass 184 by this program.

5.2 Altimeter And Attitude Control System Comparisons

For the time period from 18 April 1975 to 30 June 1975, estimates of the GEOS-3 spacecraft attitude were computed and published by the Goddard Space Flight Center [2]. These results were based upon magnetometer and sun sensor data from the GEOS-3 spacecraft and they provided estimates of the spacecraft z-axis pointing angle with respect to nadir. Due to the manner in which the altimeter antenna boresight was aligned with the spacecraft z-axis, it is possible that a 0.2 degree offset between the two axes exists [Private Communication, C. L. Purdy]. However, these spacecraft

ID HEADER: REV 184/022, COMPILE TAPE 7696 FILE 04, 06/02/76

HHMMSS.SS	ALT.STAT.	AV.PLAT.	AV.ASG	AV.RAGC	DELTA	PT.ANGLE	AV.RTP	SIGMA
234832.15	232.92	.0129	-.0172	-72.808	2.332	-9999.99	151.987	-9999.99
234842.39	210.80	.0563	.0220	-49.607	.609	-9999.99	64.716	-9999.99
234852.63	174.88	.0605	.0635	-49.983	-.050	1.34	62.890	40.55
234902.87	160.16	.0769	.0645	-51.197	.161	.83	60.158	39.02
234913.11	185.40	.1072	.1018	-52.226	.050	1.12	56.270	43.45
234923.35	216.60	.0028	-.0211	-83.004	8.569	-9999.99	178.971	-9999.99
234933.59	203.16	.0482	.0356	-71.718	.261	.46	64.840	12.46
234943.84	204.00	.0547	.0444	-72.822	.189	.75	64.840	12.32

Figure 27. Sample listing from the ten second averaging program which computes the estimated pointing angle in degrees (PT. ANGLE) and cross section σ° (SIGMA) in dB.

attitude estimates do provide data which can be used to approximately determine the adequacy of the altimeter pointing angle estimation technique. In this section, a limited comparison of the two data sets will be made.

5.2.1 Global Mode

Figures 28-33 show comparisons between altimeter derived estimates and the attitude control system estimates for the pointing angle in Global Mode. Apart from the results in Figure 31, the altimeter estimates tend to always be larger than the spacecraft estimates. In particular, the altimeter derived estimate never goes below about 0.5°. While the data base is admittedly limited, the results in Figures 28-33 do tend to indicate that the altimeter derived estimates are too large for a pointing error of less than about 0.6° in the Global Mode. It was initially thought that this discrepancy might be due to a misalignment between the altimeter antenna boresight and the spacecraft z-axis. However, subsequent inspection of Intensive Mode estimates of pointing angle did not corroborate this hypothesis. That is, the discrepancy appeared to be unique to the Global Mode of the altimeter.

For the Global Mode Ramp and Plateau gates, gain calibrations were only obtained at room ambient temperature and pressure during preflight testing/calibration of the altimeter. Thus, the temperature dependent transfer gain of the Plateau gate was unknown. Since this quantity has a direct influence upon the estimation function, see equation (85), it was felt that inadequate calibration data could be a source of error. The analysis presented in section 2.4 clearly shows that the estimation of pointing angle using (85) is relatively sensitive to changes in gain. In particular, the error is a nonlinear function of the pointing angle; that is, for a 5% error in gain, the resulting pointing angle error is 0.4° at 0° pointing angle and 0.1° at 1.0° pointing angle (see Figure 18).

For the Global Mode, it is concluded that the pointing angle estimation technique using altimeter data is not accurate for pointing angles of less than 0.6° because of inadequate calibration of the Plateau gate gain. While it is possible to obtain a correction curve for the data (using Intensive and Global mode comparisons), this would entail a rather extensive effort and, hence, a reexamination of the need for Global Mode pointing angles estimates.

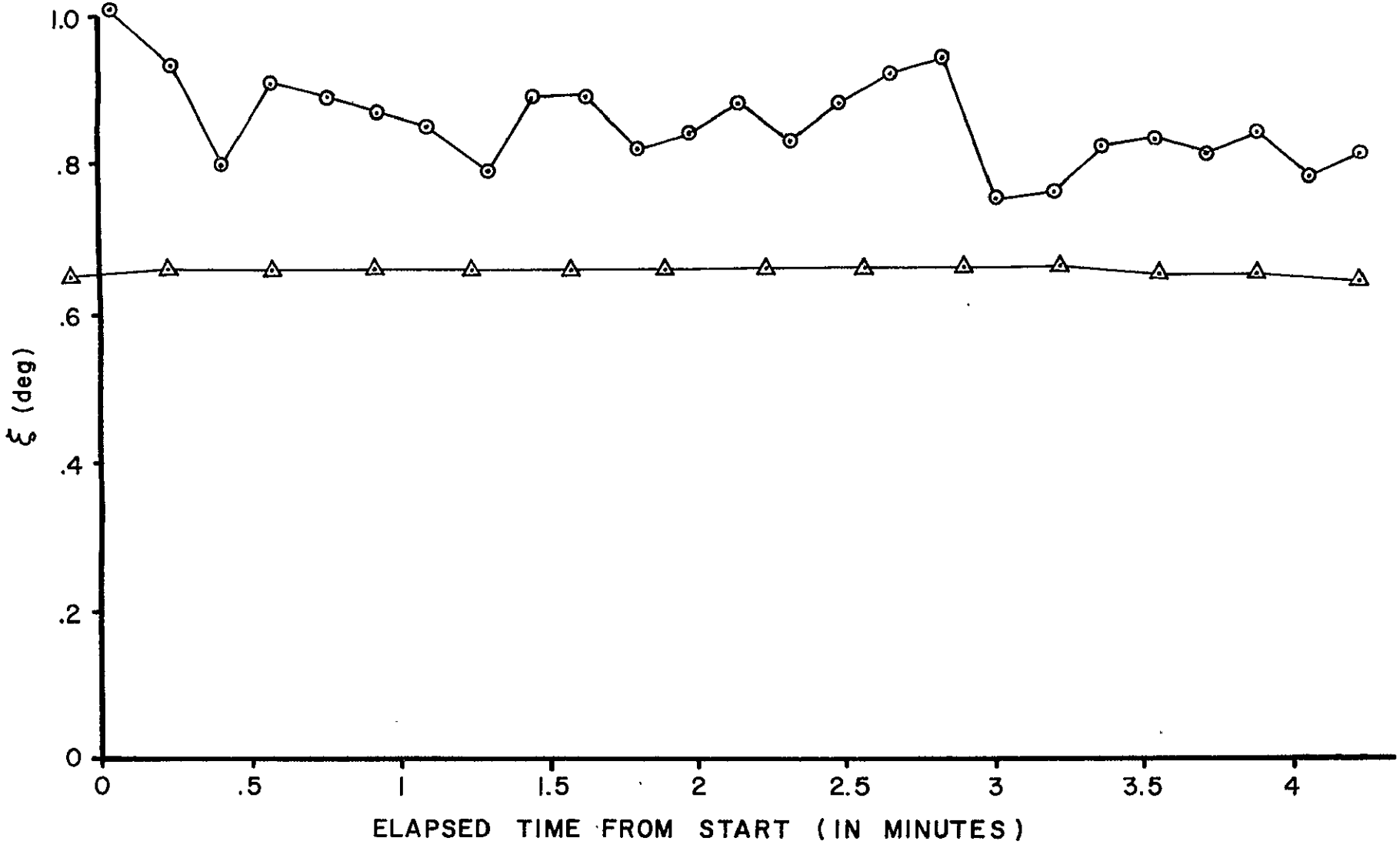

Figure 28. Comparison of attitude control system derived pointing angles (Δ—Δ—Δ) with altimeter derived estimates (o—o—o) for Global Mode, Rev 167 Start Time = 19H11M45S, 21 Apr 75. Standard deviation of altimeter estimate was 0.0506°.

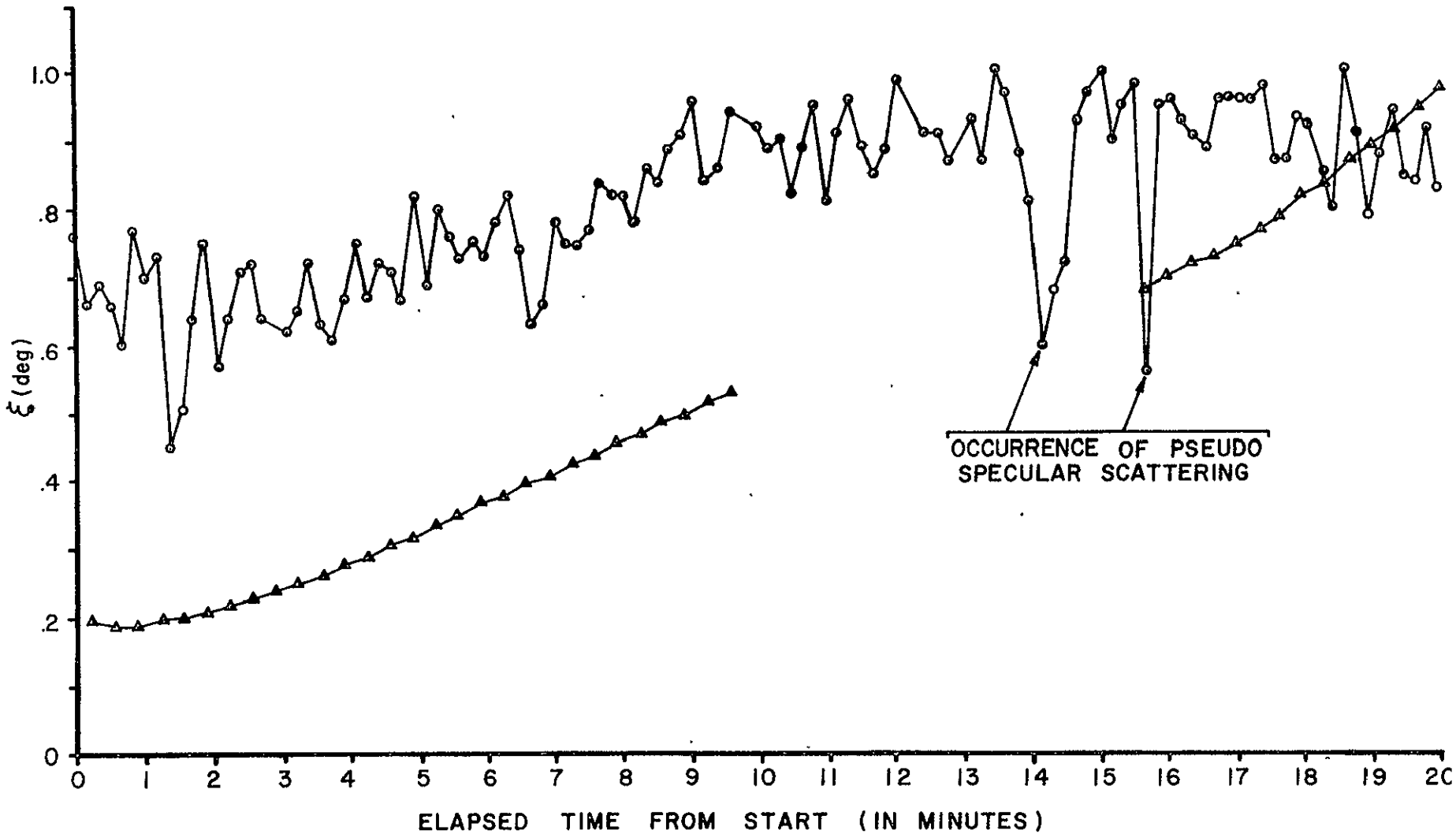

Figure 29. Comparison of attitude control system derived pointing angles (Δ–Δ–Δ) with altimeter derived estimates (o–o–o)

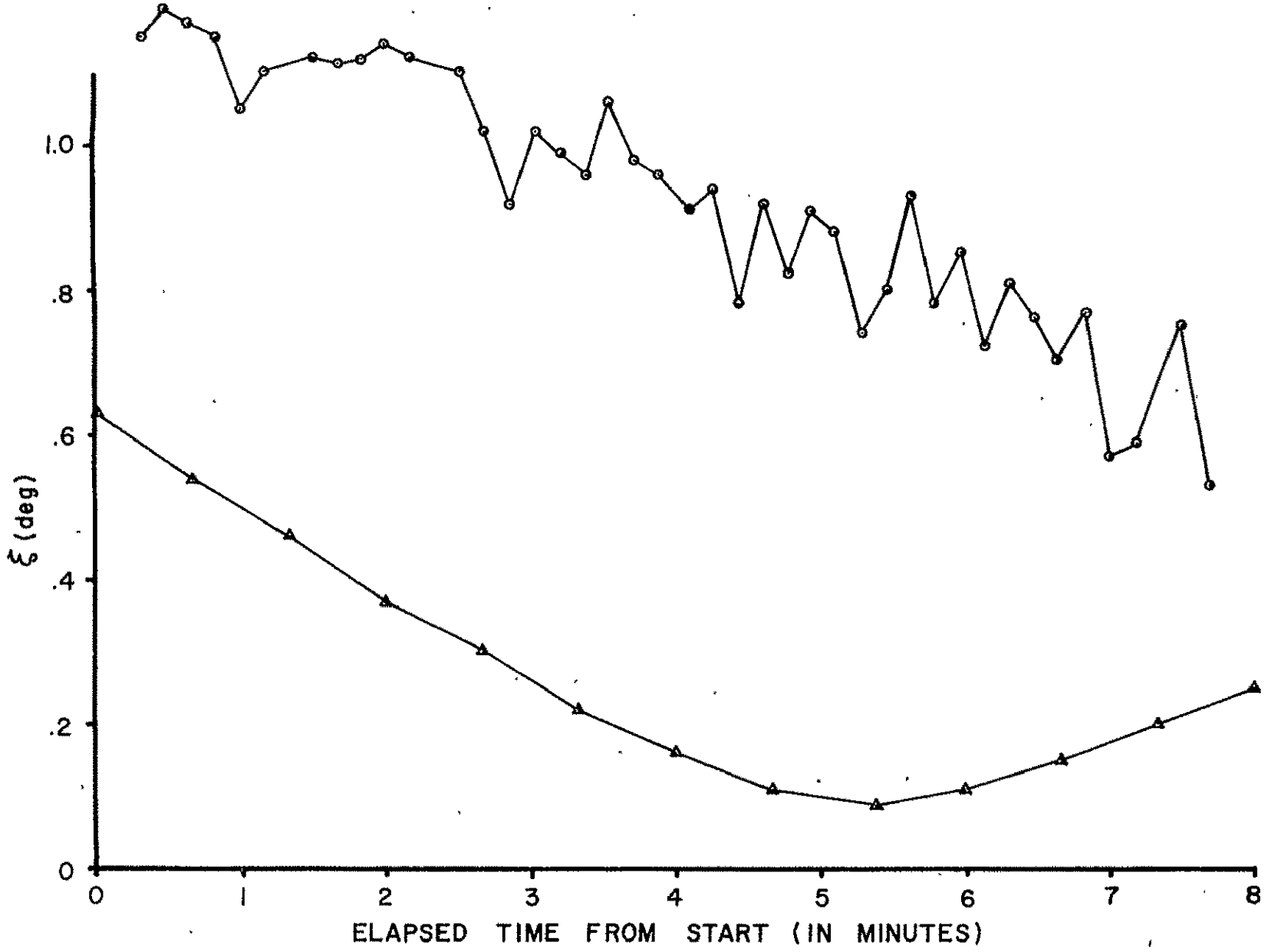

Figure 30. Comparison of attitude control system derived pointing angle (Δ—Δ—Δ) with altimeter derived estimates (o—o—o) for Global Mode, Rev 202, Start Time = 06H07M44.8S, 24 Apr 75.

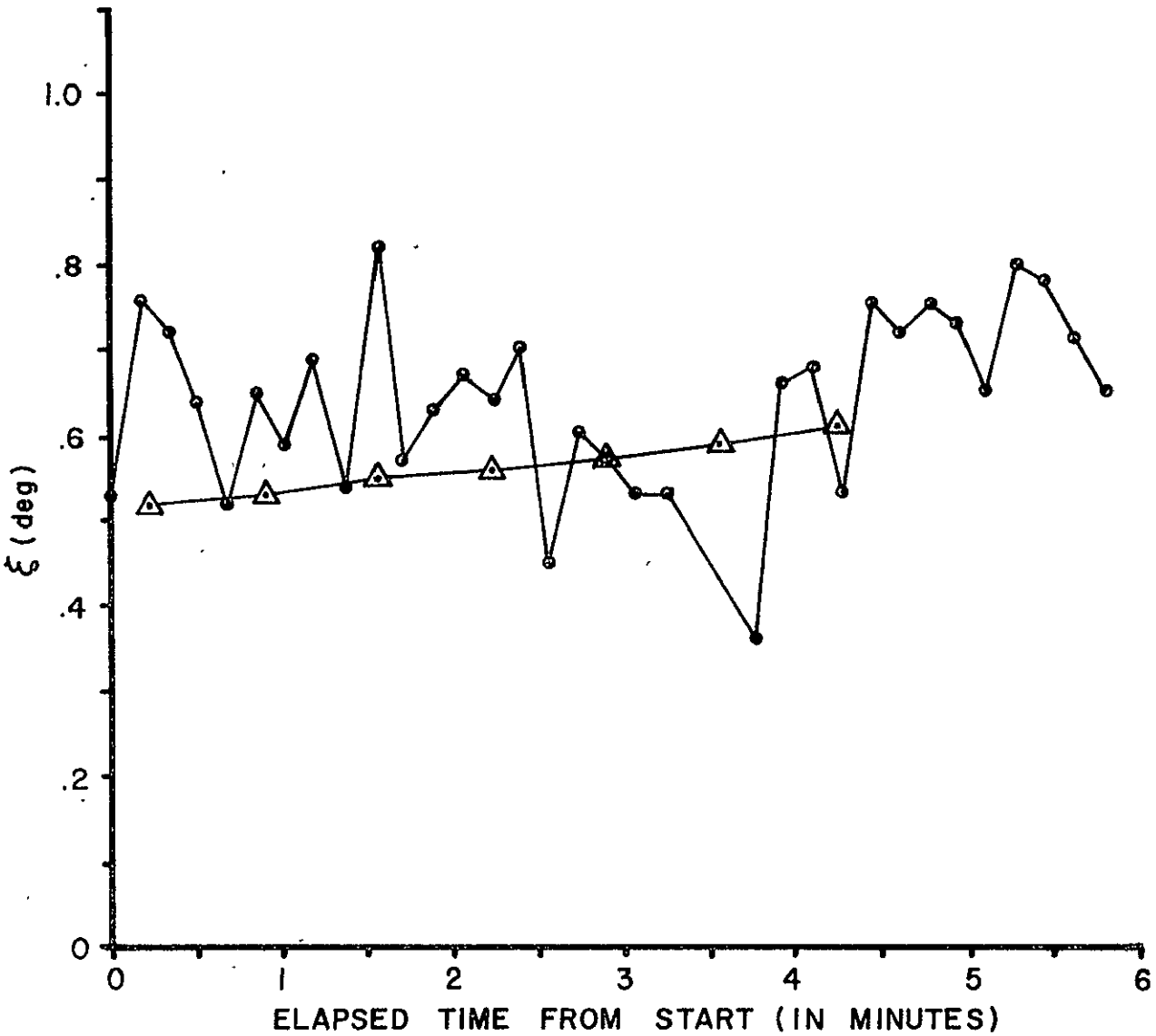

Figure 31. Comparison of attitude control system derived pointing angle (Δ—Δ—Δ) with altimeter estimates (o—o—o) for Global Mode, Rev 218, Start Time = 09H11M58.58S, 25 Apr 75.

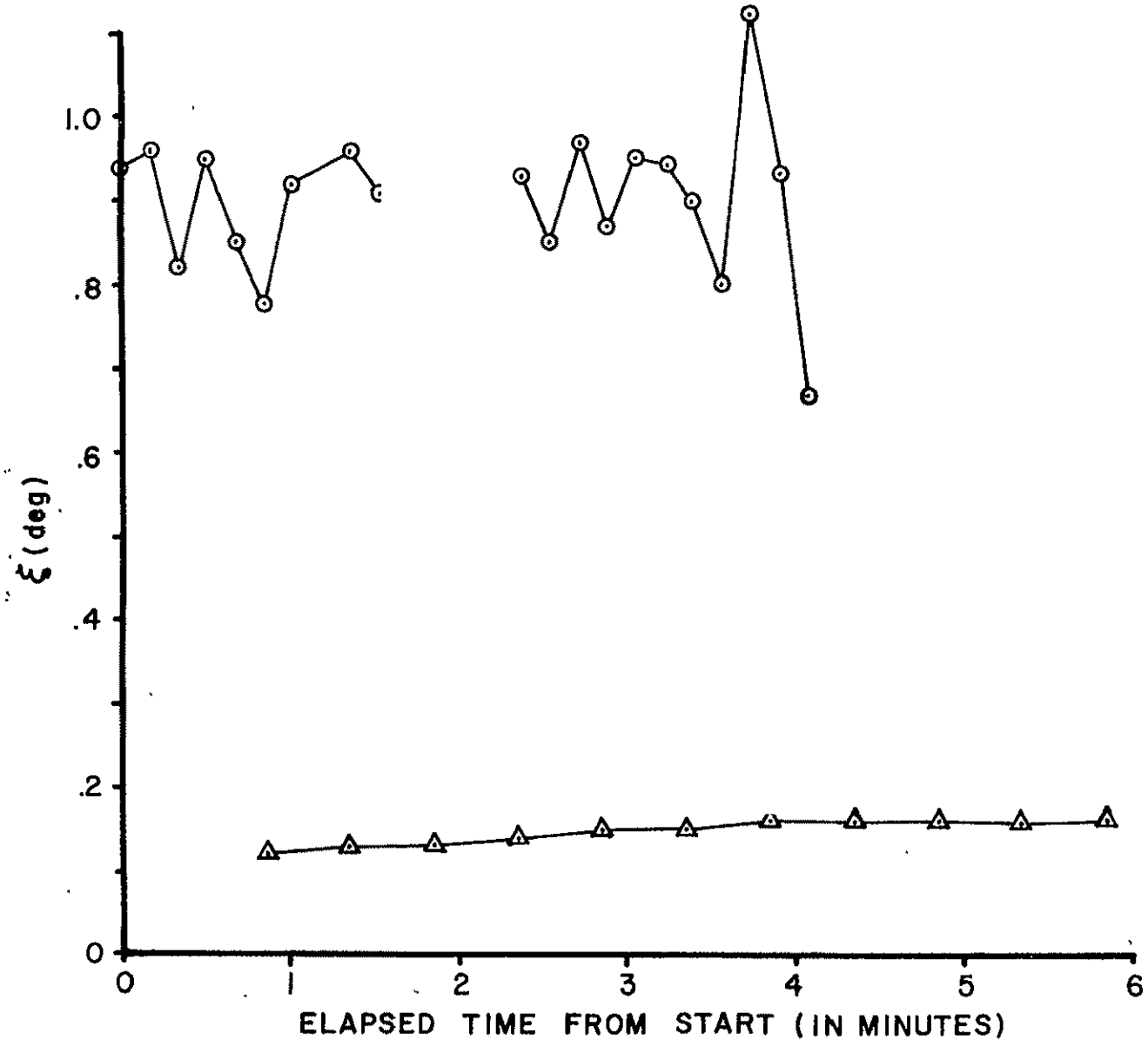

Figure 32. Comparison of attitude control system derived pointing angle (Δ–Δ–Δ) with altimeter estimates (o–o–o) for Global Mode, Rev 228, Start Time = 02H16M09.85S, 26 Apr 75.

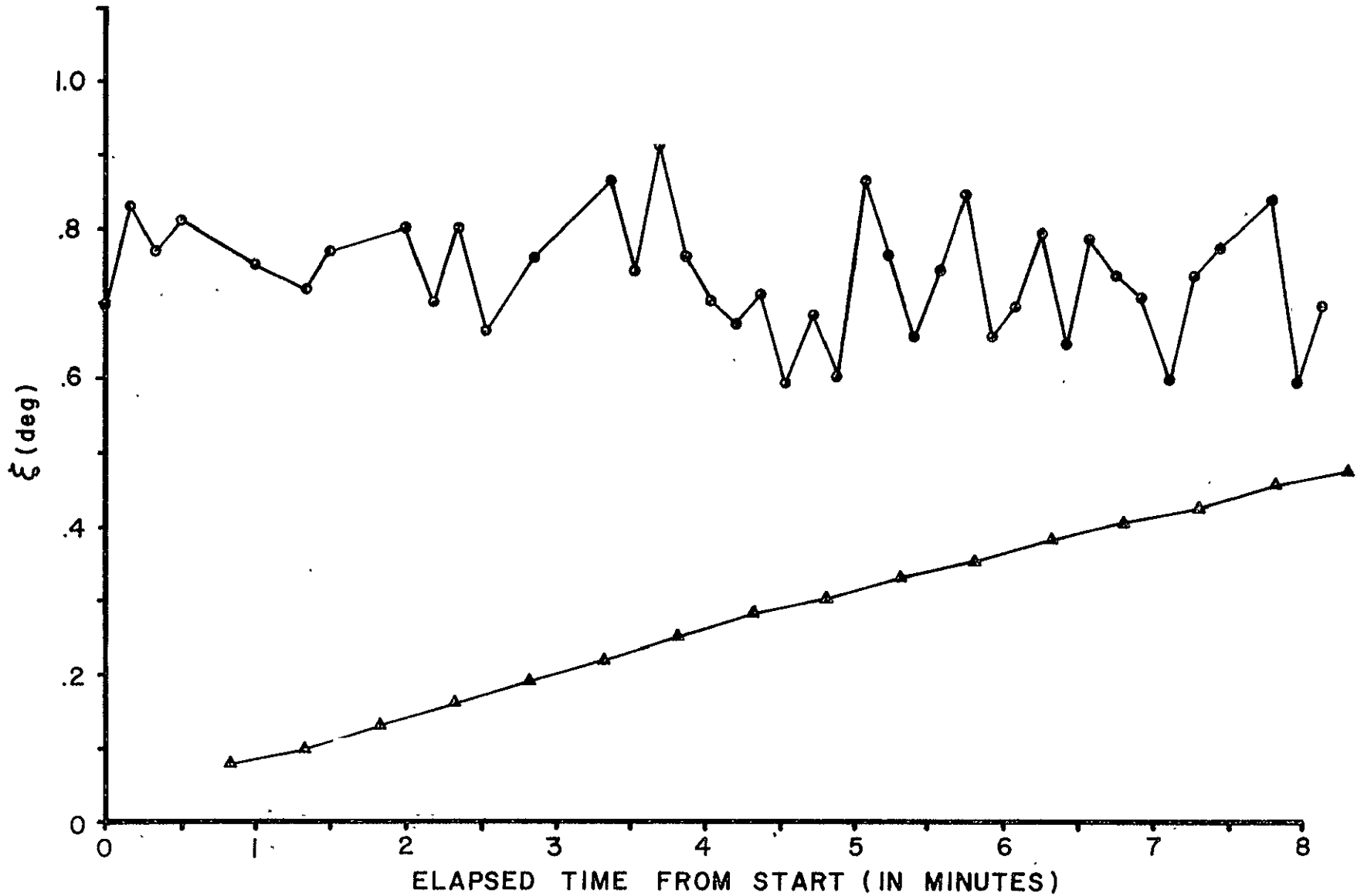

Figure 33. Comparison of attitude control system derived pointing angle (Δ–Δ–Δ) with altimeter estimates (o–o–o) for Global Mode, Rev 416, Start Time = 09H06M25.84S, 9 May 75.

5.2.2 Intensive Mode

Orbit number 2762 was first selected for study due to the availability of sufficient data. Although the ten second averaging program had not as yet been developed, a GAP (version 2.0) Summary along with the GAP and CAMIMERGE dumps were obtained. The CALIMERGE dump was used since it lists raw, uncalibrated data which can be hand-converted to account for the transfer gain of the integrating gates. The CALIMERGE results were then compared with the GAP (version 2.0) Summary and GAP dump data. It was discovered that the GAP Summary incorrectly reported the Plateau gate value as 0.13 input volts during the interval under consideration. Both the GAP dump and the hand converted CALIMERGE values agreed and indicated a lower value for per frame averages of .09 to .10 volts for the Plateau gate. It was apparent that there was a calibration problem in the GAP (version 2.0) Summary. This problem was further reflected in the failure of the pointing angle algorithm since for $\overline{APG} = 0.13$ volts, the resulting value of $\overline{\Delta}$ was larger than 0.504 (see Table V).

During this time, a revision of Reference [17] was obtained and while working with the I-Mode Plateau gate calibration table, an incorrect table entry was discovered. Under the 0°C temperature column corresponding to a functional unit value of 0.1 volt, an engineering unit value of -0.99 volt is listed. This seemed unreasonable based upon the trend in values surrounding this entry and in fact appeared as though +0.99 volt ought to be the correct value instead. Using the CALIMERGE dump again for orbit 2762, a hand conversion from engineering to functional units was repeated using the revision for the Plateau gate calibration table. The results then agreed with the incorrect GAP (version 2.0) Summary values. Evidently, the GAP Summary had been using this incorrect table and consequently generated the wrong Plateau gate per frame averages. Confirmation was made that this was an erroneous value and unfortunately was being used in recent data processing. This meant that I-mode pass data having Plateau gate engineering units and Intensive Tracker Temperature (ITT) values within range of the incorrect table entry were processed incorrectly for the conversion to Plateau gate functional units.

Dr. G. S. Hayne of Applied Science Associates has developed a Fortran subroutine capable of taking Intensive Mode APG values, which have been

incorrectly calibrated for tracker temperatures under 20°C, and reversing the calibration procedure to retrieve the original engineering unit value. This value is then re-calibrated with a procedure using the correct table value to output properly calibrated APG functional units. At present, this routine has been adapted to run with the ten second pointing angle program. Figure 34 is a typical program output before correction while Figure 35 is the same run after correction. It should be noted that the pointing angle correction also has an effect on the computed values for σ^o.

Despite the problem with the Plateau gate values, a number of passes were found to be operating in a temperature range such that the calibration was correct and the pointing angles derived from the altimeter data could be used to compare with attitude control system results. Figures 36 and 37 illustrate typical comparisons of the altimeter and attitude control system results. Although the data is very limited, there is no apparent bias as in the case of the Global Mode.

6.0 PROCESSING FOR AND INITIAL MEASUREMENTS OF σ^o

Closely associated with the computation of altimeter pointing angle is the estimation of the radar cross section per unit area, σ^o. Although the pointing angle is only computed every ten seconds, σ^o can be computed more frequently. That is, once estimates of the pointing angle are available, it is possible to go back into the data and compute σ^o at a much greater rate than one per ten seconds. However, the programs presently in use at WFC only compute σ^o at a ten second rate.

6.1 Algorithm Development

As shown by equations (62) and (64), the average received power as seen by the Plateau gate can be written in the following form;

$$\langle \bar{P}_r(t) \rangle = P_T \left[\frac{\sigma^o(\bar{\psi}_o)}{L_p} \right] f(\xi, \text{Mode}) \qquad (88)$$

where the function $f(\xi,\text{Mode})$ depends upon both the pointing angle and the operating mode. A plot of $f(\xi,\text{Mode})$ was presented in Figure 19 for both the Global and Intensive modes. A closed form approximating function was fitted to the curves in Figure 19 in order to avoid the need for a look-up table. Solving (88) for $\sigma^o(\bar{\psi}_o)/L_p$ resulted in the following algorithms; for Global Mode.

ID HEADER: REV 1164/101,COMPILE TAPE 7169,FILE 07,GETTAPE,05/25/76

HHMMSS.SS	ALT.STAT.	AV.PLAT.	AV.ASG	AV.RAGC	DELTA	PT.ANGLE	AV.RTP	SIGMA
	THE GATE VALUES WENT OUT OF RANGE							
63552.30	79.00	.0784	.0509	-70.075	.351	.71	62.214	11.84
63602.54	79.00	.0756	.0519	-70.380	.313	.78	62.214	11.92
63612.78	79.00	.0764	.0524	-70.777	.313	.78	62.214	11.52
63623.02	79.00	.0748	.0525	-70.781	.299	.81	62.214	11.67
63633.26	79.00	.0746	.0516	-70.412	.309	.79	62.214	11.93
63643.50	79.00	.0746	.0515	-70.114	.310	.79	62.214	12.22
63653.74	79.00	.0732	.0495	-69.517	.324	.76	62.214	12.67
63703.98	79.00	.0731	.0520	-70.234	.289	.83	62.214	12.31
63714.22	79.00	.0726	.0513	-69.601	.293	.82	62.214	12.90
63724.46	79.00	.0729	.0513	-69.305	.296	.82	62.214	13.17

Figure 34. Ten second pointing angle and σ° program output showing incorrect average Plateau Gate values (AV.PLAT.) resulting from erroneous calibration table entry.

ID HEADER: REV 1164/101,COMPILE TAPE 7169,FILE 07,GETTAPE,05/25/76

HHMMSS.SS	ALT.STAT.	AV.PLAT.	AV.ASG	AV.RAGC	DELTA	PT.ANGLE	AV.RTP	SIGMA
	THE GATE VALUES WENT OUT OF RANGE							
63552.30	79.00	.0952	.0509	-70.075	.465	.36	62.214	9.43
63602.54	79.00	.0939	.0519	-70.380	.447	.44	62.214	9.34
63612.78	79.00	.0953	.0524	-70.777	.450	.43	62.214	8.90
63623.02	79.00	.0946	.0525	-70.781	.445	.44	62.214	8.95
63633.26	79.00	.0949	.0516	-70.412	.456	.40	62.214	9.20
63643.50	79.00	.0956	.0515	-70.114	.461	.38	62.214	9.44
63653.74	79.00	.0951	.0495	-69.517	.480	.29	62.214	9.83
63703.98	79.00	.0954	.0520	-70.234	.455	.41	62.214	9.39
63714.22	79.00	.0953	.0513	-69.601	.462	.38	62.214	9.95
63724.46	79.00	.0961	.0513	-69.305	.466	.36	62.214	10.20

Figure 35. Ten second pointing angle and σ° program output showing results of using the Plateau Gate calibration correction subroutine.

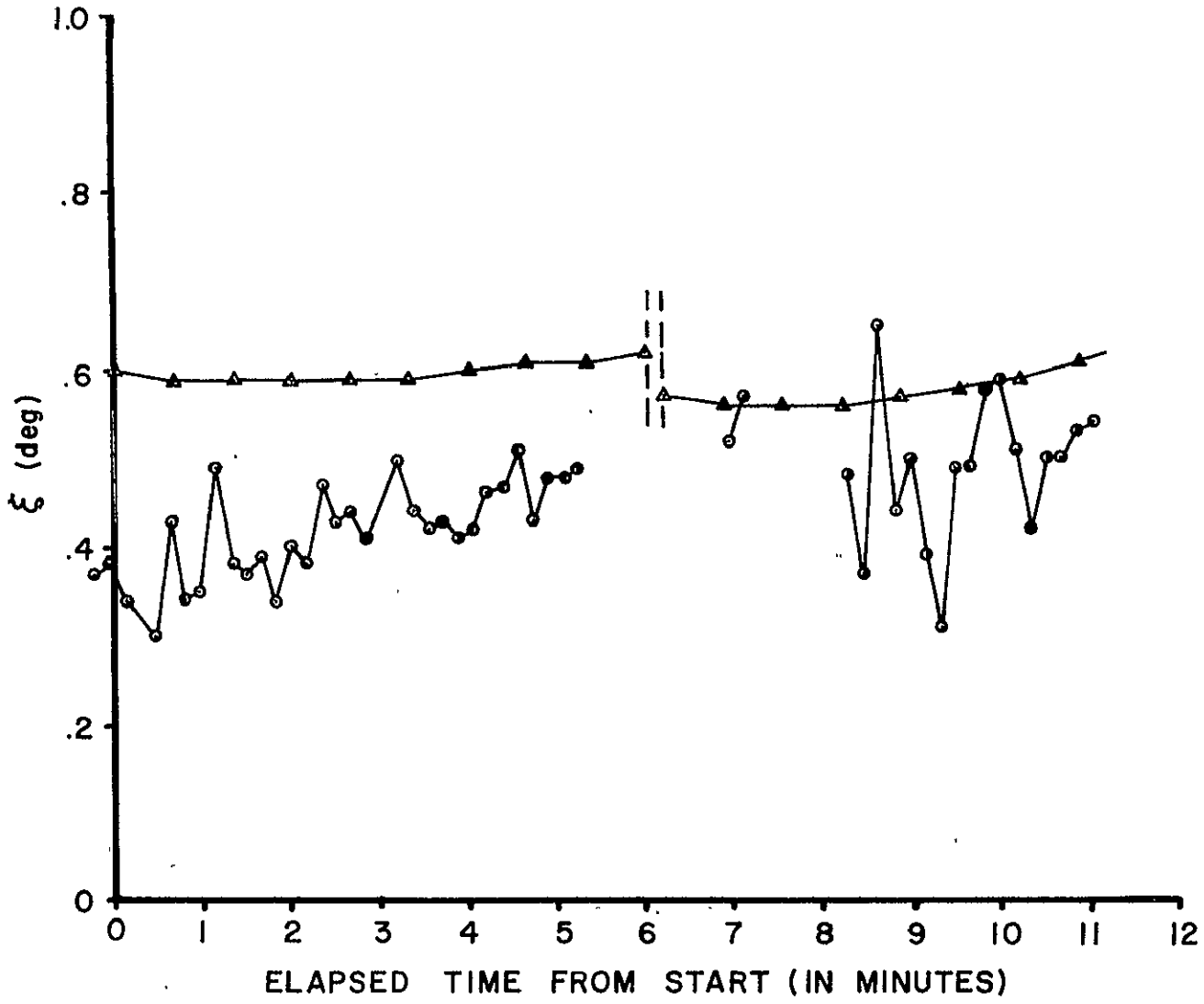

Figure 36. Comparison of attitude control system derived pointing angle (Δ–Δ–Δ) with altimeter estimates (o–o–o) for Intensive Mode, Rev 453, Start Time = 00H16M44S, 12 May 75.

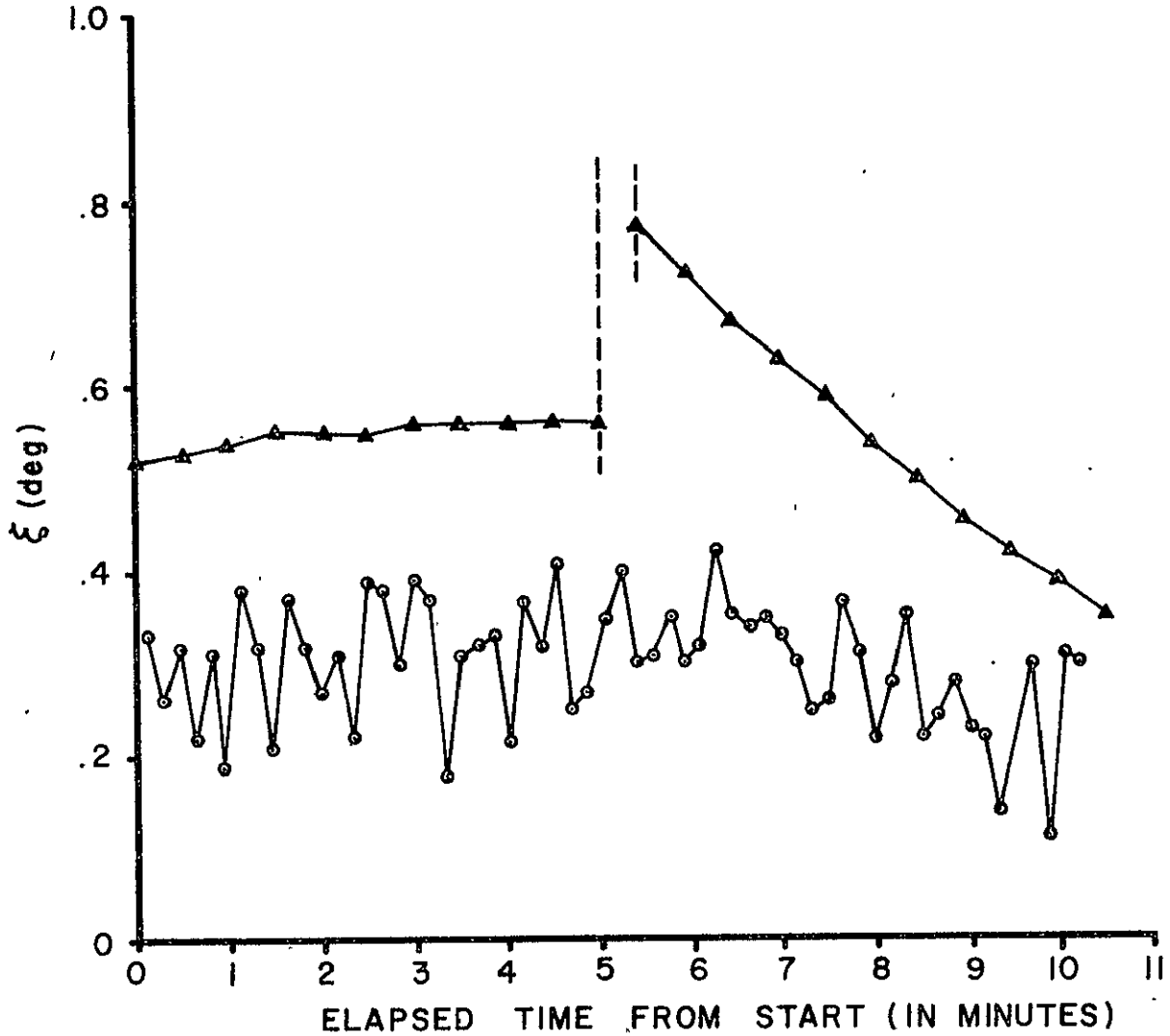

Figure 37. Comparison of attitude control system derived pointing angle (Δ—Δ—Δ) with altimeter estimates (o—o—o) for Intensive Mode, Rev 530, Start Time = 00H27M00.4S, 17 May 75.

$$\frac{\sigma^\circ(\bar{\psi}_o)}{L_p}\,(\mathrm{dB}) = (\overline{\mathrm{AGC}})_{10\mathrm{sec}} - 10\log_{10}\left\{\exp\left[-2684.56\,\sin^2\xi\right]\cdot\left[11.02\exp(1.6\xi)\right.\right.$$

$$\left.\left. + 188.98\right]\right\} + 172.15 - (\overline{\mathrm{RTP}})_{10\mathrm{sec}} \qquad (89)$$

while for Intensive Mode,

$$\frac{\sigma^\circ(\bar{\psi}_o)}{L_p}\,(\mathrm{dB}) = (\overline{\mathrm{AGC}})_{10\mathrm{sec}} - 10\log_{10}\left\{12.19\exp\left[-2684.56\sin^2\xi\right]\right.$$

$$\left. \cdot \cosh\left(\frac{\xi}{3.201}\right)\right\} + 152.15 - (\overline{\mathrm{RTP}})_{10\mathrm{sec}} \qquad (90)$$

where the average in this case corresponds to 1000 pulses or ten seconds. In (89) and (90), ξ is in degrees, $(\overline{\mathrm{RTP}})_{10\mathrm{sec}}$ is the transmit power in dBm averaged over a ten second interval, and the units of σ°/L_p are dB. The ten second average of the AGC, i.e., $(\overline{\mathrm{AGC}})_{10\mathrm{sec}}$, should be truly accomplished in the following manner; the AGC output is converted from volts to dBm to remove AGC loop nonlinearities, the dBm values are converted to numeric, a ten second average of the numeric values is formed, and then this numeric average is converted to dBm. In the actual data processing, the dBm values of the AGC-inferred power are averaged since they do not exhibit a great deal of fluctuation. This same statement also holds for the transmit power, RTP. It should be noted, however, that for periods where the AGC output is rapidly fluctuating, the values of (σ°/L_p) resulting from (89) and (90) may be in error. For the Intensive Mode, the nominal angular location of the midpoint of the Plateau gate is $\bar{\psi}_o = 0.28^\circ$, while for Global Mode it is $\bar{\psi}_o = 0.68^\circ$.

For certain cases such as quick-look data reduction, it may be desirable to decouple the σ° computation from the pointing angle estimation. That is, rather than averaging over a ten second interval to estimate the pointing angle, it may be more feasible to just list computed σ° values for some assumed pointing angle. This procedure would have the advantage of not requiring cross-frame averaging, which for quick-look data is certainly desirable. In this case, the assumption of $\xi = 0^\circ$ might as well be made. Then,

for Global Mode

$$\frac{\sigma^\circ(0^\circ)}{L_p}\,(\mathrm{dB}) = \mathrm{AGC(dBm)} - \mathrm{RTP(dBm)} + 149.14 \qquad (91)$$

while for Intensive Mode,

$$\frac{\sigma^\circ(0^\circ)}{L_p}\,(\mathrm{dB}) = \mathrm{AGC(dBm)} - \mathrm{RTP(dBm)} + 141.29 \qquad (92)$$

The AGC and transmit power outputs may either be averages or instantaneous values, depending upon the use of the data. Of course, this procedure is only intended for quick-look purposes where altimeter health or certain surface phenomenon require rapid examination of the data. Ignoring the pointing angle of the altimeter can result in more than a 3 dB error in σ° for a one degree pointing error.

6.2 Initial Cross Section Results

6.2.1 Global Mode

The results produced by the cross section algorithm used in the ten second averaging program were, for Global Mode operation, in close agreement with nominal values resulting from the Skylab data reduction effort [18]. Table VI gives one such comparison made for cross section calculations from SL-2 Pass 6 data on June 8, 1973, and the values obtained from GEOS-3, G-Mode Rev 415 on May 9, 1975, for Atlantic Ocean crossings. While these passes occurred two years apart, they are regionally similar and the sea states were not drastically different. These data may serve as a simple comparison of the values which, of course, should be system independent. It might not seem correct to present this comparison while an apparent bias in the Global Mode estimated pointing angle still exists. Justification is found, however, in the fact that the cross section computation is not very sensitive to small differences in the pointing angle up to about 1° off-nadir. For instance, the first ten second average σ° value of 13.62 dB was computed for a 0.75° estimated pointing angle. With all other parameters held constant, a 0° pointing angle would result in a ten second cross section

TABLE VI

Comparison of estimated σ° values (in dB) taken from SKYLAB S-193 and GEOS-3 altimeter data, both from Atlantic Ocean crossings in Spring.

SKYLAB SL-2, MODE V, SM-0 PASS 6 8 JUNE, 1973				GEOS-3 G-MODE REV 415 9 MAY, 1975	
	FRAME NO.	σ° 1-sec		HHMMSS.SS	σ° 10-sec.
SSM-0	4	12.7	13.5	073002.00	13.62
	5	12.8	13.6	073012.24	13.85
	6	13.2	14.0	073022.48	14.69
				073032.72	13.71
SSM-1	1	12.7	13.5	073042.96	14.06
	2	12.9	13.7	073053.20	13.78
	3	13.4	14.2	073103.44	13.69
	4	12.7	13.5	—DATA BREAK—	
	5	12.5	13.3	073251.99	13.24
				073302.23	13.38
SSM-2	1	12.7	13.5	073312.47	13.05
	2	12.7	13.5	073322.71	12.71
	3	12.3	13.1	073332.95	13.31
	4	12.7	13.5	073343.19	12.93
	5	12.3	13.1	073353.43	13.85
				073403.67	13.61
				073413.91	13.13
				073424.16	12.45
				073434.40	12.48
				073444.64	11.92
				073454.88	12.92
				073505.12	14.36
				073515.36	17.04
				—OUT OF RANGE—	
				073539.94	13.68
				073550.17	12.66

NOTE: The two columns for SKYLAB σ° values represent estimated bounds. The data rate for SKYLAB was 250 pulses/sec and 1 Frame $\approx$ 1 sec.

of 12.14 dB, less than 2 dB smaller. Given the degree of bias suspected in the estimated Global Mode pointing angle, one might expect the cross section computations to be about 1 dB too large. This 1 dB reduction places the GEOS-3 values even closer to the range of Skylab results in this case!

6.2.2 Intensive Mode

The initial application of the algorithm given by (90) to the Intensive Mode resulted in σ° values which appeared to be more than 3 dB below Global Mode and Skylab results. For example, for relatively calm seas, the Intensive Mode σ° values were below Skylab data acquired over 6 m. seas in the North Atlantic! Since the Intensive Mode estimates of pointing angle were in reasonable agreement with the attitude control system data, there was definite reason to suspect some other parameter in the algorithm. The use of the "Clean" AGC calibration curves* was suspected as the source of error and the theory presented in section 4 tended to substantiate this suspicion. When the "Clutter" AGC calibration curves were used to translate the AGC output into dBm, the resulting σ° values were in very good agreement with both Global Mode and Skylab data. The next section describes an in-orbit test that was designed to help resolve the "Clean" vs. "Clutter" AGC calibration problem.

6.3 AGC Calibration Correction

6.3.1 Rev 183-184 Crossing

A fortunate situation for purposes of this study occurred on 22 April, 1975, several hundred miles east of the coast of Iceland. Following Intensive Mode rev 183 (about 99 minutes later) Global Mode rev 184 crossed over rev 183's ground track and proceeded along for about twenty seconds in the same approximate area (see Figure 38). This provided an interesting case for comparison of the two operating mode results based on the plausible assumption that surface conditions had not changed drastically in 99 minutes. In fact, a check on ground truth information [19] indicated moderate seas

---

*See Section 4 for a discussion of the "Clean" vs. "Clutter" problem.

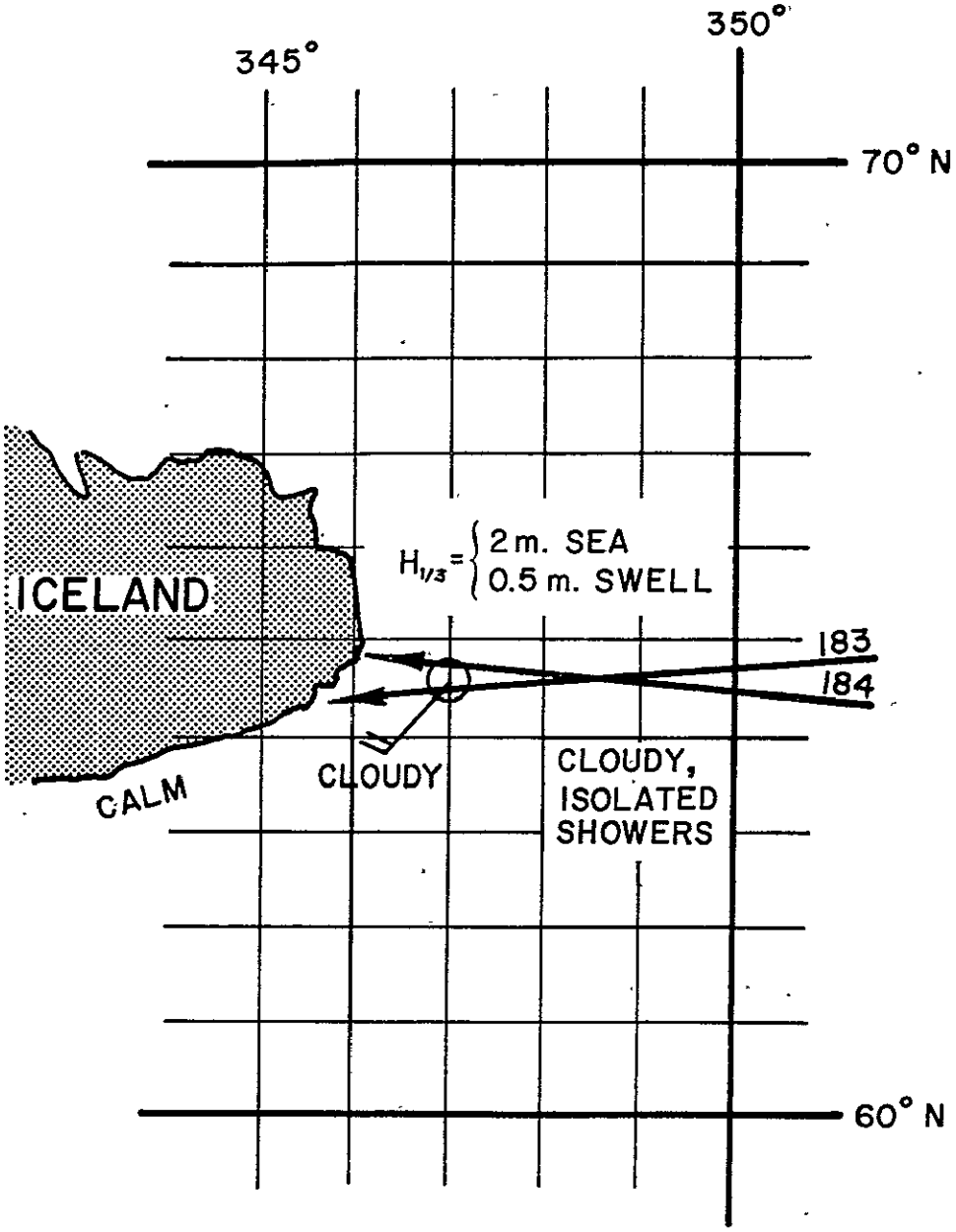

Figure 38. A plot of the ground tracks for revs 183 and 184 in the vicinity of their crossing. Note the prevailing weather and sea-state conditions.

with 20 knot winds under cloudy skies and no weather extremes occurring in the vicinity of the crossing. It therefore seemed correct to expect cross section values derived from both passes to be reasonably close in value.

6.3.2 Cross Section Comparisons

This section compares σ° values obtained from I-Mode (Rev 183) data with those obtained from G-Mode (Rev 184) in the vicinity of the crossing of each pass. Two different sets of I-Mode σ° values can be found using the two different AGC calibration curves in order to determine whether the "clean" test signal calibration or the "clutter" calibration will result in σ° values which more nearly compare with those from G-Mode. As mentioned before, the close agreement between modes is expected by the assumption that cross section did not change considerably. In order to cope with the aforementioned problem in Global Mode pointing angle estimation, a pair of constant angle values were chosen to represent bounds for the actual values. For this purpose, a lower bound of 0.2° and an upper bound of 0.7° were used. Then, σ° values were computed for each of the pointing angle values as a function of elapsed time along the pass. Table VII presents the results of these calculations. Per frame σ° values were computed for each mode and in the case of the I-Mode calculations, the altimeter estimate of pointing angle for ten second intervals was used. As can be seen, the σ° results derived from Clutter curve converted AGC values are considerably closer to G-Mode values. Since the AGC conversion process using Clutter calibration curves results in I-Mode σ° values much closer to G-Mode results, it is concluded that they should be used in data processing instead of the currently used Clean calibration curves. It would be well to further substantiate this conclusion with more comparisons using similar rev crossing situations.

A "correction" routine has been added to the ten second pointing angle and σ° program for use on the WFC ECLIPSE system. This routine accepts only Intensive Mode AGC values which have been processed using the Clean calibration data and produces a new AGC value which is equivalent to using Clutter calibration with the original raw AGC outputs. Because of the temperature dependence of this correction and the desire to keep it as simple

TABLE VII

Comparison of Intensive and Global Mode σ° values during a segment from each pass crossing the same region of ocean. Intensive Mode values show the results of applying both Clean and Clutter AGC calibration curves.

REV 183 INTENSIVE MODE				REV 184 GLOBAL MODE		
FRAME	$\bar{\xi}^\circ$	σ°_{clean}	$\sigma^\circ_{clutter}$	FRAME	$\sigma^\circ(\xi=.2^\circ)$	$\sigma^\circ(\xi=.7^\circ)$
77	.33°	5.51	9.32	89	9.54	10.76
78		6.12	9.92	90	9.54	10.76
79		5.86	9.66	91	9.62	10.84
				92	9.54	10.76
80	.24°	6.25	10.04	93	9.54	10.76
* 81		5.96	9.75	* 94	9.94	11.16
82		6.14	9.93	95	10.14	11.36
				96	10.31	11.53
83	.26°	6.02	9.82	97	10.18	11.40
84		6.15	9.95	98	10.31	11.53
85		6.23	10.03	99	10.46	11.68
				100	10.65	11.87
				101	10.75	11.97

NOTE: The two data sets have been aligned as closely as possible.
*These frames correspond to the point of intersection of Rev 183 and Rev 184.

as possible, the resultant σ° values may, at times, differ from a straightforward Clutter calibration by a dB or so. The additional time, effort, and computer storage required to reduce this error further still did not appear to be warranted.

REFERENCES

1. Miller, L. S. and G. S. Brown, "Engineering Studies Related To The GEOS-C Radar Altimeter," NASA CR-137462, Applied Science Associates, Inc., Apex, N. C., May, 1974.

2. "GEOS-3 Definitive Attitude Results, 18 April 1975 - 30 June 1975," Computer Management Branch, Goddard Space Flight Center, Greenbelt, Maryland, (no date).

3. Brown, G. S., "A Closed Form Relation for the Average Return Waveform From a Near-Nadir Pointed, Short Pulse, Satellite Based Radar Altimeter," paper presented at the USNC/URSI Conference, Boulder, Colorado, October, 1974.

4. "GEOS-C Summary Phase I Technical Report, Volume I," Contract No. APL372085, General Electric Company, Utica, New York, page 18, 31 May, 1974.

5. Miller, L. S., "Interim Report on Attitude Estimation," Unpublished Memorandum, Applied Science Associates, Inc., Apex, N. C., 1 August, 1974.

6. Hofmeister, E. L., B. N. Keeney, T. W. Godbey and T. J. Berg, "Data User's Handbook and Design Error Analysis, GEOS-C Radar Altimeter, Vol. 1," General Electric Company, Utica, New York, May, 1976.

7. Brown, G. S. (Editor), "Skylab S-193 Radar Altimeter Experiment Analyses and Results," Final Report, Contract No. NAS6-2520 (Task 3.10), Applied Science Associates, Inc., Apex, N. C., Chapter 3, May, 1976.

8. Purdy, C. L., Private Communications, NASA, Wallops Flight Center, August, 1976.

9. Papoulis, A., Probability, Random Variables, and Stochastic Processes, McGraw-Hill Book Co., New York, Pg. 197, 1965.

10. Nitzberg, R., "Limitations of a Variance Approximation," IEEE Trans. on Aerospace and Electronic Systems, Vol. AES-8, pp. 246-247, March, 1972.

11. Hofmeister, E. L., "Analysis and Measurement of the Performance of a

Signal Tracking Loop for a Satellite Radar Altimeter When Excited by a Random Process," Ph.D. Dissertation, Syracuse University, December, 1973.

12. Davenport, W. B., Jr. and W. L. Root, An Introduction to the Theory of Random Signals and Noise, McGraw-Hill Book Co., New York, pg. 168, 1958.

13. Berger, T., "Satellite Altimetry Using Ocean Backscatter," IEEE Trans. on Antennas and Propagation, Vol. AP-20, pp. 295-309, May, 1972.

14. Steenson, B. O. and N. C. Sterling, "The Amplitude Distribution and False-Alarm Rate of Filtered Noise," Proc. of IEEE, pp. 42-55, January, 1965.

15. Zrnic, D. S., "Moments Of Estimated Input Power For Finite Sample Averages Of Radar Receiver Outputs," IEEE Trans. on Aerospace and Electronic Systems, Vol. AES-11, pp. 109-113, January, 1975.

16. Gradshteyn, I. S. and I. M. Ryzhik, Tables of Integrals, Series, and Products, 4 th edition, Academic Press, New York, 1965.

17. Leitao, C. D., C. L. Purdy and R. L. Brooks, "Wallops GEOS-C Altimeter Preprocessing Report," NASA TMX-69357, Wallops Fligth Center, Wallops Island, Virginia, May, 1975.

18. Brown, G. S., "Reduced Backscattering Cross Section (σ°) Data From The Skylab S-193 Radar Altimeter," NASA CR-141401, Applied Science Associates, Inc., Apex, N. C., October, 1975.

19. Parsons, C. L. and L. R. Goodman, "GEOS-3 Phase B Ground Truth Summary," NASA TMX-69360, Wallops Flight Center, Wallops Island, Virginia, November, 1975.

APPENDIX

The basic integrals to be evaluated are of the following form;

$$I_n = \int_{-\infty}^{\infty} x^n \exp\left[\mu x - \alpha \exp(x)\right] dx \qquad \text{(A-1)}$$

where n is an integer and μ and α are constants. To accomplish (A-1), it is first necessary to start with the case of $n = 0$, i.e.

$$I_o = \int_{-\infty}^{\infty} \exp\left[\mu x - \alpha \exp(x)\right] dx \qquad \text{(A-2)}$$

and substitute

$$\alpha \exp(x) = \exp(z) \quad .$$

Since

$$x = -\ell n(\alpha) + z$$

and the limits are invariant under the transformation, (A-2) becomes

$$I_o = \exp\left[-\mu \ell n(\alpha)\right] \int_{-\infty}^{\infty} \exp\left[\mu z - \exp(z)\right] dz \qquad \text{(A-3)}$$

The integral in (A-3) is given in [16] page 308 (equation 3.328);

$$I_o = \exp\left[-\mu\, \ell n(\alpha)\right] \Gamma(\mu) \qquad \text{(A-4)}$$

where $\Gamma(\cdot)$ is the gamma function.

Combining equations (A-2) and (A-4) yields

$$\int_{-\infty}^{\infty} \exp\left[\mu x - \alpha \exp(x)\right] dx = \exp\left[-\mu \ln(\alpha)\right] \Gamma(\mu) \qquad \text{(A-5)}$$

Differentiating both sides of (A-5) n times with respect to μ produces the following;

$$\int_{-\infty}^{\infty} x^n \exp\left[\mu x - \alpha \exp(x)\right] dx = \frac{d^n}{d\mu^n}\left\{\exp\left[-\mu \ln(\alpha)\right] \Gamma(\mu)\right\} \qquad \text{(A-6)}$$

Equation (A-6) is the general result; for $n = 1$ (A-6) becomes

$$\int_{-\infty}^{\infty} x \exp\left[\mu x - \alpha \exp(x)\right] dx = \exp\left[-\mu \ln(\alpha)\right] \left\{ - \ln(\alpha)\Gamma(\mu) + \Gamma'(\mu)\right\} \qquad \text{(A-7)}$$

which is the result required in Section 4.2 for $\mu = N$ and $\alpha = N/\overline{P}_r$.